

Università degli Studi di Torino
Dipartimento di Fisica Sperimentale
Scuola di Dottorato in Scienza e Alta Tecnologia
Ciclo XXIII



**ION AND ELECTRON MICROSCOPY
FOR THE CHARACTERIZATION OF MATERIALS
OF ARCHAEOLOGICAL, HISTORICAL AND ARTISTIC
INTEREST: DETERMINATION OF THE PROVENANCE
OF LAPIS LAZULI USED FOR GLYPTIC**

Alessandro Re

Tutor: dott. Alessandro Lo Giudice

Coordinatore del Dottorato: prof. Guido Boffetta
Anni Accademici: 2008-2010
Settore scientifico-disciplinare di afferenza: FIS/07

Università degli Studi di Torino
Scuola di Dottorato in Scienza e Alta Tecnologia

Tesi di Dottorato di Ricerca in Scienza e Alta Tecnologia
Indirizzo: Fisica e Astrofisica

**ION AND ELECTRON MICROSCOPY
FOR THE CHARACTERIZATION
OF MATERIALS OF ARCHAEOLOGICAL,
HISTORICAL AND ARTISTIC INTEREST:
DETERMINATION OF THE PROVENANCE OF
LAPIS LAZULI USED FOR GLYPTIC**



Alessandro Re

Tutor: Dott. Alessandro Lo Giudice

XXIII Ciclo, Marzo 2011

[...] Then Gilgamesh issued a proclamation through the land, he summoned them all, the coppersmiths, the goldsmiths, the stone-workers, and commanded them, "Make a statue of my friend". The statue was fashioned with a great weight of lapis lazuli for the breast and of gold for the body. A table of hard-wood was set out, and on it a bowl of carnelian filled with honey, and a bowl of lapis lazuli filled with butter. These he exposed and offered to the Sun; and weeping he went away. [...]

The Epic Of Gilgamesh – "Ishtar and Gilgamesh, and the death of Enkidu"

TABLE OF CONTENTS

INTRODUCTION	1
THE HISTORICAL PROBLEM	3
THE USES OF LAPIS LAZULI	3
THE QUARRIES OF LAPIS LAZULI	5
<i>Badakhshan, Afghanistan.....</i>	<i>6</i>
<i>Pamir Mountains, Tajikistan</i>	<i>6</i>
<i>Chagai Hills, Pakistan</i>	<i>7</i>
<i>Lake Baikal, Siberia</i>	<i>7</i>
<i>Chile, Coquimbo region.....</i>	<i>7</i>
<i>Other quarries</i>	<i>8</i>
PETROGRAPHY OF LAPIS LAZULI.....	9
LAZURITE.....	9
DIOPSIDE	10
OTHER MINERALOGICAL PHASES.....	11
THE SAMPLES	16
ROCKS	16
<i>Sample preparation</i>	<i>16</i>
ARTWORKS OF THE "COLLEZIONE MEDICEA DI PIETRE LAVORATE"	18

ANALYTICAL TECHNIQUES	20
ION BEAM ANALYSIS	21
<i>PIXE: Particle Induced X-ray Emission</i>	22
<i>IL: Ionoluminescence</i>	24
ELECTRON PROBE ANALYSIS.....	26
<i>EPMA: Electron Probe Micro-Analysis</i>	28
<i>CL: Cathodoluminescence</i>	28
RS: RAMAN SPECTROSCOPY	29
THE PREVIOUS PROVENANCE STUDIES	30
EXPERIMENTAL SETUP	35
ION BEAM MICROPROBE FACILITIES	35
<i>LNL (Legnaro)</i>	35
μ -PIXE set-up at LNL.....	36
<i>LABEC (Firenze)</i>	37
μ -PIXE set-ups at LABEC	38
μ -IL set-up at LABEC.....	39
<i>Defocused-IBIL setup at LABEC</i>	41
ELECTRON PROBE INSTRUMENTS	42
<i>cold-CL</i>	42
<i>SEM-EDX</i>	43
<i>SEM-CL</i>	44
SIMULATIONS.....	46
μ -RAMAN SPECTROSCOPY	48

RESULTS ON ROCKS	49
PRELIMINARY CHARACTERISATION	49
LAZURITE.....	55
DIOPSIDE	59
OTHER PHASES.....	63
<i>Wollastonite</i>	63
<i>Calcite</i>	64
<i>Phlogopite</i>	65
<i>K-feldspar</i>	65
<i>Phase of the cancrinite group</i>	66
<i>Phase rich in titanium</i>	68
MARKERS.....	70
CHECK ON A SAMPLE OF UNKNOWN PROVENANCE.....	71
RESULTS ON ARTWORKS.....	72
EXPERIMENTAL PROCEDURE	72
RESULTS.....	73
<i>Oval bowl (13682)</i>	74
<i>Small case (13684)</i>	76
<i>Saltcellar (13687)</i>	76
<i>Oval panel (13688)</i>	76
<i>Summary</i>	77
CONCLUSION.....	78
BIBLIOGRAPHY	80

INTRODUCTION

Ion and electron microscopy are widely used to characterize materials in many fields. The study of samples of archaeological, historical and artistic interest is a case in which these techniques are of extreme importance. In particular Ion Beam Analysis techniques are of great interest in the Cultural Heritage field for many reasons: they do not require any sample preparation, they can be performed in air and they do not damage the sample at low ion fluences.

An interesting material to be analyzed by means of Ion Beam Analysis is lapis lazuli; it is a semi-precious blue stone widely used for different purposes since the antiquity but, at present, there are still some lacking information about both its trade in ancient times and the quarries exploited from different civilizations. Although the Badakhshan mines in Afghanistan (the most famous being Sar-e-Sang) are widely considered as now as the only sources of lapis lazuli in ancient times, other sources have been taken in consideration, even if a systematic and exhaustive provenance study of the raw material utilized in works of art is still lacking.

To contribute in the solving of the lapis lazuli provenance problem we started a systematic study of this fascinating stone comparing physico-chemical properties of rocks and historical objects. Since often it is impossible to take a sample from the object under analysis due of its extreme value, it is fundamental to use only non-destructive techniques. Nowadays there are many instruments that permits not to damage the sample under analysis and among these we concentrate our efforts on Ion Beam Analysis, to identify the provenance of lapis lazuli only by means of them. We often used also destructive techniques, like Electron Microscopy, just to speed up the characterization of geological samples and to gain experience with the material, but these techniques are not necessary for the study of precious objects.

With these bases we started to go deeper in the problem surveying all the bibliography about this stone, its characteristics and the studies done on it, both from the historical, geological, geochemical and archaeometrical points of view. As we will see, a lot of people already worked on lapis lazuli, but up to now nobody performed an exhaustive provenance study in a non destructive way.

This work rose from the Solid State Physics group of the Experimental Physics Department of the University of Torino and is part of a wide experiment of the Italian National Institute of Nuclear Physics (INFN) called FARE (External Rarefied Beams) continuation of the experiment DANTE (Developments in Analytical Nuclear TEchniques). One of the main goals of

these experiments is to develop, install and test new apparatuses (among which a Ionoluminescence device) on the external microbeam line at the LABEC in Firenze, an INFN laboratory mainly devoted to non-destructive analyses in the field of Cultural Heritage.

In this work we were lucky to have the support and the interest of the "Museo di Storia Naturale di Firenze" in studying its collections and in particular the section "Mineralogy and Lithology" very rich in lapis lazuli, featuring both precious objects of the "Collezione Medicea" (16th-17th century) and rocks of various certain provenance. Besides the "Collezione Medicea" this study can be extended to archaeological findings to try to reconstruct the old trade-routes between ancient populations that already used this material.

Going into the structure of this work, the first chapter is about the historical problem and the open questions about the origin and the provenance of lapis lazuli; in particular we will focus on the uses of this stone and the main quarries in the world. In the second chapter we present a short mineralogical contextualization of the material, while the third one contains a short description of the samples available for this provenance study and how they have been treated to speed up the measurements. The fourth chapter details the analytical techniques employed in this work and in the previous provenance studies of lapis lazuli, while the results obtained using them are presented in the fifth chapter. The sixth chapter describes the instruments optimized for this work while in the seventh one the approach we used to face the problem is presented, trying to find some markers to identify the different provenances. In the same chapter there are also the details of the experimental results we obtained and some tests we performed to check if our method works with samples of unknown provenance. The eighth chapter shows the results obtained on the artworks of the "Collezione Medicea", while in the last chapter I'll try to summarize the results obtained in this work, concluding with some proposals for future improvements and how to continue with this intriguing work.

Most of the results presented in this work have already been published in two papers [Lo Giudice et al, 2009; Re et al, 2011] and have been presented at national and international conferences; among these there are TECHNART 2009 (Athens, Greece), ICNMTA 2010 (Leipzig, Germany), SEM2010 (London, UK) and in the near future it will be presented at TECHNART 2011 (Berlin, Germany).

THE HISTORICAL PROBLEM

Semi-precious stones were used since Neolithic Age for the manufacture of jewels, objects of social prestige and veneration objects. The few fragments of Sumer cuneiform script, survived till now through clay tablets, exalts not only the beauty of the semi-precious stones but also their meaning in the connections between the people and the divinity [Bulgarelli and Tosi, 1977]. Some of these stones are very rare, because they can be found in very few places on the Earth, and so they were procured through complex networks of exchanges and trades routes and transported thousands kilometres away from their origin. This has been proved by archaeological findings, mostly coming from rich graves, among which there were also many lapis lazuli, one of the first semi-precious stones used in Middle East, Asia and Europe. In next paragraph there is a brief description of the different use of lapis lazuli by different civilizations in different periods. In any case, the rarity and the importance of the lapis lazuli in the culture of civilization is confirmed by two discoveries. The first consisting in a systematically reuse, as can be observed in the progressive decrease in the average size of lapis lazuli cylinder seals in the third millennium B.C. [Bussers, 1984; Collon, 1986] and their reuse as beads [Herrmann, 1968]. The second consisting in glass imitation ("lapis lazuli from the kiln") of the genuine stone ("lapis lazuli from the mountain") that begins to appear in the second half of the second millennium B.C. [Moorey, 1994].

The uses of lapis lazuli

In Mesopotamia the earliest archaeological evidence of lapis lazuli's use was traced back to the 5th millennium B.C. [Von Rosen, 1990] with the discovery of beads at a cemetery outside the temple walls of Eridu (Sumer) in southern Babylonia. Artistic works containing lapis lazuli used between 2700 and 2500 B.C. were recovered in the 1920's during excavations of the ancient Chaldean city of Ur. The most famous of these were recovered from the royal tomb of Queen Pu-abi (2500 BC), including three gold headdresses, and two bead necklaces [Sofianides and Harlow, 1990; Sutherland, 1991], as well as two statues of male goats with shoulders, eyes and horns of lapis lazuli [Coenraads and Canut de Bon, 2000]. There were many other applications of lapis lazuli, some of them discovered only in recent periods: small objects (such as seals, amulets and jewels), larger objects (such as vessels, votive cylinders, dagger handles, etc.) and fragments of inlays are just some examples [Herrmann and Moorey, 1983; Moorey, 1994].

In Egypt, prior to 3100 B.C., lapis lazuli was used for scarabs, pendants, beads and inlaid jewels [Sofianides and Harlow, 1990]. The tombs of Ramses II (about 1279 B.C.) and Tutankhamon (1361-1352 B.C.) revealed rings and other jewels made of lapis lazuli. In fact, the golden mask over the head and shoulders of Tutankhamon's mummy has eyebrows and areas around the eyes that are inlaid with lapis lazuli [Silverman, 1978].

Also in Asia lapis lazuli was known and used since long time: the Indus Valley Civilization used it together with other stones to manufacture beads from the 3300 B.C., as proved by some findings in the archaeological sites of Harappa, Pakistan [Kenoyer, 1997].

In China the use of lapis lazuli was mentioned the first time in Chinese annuals of the 6th and 8th centuries B.C., as the stone was a favourite of Chinese carvers [Bowersox and Chamberlin, 1995]. Some Chinese hair and belt ornaments carved from lapis lazuli have been dated to 551-479 B.C. [Sofianides and Harlow, 1990].

In Europe, from the eleventh century A.D. [Herrmann and Moorey, 1983] until last centuries, lapis lazuli was crushed to be used as a blue pigment called "ultramarine". During the Renaissance, lapis lazuli, was used for cups, bowls and urns, and was inlaid into clock faces and tables. An example of application of lapis lazuli it is visible in Italy with the popular flowers, bird and butterfly mosaics of Florence [Hinks, 1975]. More recently, at the beginning of 20th century, French jewellery and artist Peter Carl Fabergè (1846-1920 A.D.) used lapis lazuli in many of his major works. Among these was one of his 58 Imperial Easter Eggs, a gift from Czar Nicholas II of Russia to Czarina Alexandra in 1912 [Coenraads and Canut de Bon, 2000].

In Russia, lapis lazuli was used as a decorative stone, as at the Winter Palace in St. Petersburg and the Palace of Catherine the Great in the city Pushkin [Bauer, 1904].

In more recent times, during the 20th century, lapis lazuli were used also in North and South America primarily for local ornamental use. In South America, there have been several recent references to the use of lapis lazuli by the Moche (800-100 B.C.) and the Inca (1100-1537 A.D.) cultures, which occupied present day Peru, Ecuador, Bolivia, Northern Chile and north-western Argentina [Sofianides and Harlow, 1990] but the Columbian artefacts studied at the University of La Serena have been found to contain sodalite or other blue minerals, but not lapis lazuli [Canut de Bon, 1991]. However, evidences of ancient human activity near the lapis lazuli mining area suggest that the deposit could have been known to early inhabitants of the region, but further research is needed to determine if the Chilean deposit was worked in ancient time [Rivano, 1975; Rivano and Sepúlveda, 1991].

The quarries of lapis lazuli

Only few sources of Lapis Lazuli exist in the world due to the low probability of geological conditions in which it can form (Figure 1) [Voskoboinikova, 1938; Wyart et al, 1981], so that the possibility to associate the raw material to man-made objects is helpful to reconstruct trade routes. Historical sources were in very inaccessible places, such as Afghan and Pamir Mountains, and stones were transported for thousand of kilometres, in times for which the knowledge of trade routes is still largely incomplete. This is especially true for ancient contexts where there is an absence or scarceness of written evidences [Tosi, 1974]. Although the Badakhshan mines in Afghanistan (the most famous being Sar-e-Sang) are widely considered till now as the only sources of the Lapis Lazuli in ancient times [Herrmann, 1968; Sarianidi, 1971; Tosi, 1974; Bulgarelli and Tosi, 1977; Herrmann and Moorey, 1983], other sources have been considered: Tajikistan (Lyadzhuar Dara, Pamir Mountains), Pakistan (Chagai Hills), Siberia (Irkutsk, near Lake Baikal), Iran [Herrmann, 1968] and Egypt (Sinai) [Nibbi, 1981]. The last two possibilities are not geologically confirmed and their interpretations are still debated [Herrmann and Moorey, 1983; Von Rosen, 1988; Delmas and Casanova, 1990; Nicholson and Shaw, 2000], so that the provenance of ancient lapis lazuli is still an open question. Other sources [Le Strange, 1919] are: Mazanderan (but there are many doubts about it and it seem quite unlikely [Herrmann, 1968]), Dizmar in Azerbaijan and Kerman (there are doubts about the presence of metamorphic rocks and there are no evidences of lapis lazuli [Herrmann, 1968; Bowersox and Chamberlin, 1995]). Moreover there are references to other



Figure 1. Map of the geological occurrences of lapis lazuli in the world

sources [Von Rosen, 1988], in particular to northern China and Tibet, but neither in this case there are any geological confirmation.

Badakhshan, Afghanistan

Badakhshan, in north-eastern Afghanistan, has been considered for long time the only historical source for the ancient Near East and is now considered as one of the principal sources. It is located at 2400 km from Mesopotamia in an inhospitable country of bare mountain and deep ravine. There are today four known mines in the Kerano-Munjan valley located at Chimlak, Shaga-Darra-i-Robat-i-Paskaran, Stromby and Sar-e-Sang, at altitudes ranging from 2000 to 5500 m. Of the four, the latter is the only one worked today.

At Sar-e-Sang the materials required for the formation of lapis lazuli must have been deposited with the original limestone. The lapis lazuli occurs in a thick, rather ill-defined band varying considerably in the concentration of lazurite and the number of accessory minerals.

The specimens of lapis lazuli collected at Sar-e-Sang cover a wide range of colours from a deep violet-blue through the royal blue of the gem quality to a light blue, a turquoise and finally, a few pieces of brilliant green. The finest quality should be a pure royal blue without blemish: impurities often present include iron pyrites, calcite and dark smudges [Herrmann, 1968].

One of the first explorer of this region reported the method to extract the lapis lazuli [Wood, 1841]: for mining camelthorn and tamarisk twigs were used, collected from the valley below and carried up the steep path to the mine. When sufficient fuel had been collected, it was piled against the rock face and a fire was lit. When the rock was hot, cold water, which also had to be carried up the 350 m ascent, was thrown onto it. The rock cracked and split, enabling further work to be done with the primitive tools available (pick, hammer and chisel) to extract the lapis lazuli from its marble host rock.

Many other authors studied and cited this quarry from many point of view [Tosi and Piperno, 1973; Tosi, 1974; Bulgarelli and Tosi, 1977; Wyart et al, 1981; Majidzadeh 1982; Herrmann and Moorey, 1983; Yurgenson and Sukharev, 1985; Grew, 1988; Von Rosen, 1988; Delmas and Casanova, 1990; Moorey, 1994; Faryad, 1999; Faryad, 2002].

Pamir Mountains, Tajikistan

Another source that could have been exploited in ancient time is in Pamir Mountains, on the Liadjuar-Dara ("River of Lazurite") at an altitude of 5000 m. Legend had recorded a deposit of lapis lazuli high in the Pamir range and this source was authenticated in 1930 when it was located by a Russian expedition. They found the route extremely difficult and had to leave their horses at 3500 m, climbing the remaining 1500 m. The lapis lazuli occurred in a steep wall of

marble and gneiss, at the border of an immense glacier. In this white marble there are veins and lenses of lapis lazuli, some bright-blue, some delicately blue with beautiful passages into violet and green tints [Herrmann, 1968; Webster, 1975]. Pamir lapis lazuli results to have the same quality as those from Badakhshan [Goldstein, 1981; Delmas and Casanova, 1990]. Also other authors cite this quarry [Tosi, 1974; Hogarth and Griffin, 1978; Herrmann and Moorey, 1983; Von Rosen, 1988; Casanova, 1992; Moorey, 1994].

Chagai Hills, Pakistan

Some deposits are reported in the Chagai Hills which are located in Pakistan at the northwest boundary with Afghanistan, between the Quetta district and the Iranian border. However, their existence is not recognized in the literature, probably because they are not subject to geological studies similar to those undertaken in Afghanistan. These deposits are very near to Shahr-i Sokhta from where several objects and cutting remain have been discovered. Chagai Hills lapis lazuli are reported to have the same quality as those from Badakhshan [Delmas and Casanova, 1990]. Other authors cite this quarry [Berthoud et al, 1982; Jarrige, 1988; Tosi and Vidale, 1990; Casanova, 1992; Ballirano and Maras, 2006].

Lake Baikal, Siberia

The Baikal source of lapis lazuli is the most distant from Mesopotamia, lying some 4800 km away. It is situated in the valley of the River Sljudjanka at the southwest end of Lake Baikal. The Malaja Bystraja deposits are situated on the right slope of the valley of the River Lazur where its outlet runs into the River Malaja Bystraja a southern tributary of the River Irkut, which is about 22 km from the Sljudjanka deposits [Korzinskij, 1947]. There are different qualities of the stone attributed to this source: poor quality and "grainy" in texture [Herrmann, 1968], but also fine quality [Hogarth, 1970]. Other authors studied and cited this quarry [Tosi, 1974; Webster, 1975; Hogarth and Griffin, 1976; Ivanov, 1976; Ivanov et al, 1976; Herrmann and Moorey, 1983, Von Rosen, 1988; Delmas and Casanova, 1990; Moorey, 1994].

Chile, Coquimbo region

This quarry has been taken into account in this work because of its possible use during ancient time in the American continent. Even if the first reference to Chilean lapis lazuli in "recent times" dates back to the 19th century [Field, 1850], there are some hypothesis that suggest the use of Chilean lapis lazuli before the 19th century; this question has to be investigated in future researches [Coenraads and Canut de Bon, 2000].

The only known source of lapis lazuli in Chile lies in the Coquimbo Region, near Ovalle, in the Andes Mountains at an altitude of 3500 m. Although reference is sometimes made to

another Chilean deposit at Vicuña Mackenna Mountain near Antofagasta [Webster, 1975; Sofianides and Harlow, 1990] but this material has been identified as dumortierite [Canut de Bon, 1991]. Once considered a minor or unimportant locality, with the lapis lazuli described as "at best mediocre" [Wyart et al, 1981], the Chilean deposit has produced significant quantities of attractive material in recent years. Today, Chilean lapis lazuli is exported as raw material, or incorporated into jewelry, carvings and decorative building materials by local artisans [Coenraads and Canut de Bon, 2000]. Other authors studied this quarry [Bruggen 1921; Tosi, 1974; Hogarth and Griffin, 1976; Cuitiño, 1986; Moorey, 1994; Corona Esquivel and Benavides Muñoz, 2005].

Other quarries

There are also other quarries mentioned but not very used because they produce some poor quality lapis or find out in lands far from Ancient East or exploited only in recent periods. Here is just a list of the places and some of the authors that cited them:

- Russia (Ural Mountains) [Zöldföldi and Kasztovszky, 2003];
- Myanmar or Burma (Mogok region) [Webster, 1975; Hogarth and Griffin, 1976; Von Rosen, 1988; Moorey, 1994];
- Italy (Latium) [Hogarth and Griffin, 1975; Hogarth and Griffin, 1976; Von Rosen, 1988];
- Angola (Dattawa Valley) [Webster, 1975; Von Rosen, 1988];
- North Africa (Atlas Mountains) [Kulke, 1976; Von Rosen, 1988];
- California (Cascade Canyon) [Rogers, 1938; Webster, 1975; Hogarth and Griffin, 1976; Moorey, 1994];
- Colorado/Wyoming/Utah (Italian Mountain and Green River) [Bradley, 1964; Webster, 1975; Hogarth and Griffin, 1976; Hogarth and Griffin, 1980; Von Rosen, 1988; Moorey, 1994];
- N.Y. State (Edwards) [Jensen, 1976];
- Canada (Baffin Island) [Webster, 1975; Kulke, 1976; Hogarth and Griffin, 1976; Hogarth and Griffin, 1978; Von Rosen, 1988];
- Cuba [Tosi, 1974];
- Brazil [Tosi, 1974].

PETROGRAPHY OF LAPIS LAZULI

Lapis lazuli is a metamorphic rock characterized by the presence of the mineral lazurite, combined with other types of minerals whose presence and relative amount varies from and within deposits. The typical blue colour of the rock is due to the mineral lazurite, that seldom presents well-formed crystals, since usually is an aggregate of quite small crystals. Lazurite is traversed by gray-white or yellowish veins, due to the presence of various accessory minerals such as calcite, wollastonite, phlogopite, plagioclase, diopside and others. There may be also other feldspathoids of the same lazurite family such as haüyne, sodalite or nosean. Furthermore, lapis lazuli of all deposits contain small inclusions of pyrite, mistaken in the past for golden inclusions.

The first attempts to classify the lapis lazuli from a mineralogical point of view have been done in the 18th century [Sage, 1777; Buffon, 1787] but there were still a lot of confusion between the rock lapis lazuli and the mineral lazurite, often mistaken. Only at the end of the 19th century there were the first scientific characterization [Brögger and Bäckström, 1891], with the analysis of the lazurite separated by all the other minerals.

Also the metamorphic conditions of the formation of lapis lazuli have been investigated in a lot of works, usually together with the mineralogical characterization of the rock; most of them are focused mainly on the deposit sited in Afghanistan [Blaise and Cesbron, 1966; Schreyer and Abraham, 1976; Wyart et al, 1981; Yurgenson and Sukharev, 1985; Grew, 1988; Faryad, 1999; Faryad, 2002], in Siberia [Ivanov, 1976; Ivanov et al, 1976], in Chile [Cuitiño, 1986; Corona Esquivel and Benavides Muñoz, 2005], in Canada [Hogarth and Griffin, 1978] and in Colorado [Hogarth and Griffin, 1980], but more recent works try to compare the genesis of different deposits [Aleksandrov and Senin, 2006; Dill, 2010].

Due to the heterogeneity of lapis lazuli is convenient to analyse the single phases to find some marker useful for a provenance study. For this reason this work is mainly focused on two mineral phases, i.e. the main phase lazurite and the accessory phase diopside that is present in all the samples of the three Asian provenances under investigation.

Lazurite

Lazurite is a tectosilicate belonging to the feldspathoids family; more specifically, it belongs to the sodalite group. This group consists of eight minerals, among which the main ones are: sodalite ($\text{Na}_8\text{Al}_6\text{Si}_6\text{O}_{24}\text{Cl}_2$), nosean ($\text{Na}_8\text{Al}_6\text{Si}_6\text{O}_{24}(\text{SO}_4)$), haüyne ($(\text{Na,Ca})_{4-8}\text{Al}_6\text{Si}_6(\text{O,S})_{24}$)

(SO₄,Cl)₁₋₂) and lazurite (Na₆Ca₂Al₆Si₆O₂₄[(SO₄),S,Cl,(OH)]₂) [Anthony et al, 2001], even if there is a tendency to consider the lazurite as a variety of haüyne rich in sulphur [Rogers, 1938; Van Peteghem and Burley, 1963] rather than a distinct mineral; however it is better to keep its name for convenience [Cipriani et al, 1988]. The first description of the structure of the sodalite is dated back to 1930 [Pauling, 1930]; after that date there were many other works with a wide description of the first three minerals of the group [Deer et al, 1978; Taylor, 1967] and others centred on the lazurite [Bradley, 1964; Hogarth and Griffin, 1976; Hassan et al, 1985], reporting the fundamental data about this mineral, its structure, its chemical composition and its physical properties.

The diffuse general chemical formula of lazurite is (Na,Ca)₈Al₆Si₆O₂₄(SO₄,S,Cl)₂ [Strunz 1970]; the central part of the formula is the aluminosilicate framework (Al₆Si₆O₂₄)⁶⁻, the same of the whole group. It is well defined with a 1:1 ratio of AlO₄ and SiO₄ tetrahedra and consists of alternating AlO₄ and SiO₄ tetrahedra which are cornered-linked to give cubo-octahedral cavities called sodalite cages. The cages can accommodate a variety of cations and anions by adapting to different sizes due to the cooperative rotations of the framework tetrahedra. The diversity of interframework ions is limited by spatial requirements and by the requirements of electrical neutrality of the negatively charged framework oxygens [Hassan et al, 1985].

The blue colour of the lazurite and its intensity can be explained by an anion-anion charge transfer [Nassau, 1983]: the S₃⁻ ion, the chromophore inside the sodalite cage, is composed by three atoms with the configuration 3 s² p⁴, so that the S₃⁻ ion has a total number of 19 outer electrons in molecular orbitals. A transition among these orbitals produces a strong absorption band at 590 nm in the yellow, leading the blue colour with purple overtones [Schwarz and Hofmann, 1970].

A summary of the main features of lazurite is reported in Table 2 [Anthony et al, 2001].

Diopside

Diopside is a mineral belonging to the pyroxene family; in particular it is an inosilicate with a single calcium and magnesium chain, whose chemical formula is CaMgSi₂O₆. Historically, the first pyroxene structures determined was right that of diopside [Warren and Bragg, 1928] and after that work a lot of information about this mineral have been collected, with a good description of all its characteristics [Deer et al, 1978].

Diopside forms a solid solution with hedembergite (CaFeSi₂O₆) and the mineral with the intermediate composition is called salite. A common practice to evaluate the composition of a pyroxene from the chemical analysis of the mineral consists in calculating the end members (pure terms) percentage and to report the results on a triangular diagram [Morimoto, 1988]

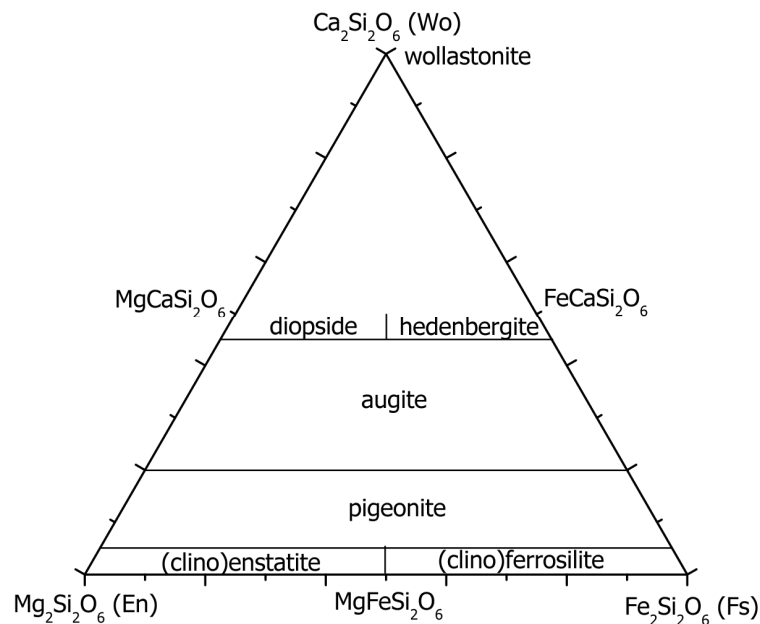


Figure 2. Composition ranges of the Ca-Mg-Fe Clinopyroxenes [Morimoto, 1988]

shown in Figure 2. In the corners there are the pure terms (100% composition of the indicated mineral), while inside the triangle the names of the intermediate composition minerals are reported.

About the paragenesis of diopside, it is a common constituent of igneous basic rocks, especially alkaline, and ultra-basic rocks; the terms more rich in iron are present in various metamorphic rocks, in particular contact-metamorphic ones rich in calcium, but can also be formed in conditions of pressure and temperature typical of regional metamorphism.

Despite it is a complete solid solution, many minerals belonging to this series contain other ions; aluminium can substitute silicon and the content of Al_2O_3 can vary between 1 and 3%. Diopside can also contain titanium (a mean of 0.54% of TiO_2), manganese (a mean of 0.13% of MnO) and chromium (up to 1% of Cr_2O_3); besides, depending on the provenance, it could contain also other elements, among which there are: vanadium, potassium, rubidium, strontium and barium [Deer et al, 1978]. Other characteristic of diopside are reported in Table 2.

Other mineralogical phases

Besides lazurite and diopside, many other mineralogical phases can be found in lapis lazuli, as shown in Table 1. The main ones are: sodalite, haüyne, pyrite, calcite, phlogopite, feldspars, scapolite, forsterite, nepheline, afghanite, and wollastonite. Their principal features are presented in Table 2.

Table 1. Mineralogical phases present in lapis lazuli samples coming from the same provenances analysed in this work.

(•): principal minerals (more than 0.3%);

(x): minor minerals (less than 0.3%);

(◦): secondary minerals.

Minerals associated to lazurite-bearing rocks are indicated with (*).

Minerals	Year / Authors		Afghanistan					Siberia					Chile		Pamir		
	1981	1985	1986	2001	2003	2004	2006	1970	1976	1986	2003	2006	1986	1986	2005	2006	
Quarries / Provenances		Badakhshan (Sar-e-sang)	Badakhshan	-	Badakhshan (Sar-e-Sang)	Badakhshan	Badakhshan	Badakhshan (Sar-e-Sang)	Malaya Bystraya (Staryi)	Malo Bystrinsk, Slyudyansk, Tultuysk	-	Lake Baikal	Baikal area	Flor de Los Andes	-	Flor de Los Andes	Lyadzhvardara
Lazurite	•	•	•	•	•	•	•	•	•	•	•	•	•	•	•	•	*
Diopside	•	•	•	•	•	•	•	•	•	•	•	•	•	•	•	*	*
Pyrite	•	•	x	•	•	•	•	•	•	•	•	•	•	•	•	•	•
Calcite	•	•	•	•	•	•	*	•	•	x	•	*	•	•	•	•	*
Phlogopite		•	x		•	•		•	•	•	•	•	•		*	*	
Scapolite	•	•			•	•		•	•		•	*	•		*		
Feldspars	•		•		•	•	*	•		•	•		•				*
Forsterite	•	•		•	•	•		•				•	•				*
Häüyne		•		•			•	•					•			•	
Nepheline		•			•		•				•	•					
Afghanite		•			•		•		•			*	x				*
Wollastonite									•				•	•	•	•	
Sodalite		•	•			•	*			•			•				
Pyrrhotite		•					•	•								*	
Apatite					•			•			•	*					
Tremolite		•				•	*						•				
Epidote					•						•		•				
Garnet					•						•						
Quartz						•	*	•									
Dolomite					•						•	*					*
Biotite					•						•						*
Native Sulphur								•				•					
Titanite					•						•						
Olivine					•						•						
Ilmenite					•						•						
Feldspathoids												•			•		
Amphibole						•	*										*
Chalcopyrite													•		*		
Muscovite				•													
Cancrinite												•					
Graphite						•											
Siderite													•				
Humite				•													
Spinel												•					

Table 2. Main features of the principal phases of lapis lazuli [Anthony et al, 2001]

Mineral	Lazurite	Sodalite	Häüyne	Diopside	Pyrite	
Formula	$\text{Na}_6\text{Ca}_2\text{Al}_6\text{Si}_6\text{O}_{24}[(\text{SO}_4)_2\text{S};\text{Cl};(\text{OH})]_2$	$\text{Na}_8\text{Al}_6\text{Si}_6\text{O}_{24}\text{Cl}_2$	$(\text{Na,Ca})_{4+8}\text{Al}_6\text{Si}_6(\text{O,S})_{24}(\text{SO}_4,\text{Cl})_{1+2}$	$\text{CaMgSi}_2\text{O}_6$	FeS_2	
Mineral Group	Sodalite group	Sodalite group	Sodalite group	Pyroxene group	Pyrite group	
Main occurrences	A contact metamorphic mineral in limestones	Formed in nepheline syenites, phonolites, and related rock types. In metasomatized calcareous rocks, and in cavities in ejected volcanic blocks.	In phonolites and related leucite- or nepheline-rich igneous rocks; less commonly in nepheline-free extrusives	Typical of metamorphosed siliceous Ca, Mg-rich rocks	Formed under a wide variety of conditions, also in metamorphic rocks	
Name	From the Persian "lazzward", for blue	In allusion to its sodium content	To honor Abbé René Just Häüy (1743-1822), French crystallographer and mineralogist	From the Latin "di" and the Greek "opsis", for double appearance	From the Greek for fire, as sparks may be struck from it	
Crystal Data	Cubic; also monoclinic or triclinic	Cubic	Cubic	Monoclinic	Cubic	
Physical Properties	Fracture	Uneven	Uneven to conchoidal	Uneven to conchoidal	Uneven to conchoidal	Conchoidal to uneven
	Tenacity	Brittle	Brittle	Brittle	Brittle	Brittle
	Hardness	5÷5.5	5.5÷6.0	5.5÷6.0	5.5÷6.5	6.0÷6.5
	Density measured (g/cm^3)	2.38÷2.45	2.27÷2.33	2.44÷2.50	3.22÷3.38	5.018
	Density calculated (g/cm^3)	2.39÷2.42	2.31	n.d.	3.278	5.013
Optical Properties	Color	Translucent to opaque	Transparent to translucent	Transparent to translucent	Transparent to opaque	Opaque
		Deep blue, azure, violet blue, greenish blue	Colorless, white, yellowish, greenish, light to dark blue, reddish	Bright blue to greenish blue; white or shades of black, gray, brown, green, yellow, red, may be patchy	Colorless, white, yellow, pale to dark green, black	Pale brass-yellow, tarnishes darker and iridescent
		blue in thin section	colorless to gray in thin section	colorless or pale blue in thin section	colorless in thin section	creamy white in polished section
	Streak	Bright blue	White	Slightly bluish to colorless	White, gray, gray-green	Greenish black to brownish black
	Luster	Vitreous	Vitreous to greasy	Vitreous to greasy	Vitreous or dull	Metallic, splendent
	Optical Class	Isotropic; anomalously anisotropic	Isotropic	Isotropic; weakly birefringent when included	Biaxial (+)	Rarely anisotropic
	Refr. index (n)	1.502÷1.522	1.483÷1.487	1.494÷1.509		
Chemistry	sample provenance	Sar-e-Sang, Afghanistan	Mont Saint-Hilaire, Canada	Monte Vulture, Italy	Dutoitspan mine, South Africa	Elba, Italy
	composition (%w)	SiO ₂ : 31.34 Al ₂ O ₃ : 26.27 Fe ₂ O ₃ : 0.27 CaO: 7.97 MgO: 2.47 Na ₂ O: 15.75 K ₂ O: 1.02 Cl: 0.78 H ₂ O: 3.87 SO ₃ : 8.71 S: 1.84 -O=S, Cl ₂ : 0.67 total: 99.62	SiO ₂ : 37.95 Al ₂ O ₃ : 31.42 FeO: 0.39 MnO: 0.08 Na ₂ O: 24.16 K ₂ O: 0.05 Cl: 7.33 SO ₃ : 0.09 -O=Cl ₂ : 1.65 total: 99.82	SiO ₂ : 34.04 Al ₂ O ₃ : 28.27 FeO: 0.69 MgO: 0.48 CaO: 9.51 Na ₂ O: 10.39 K ₂ O: 5.44 Cl: 0.76 H ₂ O: 0.34 CO ₂ : 0.4 SO ₃ : 10.02 -O=Cl ₂ : 0.17 total: 100.17	SiO ₂ : 54.09 TiO ₂ : 0.28 Al ₂ O ₃ : 1.57 Fe ₂ O ₃ : 0.74 Cr ₂ O ₃ : 2.03 FeO: 1.47 MnO: 0.09 MgO: 16.96 CaO: 21.10 Na ₂ O: 1.37 K ₂ O: 0.15 H ₂ O ⁺ : 0.22 H ₂ O ⁰ : 0.08 rem: 0.49 total: 100.64	Fe: 46.49 S: 53.49 SiO ₂ : 0.04 total: 100.02

Table 2 (continue). Main features of the principal phases of lapis lazuli [Anthony et al, 2001]

Mineral	Calcite	Phlogopite	Orthoclase	Anorthite	Albite	
Formula	CaCO ₃	KMg ₃ Si ₃ AlO ₁₀ (F,OH) ₂	KAlSi ₃ O ₈	Na _{0.1+0.0} Ca _{0.9+1.0} Al _{1.9+2.0} Si _{2.1+2.0} O ₈	Na _{1.0+0.9} Ca _{0.0+0.1} Al _{1.0+1.1} Si _{3.0+2.9} O ₈	
Mineral Group	Calcite group	Mica group	Feldspar (alkali) group	Feldspar group, plagioclase series	Feldspar group, plagioclase series	
Main occurrences	A major rock-forming mineral; in limestones, marbles, chalks, in clastic sedimentary rocks, in hydrothermal veins; in alkalic to mafic igneous rocks; common as speleothems in caves	In metamorphosed dolostones and magnesium-rich limestones; in ultramafic rocks as kimberlites, peridotites, lamproites, and serpentinites	The common feldspar of granites, granite pegmatites, and syenites. In cavities in basalts; in high-grade metamorphic rocks and as a result of potassic hydrothermal alteration; also authigenic and detrital.	A rare constituent of mafic plutonic and volcanic rocks. In some granulite facies metamorphic rocks; in metamorphosed carbonate rocks; with corundum deposits. Known from meteorites.	A major constituent of granites and granite pegmatites, alkalic diorites, basalts, and in hydrothermal and alpine veins. A product of potassium metasomatism and in low-temperature and low-pressure metamorphic facies and in some schists.	
Name	From the Latin "calx", for burnt lime, an allusion to an important commercial use	From the Greek for firelike, referring to an oft-seen reddish tint	From the Greek for straight and fracture, in allusion to the cleavage angle	From the Greek for oblique, for its triclinicity	From the Latin, "albus", for white, its characteristic color	
Crystal Data	Hexagonal	Monoclinic	Monoclinic	Triclinic	Triclinic	
Physical Properties	Fracture	Conchoidal		Conchoidal to uneven	Uneven to conchoidal	
	Tenacity	Brittle	Thin laminae flexible and elastic, tough	Brittle	Brittle	
	Hardness	3.0	2.0÷3.0	6.0÷6.5	6.0÷6.5	6.0÷6.5
	Density measured (g/cm ³) calculated (g/cm ³)	2.7102(2) 2.711	2.78÷2.85 2.79	2.55÷2.63 2.563	2.74÷2.76 2.76	2.60÷2.65 2.609÷2.621
Optical Properties	Color	Transparent to opaque	Transparent to translucent	Transparent to translucent	Transparent to translucent	
		Colorless or white, also gray, yellow, green, many other colors from included minerals	Brownish red, dark brown, yellowish brown, green, white	Colorless, white, gray, pale yellow, flesh-red, green	White, grayish, reddish	White to gray, bluish, greenish, reddish; may be chatoyant
		colorless in transmitted light	colorless, pale yellow, or green in thin section	colorless in thin section	colorless in thin section	
	Streak	White	White	White	White	White
	Luster	Vitreous; pearly on cleavages and {0001}	Pearly to submetallic on cleavage	Vitreous, pearly on cleavages	Vitreous	Vitreous, typically pearly on cleavages
	Optical Class	Uniaxial (-); anomalously biaxial	Biaxial (-)	Biaxial (-)	Biaxial (-)	Biaxial (+) (low); (-) (high)
	Refr. index (n)					
Chemistry	sample provenance	California, USA	New Jersey, USA	California, USA	Northumberland, England	Alp Rischuna, Switzerland
	composition (%w)	CO ₂ : 44.22* FeO: 0.43 MgO: 1.74 CaO: 53.60 total: 99.99 * calculated from stoichiometry	SiO ₂ : 42.0 TiO ₂ : 0.22 Al ₂ O ₃ : 12.7 FeO: 0.25 MnO: 0.08 NiO: 0.02 ZnO: 0.01 MgO: 28.6 CaO: 0.04 BaO: 1.70 Li ₂ O: 0.02 Na ₂ O: 1.19 K ₂ O: 8.46 Rb ₂ O: 0.01 F: 5.85 H ₂ O ⁺ : 1.51 -O=F ₂ : [2.46] total: [100.19]	SiO ₂ : 64.76 Al ₂ O ₃ : 18.45 BaO: 0.02 Na ₂ O: 1.08 K ₂ O: 14.76 Rb ₂ O: 0.49 total: 100.19	SiO ₂ : 45.88 TiO ₂ : 0.04 Al ₂ O ₃ : 34.31 Fe ₂ O ₃ : 0.83 CaO: 18.28 Na ₂ O: 0.82 K ₂ O: 0.11 H ₂ O ⁺ : 0.14 total: 100.41	SiO ₂ : 68.71 Al ₂ O ₃ : 19.63 CaO: 0.22 Na ₂ O: 11.72 K ₂ O: 0.03 total: 100.31

Table 2 (continue). Main features of the principal phases of lapis lazuli [Anthony et al, 2001]

Mineral	Scapolite*	Forsterite	Nepheline	Afghanite	Wollastonite	
Formula	(Na,Ca) ₄ [Al ₃ Si ₉ O ₂₄]Cl	Mg ₂ SiO ₄	(Na,K)AlSiO ₄	(Na,Ca,K) ₈ (Si,Al) ₁₂ O ₂₄ (SO ₄ ,Cl,CO ₃) ₃ ·H ₂ O	CaSiO ₃	
Mineral Group		Olivine group		Cancrinite group	Wollastonite group	
Main occurrences		In mafic and ultramafic igneous rocks and thermally metamorphosed impure dolomitic limestones	Characteristic of alkalic rocks as nepheline syenites and gneisses, alkalic gabbros; in sodium-rich hypabyssal rocks, tuffs and lavas, and pegmatites; as a product of sodium metasomatism	In thin veinlets cutting lazurite crystals (Sar-e-Sang, Afghanistan); in silicified limestone xenoliths in pumice (Pitigliano quarry, Italy)	Common in thermally metamorphosed siliceous carbonates, the intruding igneous rock, and skarn deposits along their contact; also in some alkalic igneous rocks and carbonatites	
Name	Named in 1800 from the Greek skapos - "rod" and lithos - "stone".	After Adolarius Jacob Forster (1739-1806), English mineral collector and dealer	From the Greek for cloud, as it becomes cloudy when treated with strong acid	For the country of first occurrence, Afghanistan	For William Hyde Wollaston (1766-1828), English chemist and mineralogist	
Crystal Data	Tetragonal - Dipyramidal	Orthorhombic	Hexagonal	Hexagonal	Monoclinic or triclinic	
Physical Properties	Fracture	Splintery - Thin,	Conchoidal	Subconchoidal	Conchoidal	Uneven
	Tenacity		Brittle	Brittle		Brittle
	Hardness	5.5 ÷ 6.0	7	5.5 ÷ 6.0	5.5 ÷ 6.0	4.5 ÷ 5.0
	Density measured (g/cm ³) calculated (g/cm ³)	2.56 ÷ 2.77	3.275	2.55 ÷ 2.66	2.55	2.86 ÷ 3.09
Optical Properties	Color		Transparent to translucent	Transparent to nearly opaque	Transparent	Transparent to translucent
		White, Gray, Pale brown, Pink, Yellow	Green, yellowish, lemon-yellow, white, grayish, blue-gray	Colorless, white, gray, yellowish; variously colored by impurities	Blue	White, colorless, brown, red, yellow, pale green
		colorless in thin section	colorless in thin section	colorless in thin section	colorless in thin section	colorless in thin section
	Streak	White	White			White
	Luster	Vitreous (Glassy)	Vitreous	Vitreous to greasy	Vitreous	Vitreous, pearly on cleavage
	Optical Class	Uniaxial (-)	Biaxial (+)	Uniaxial (-)	Uniaxial (+)	Biaxial (-)
	Refr. index (n)	1.55 ÷ 1.59				
Chemistry	sample provenance	Otter Lake, Canada	Mogok district, Myanmar	Monte Somma, Italy	Sar-e-Sang, Afghanistan	Remonmaki, Finland
	composition (%w)	SiO ₂ : 47.95 Al ₂ O ₃ : 29.06 CaO: 12.79 Na ₂ O: 7.07 Cl: 4.04 -O=Cl ₂ : -0.91 total: 100	SiO ₂ : 41.72 FeO: 1.11 MgO: 57.83 total: 100.66	SiO ₂ : 43.55 Al ₂ O ₃ : 34.66 MgO: 0.05 CaO: 4.44 Na ₂ O: 12.09 K ₂ O: 4.87 H ₂ O ⁺ : 0.25 H ₂ O ⁻ : 0.25 total: 100.16	SiO ₂ : 30.8 Al ₂ O ₃ : 25.0 CaO: 16.5 Na ₂ O: 12.6 K ₂ O: 2.7 Cl: 4.6 H ₂ O: 0.7 CO ₂ : 0.4 SO ₃ : 8.5 -O=Cl ₂ : 1.0 total: 100.8	SiO ₂ : 50.82 FeO: 0.18 MnO: 0.03 MgO: 0.22 CaO: 48.16 Na ₂ O: 0.12 K ₂ O: 0.07 H ₂ O ⁺ : 0.08 total: 99.68
	* Data taken from: • webmineral.com • mindat.org					

THE SAMPLES

All the lapis lazuli analysed in this work are part of the collections of the "Museo di Storia Naturale" of the University of Firenze. This museum conserves about fifty pieces of lapis lazuli: half of them are blocks of rock, rough or partially polished, but the other half consists of carved objects of exquisite workmanship and fragments or whole tessera for inlays. Some of them have already been studied in the 1980's [Borelli et al, 1986; Cipriani et al, 1988].

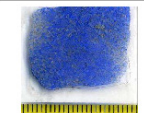
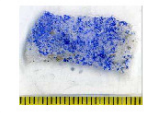
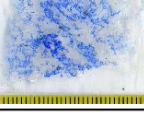
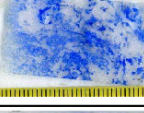
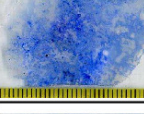
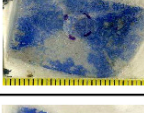
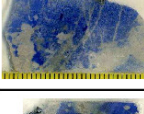
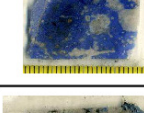
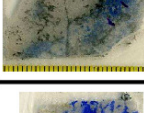
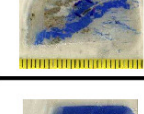
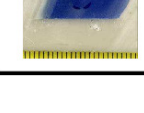
Rocks

The lapis lazuli stones of the section "Mineralogy and Lithology" of the museum are fragments, thin slices or pieces of different sizes, some rough and other polished or partially polished. In Table 3 the catalogue number, a brief description of the starting material, the acquisition conditions and the provenances of the different samples are reported. As already pointed out by other authors [Ballirano and Maras, 2006; Cipriani et al, 1988], there is a lack of precise geographical information for some specimens. In our case, for most of the samples studied only the provenance area is specified, but the exact mines are not known: 3 samples come from Badakhshan in Afghanistan (probably Sar-e-Sang mine), 4 samples from Chile (only 2 samples are catalogued as Chilean, but probably are all from Ovalle), 1 sample from Irkutsk in Siberia, and 4 samples from Pamir mountains in Tajikistan (Lyadzhuar Dara lazurite deposit at 4800 m above sea level and 76 km south of Khorugh in Gorno-Badakhshan). One more sample, *RI 571*, was catalogued as "South America", but was later attributed to the Siberian provenance [Cipriani et al, 1988]: for this reason we will consider this sample as an "unknown provenance" sample and we'll use it to test if our method is able to attribute a provenance to a doubt sample or not.

Sample preparation

Samples were prepared as semi-thin sections and mounted on special slides with a 3 mm diameter hole in the centre (Table 3). The holes were made to avoid any interference from the sample-holder during ion beam analysis, being the penetration depth of the proton probe up to about 60÷80 µm, depending on the mineral (SRIM calculation). The choice to have thicker sections (from 60 to 100 µm) compared to classical thin sections (about 30 µm) is necessary because of the hole, that makes samples more fragile. Obviously this fact, essential for our purpose, makes impossible an accurate petrographical analysis by means of transmitted

Table 3. Catalogue number, description, acquisition, and provenance of the analysed samples; the last column is from a previous work on these samples [Cipriani et al, 1988].

	Catalogue number	Description	Acquisition	Provenance (catalogue)	Attribution [Cipriani et al, 1988]
	RI 388	Cut and partially polished fragment	Bought in Munich, 1985.	Badakshan (Afghanistan)	Badakshan (Afghanistan)
	12397	Polished thin slice	Ciampi collection n.3780.	Badakshan (Afghanistan)	Badakshan (Afghanistan)
	47860	Big piece, partially polished	Afghan Gems (Germany) Mineralientage, 1999.	Badakshan (Afghanistan)	----
	RI 3063	Rough small piece	Bought from C. Djankoff Global Mining LLC 2007	Ladjvardara (Tajikistan)	----
	RI 3064	Rough medium piece	Bought from C. Djankoff Global Mining LLC 2007	Ladjvardara (Tajikistan)	----
	RI 3065	Rough small piece	Bought from C. Djankoff Global Mining LLC 2007	Ladjvardara (Tajikistan)	----
	RI 3066	Rough big piece	Bought from C. Djankoff Global Mining LLC 2007	Ladjvardara (Tajikistan)	----
	12394	Rough small piece	Magistero collection	America	Ovalle (Chile)
	12403	Rough small piece	Capacci donation	Chile	Ovalle (Chile)
	12405	Partially polished piece	Bought from Brogi, Siena	----	Ovalle (Chile)
	16980	Big piece, partially polished	Le Pietre, 1980	Chile	Ovalle (Chile)
	RI 390	Cut and partially polished fragment	Mineralientage, Munich, 1985	Irkutsk (Siberia)	Irkutsk (Siberia)
	RI 571	Small piece, partially polished	from Archives, n.188	South America	Irkutsk (Siberia)

light, but it is important to remember that this kind of measurements has to be excluded when analysing art-works and so it is not among the main techniques of this work.

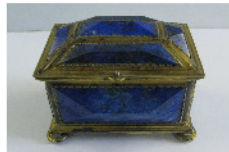
It is worth stressing that this procedure for samples preparation was useful only in the first characterization stage, to permit the use of SEM-EDX and SEM-CL, simplifying and speeding up the measurements on rocks. The same semi-thin sections has been characterised also by means of IBA techniques, but just for convenience; it will not be necessary to perform this sample preparation when works of art are analysed by means of IBA techniques.

Artworks of the "Collezione Medicea di pietre lavorate"

This collection has a great historical value: in fact almost all the objects are described in the catalogues since the end of the 18th century. It is composed by precious stones, both polished and carved: part of them are present in the inventories of the 16th century and part of them have been manufactured in the ancient glyptic school in the gardens of "S. Marco" in the middle of the 16th century.

In this work we analysed four of these precious objects made in lapis lazuli, whose main characteristic are reported in Table 4. The largest and more precious of them is an oval bowl (catalogue number: 13682) with the outline of a small palm and a big leaf. On the rear there are two carvings: the Grand-Ducal crown and the initials "FM 1600". It was manufactured in the

Table 4. Catalogue number, description, provenance and dimensions of the analysed samples of the "Collezione Medicea" of "Museo di Storia Naturale" in Firenze. The column "Attribution" is referred to a previous work [Cipriani et al, 1988]

	Catalogue number	Description	Provenance (catalogue)	Attribution [Cipriani et al, 1988]	Dimensions (cm)
	13682	Oval bowl in lapis lazuli signed "F.M. 1600"	Levante	---	22 × 11 × 5
	13684	Small case in lapis lazuli mounted in golden metal	Persia	Afghanistan or Siberia	7 × 4.5 × 3.5
	13687	Saltcellar in lapis lazuli	Persia	Afghanistan or Siberia	5.8 × 4.6 × 4
	13688	Oval panel in lapis lazuli	Siberia	Siberia	9 × 5 × 1

workshops "Galleria dei Lavori" during the reign of Ferdinando I de' Medici and it results in the list of objects delivered to the Gran Duke's Private Secretariat in 1782.

The second object is a "Small case", rectangular, with carved faces (catalogue number: 13684); its borders, base and feet are made in golden metal. The inside is subdivided in six spaces and from the description results that it was used as a container for teeth. It has been realized in the end of the 16th century or at the beginning of 17th century in the Gran Duke's workshops "Galleria dei Lavori" and it arrived at the "Imperial Regio Museo di Fisica e Storia Naturale" in 1787.

On the other two objects there are less historical information: both the "Saltcellar" (catalogue number: 13687) and the "Oval panel" (catalogue number: 13688) have been manufactured in the workshops "Galleria dei Lavori". The period of realization of these objects is the end of the 16th century or the beginning of 17th century for the "Saltcellar", while for the "Oval panel" it is probably the same, but the only certainty is that it comes from the Grand-Ducal collections.

ANALYTICAL TECHNIQUES

Many techniques can be used to study rocks and gems and each one can give different information. In Table 5 a list of the techniques already used by various authors to study lapis lazuli is reported, together with the acronym used to identify them and the probe used. Most of these have been used both to recognize lapis lazuli from other stones [Da Cunha, 1989], and for provenance studies, as will be explained in next chapter. It is worth noting that the results that can be obtained with each technique mainly depend on the possibility to destroy the sample or to take a sample from the object to analyse. Since art objects produced using lapis lazuli are valuable, only non-destructive investigations can be carried out to identify the provenance of the raw materials used for their realization. Many techniques are good candidates for this purpose and in this work we adopted a multi-technique approach: Ion Beam Analyses (IBA) have been chosen because of their absolute non-destructivity and because they can give a lot of information about a sample at the same time. In particular we can analyse a single crystal of interest thanks to the dimension of the beam (some microns) and obtain both the elemental composition up to trace elements using Particle Induced X-ray Emission (PIXE)

Table 5. Some of the analytical techniques used for the study of lapis lazuli in many works from other authors (see next chapter); in bold type the techniques used in this work

<i>Probe</i>	<i>Techniques</i>	
light	OM	Optical Microscopy
	OS	Optical Spectroscopy
	RS	Raman Spectroscopy
	PL	Photo-Luminescence
X-ray	FTIR	Fourier Transform Infrared Spectroscopy
	XRF	X-Ray Fluorescence
electrons	XRD	X-Ray Diffraction
	SEM-EPMA	Scanning Electron Microscopy - Electron Probe Micro-Analysis
	SEM-EDX	Scanning Electron Microscopy - Energy Dispersive X-Ray Spectrometry
	SEM-WDS	Scanning Electron Microscopy - Wavelength Dispersive Spectrometry
	TEM	Transmission Electron Microscopy
ions	CL	Cathodo-Luminescence
	PIXE	Particle Induced X-Ray Emission
	IL	Iono-Luminescence
neutron	AMS	Atomic Mass Spectroscopy
	NAA	Neutron Activation Analysis
plasma	PGAA	Prompt Gamma Activation Analysis
	AAS	Atomic Absorption Spectroscopy
magnetic field	NMR	Nuclear Magnetic Resonance

and the luminescence spectrum of it using Ionoluminescence (IL). In this work these techniques were preceded and completed by systematic measurements using both electron-beam analyses (SEM-EDX, SEM-CL, cold-Cathodoluminescence) and optical ones (Optical Microscopy, Raman Spectroscopy). The firsts are vacuum-operating techniques and normally are not suitable to art objects, but proved to be useful in the first stage of the work, in which rocks have been characterised. This characterisation was propaedeutic to IL/PIXE measurements, carried out on significant areas selected on the basis of results obtained by means of electron probe techniques. Such articulated use of complementary techniques is motivated by the less time required in measurements with respect to IBA techniques and by the fact that it is very difficult to have a sure identification of a mineral phase using IBA only.

In the following paragraphs there are some general information about the analytical techniques used in this work.

Ion Beam Analysis

In this paragraph I'll introduce Ion Beam Analysis, mainly focusing on the main features of the IBA techniques I used, that are PIXE and IL. Obviously it will not be an exhaustive description, but IBA characteristic and potential are fully explained elsewhere [Breese et al, 1996].

IBA consists in the collection of different signals (visible photons, X-rays, gamma-rays and charged particles) induced by MeV ion (usually protons) irradiation. When a light MeV ion beam is aimed at a sample, every ion/projectile penetrates the matter losing energy continuously at a well-known rate. Along its trajectory there is a chance for collision with nuclei and electrons. The products of these interactions are emitted from the sample with probabilities determined by the respective interaction cross-sections and their energy is measured and collected as spectra carrying information on the sample chemical composition, structure, electrical and chemical properties [Bettioli, 1999].

In principle, most of these information can be obtained with electrons or X-rays probes, but often where those ones are limited, IBA techniques are not. The different interactions of light MeV ions with matter with respect to the other kind of probes make the nuclear microprobe technique a complementary method to investigate materials. Moreover, more than one IBA technique can be used simultaneously, improving materials characterization with respect to other single techniques, thanks to the possibility to gather several different complementary information. Let's consider for example the comparison between an ion probe and an electron probe: Figure 3 helps understanding which are the main differences: these simulations show a visible smaller lateral and longitudinal straggling of ions with respect to

electrons and a deeper penetration. Moreover, modulating the energy of the ion beam, different depths of a sample can be analyzed.

Another advantage, that also explain why IBA have been widely used in cultural heritage investigations, is the possibility to work in air on large objects without any pre-treatment. Moreover, IBA techniques exploiting proton beams, can be used in most

materials without damaging. Particle-Induced Gamma ray Emission (PIGE), Backscattering Spectrometry (BS) and especially PIXE can be considered as the chief techniques, but also IL has been successfully employed in this field [Calvo del Castillo et al, 2007; Quaranta et al, 2007; Mathis et al, 2010]. The availability of scanning micro-beam allows the investigation of details down to the micrometer scale which can be very useful in many cases [Dran et al, 2004] and in our case is generally sufficient to distinguish mineral phases inside the samples.

PIXE: Particle Induced X-ray Emission

PIXE is the most commonly used nuclear microprobe technique since 1970, when the Lund (Sweden) group introduced it as a new powerful analytical method for trace element analysis. PIXE relies on the interaction of the incident ions, usually protons or alpha particles, with the inner-shell electrons of the sample, detecting characteristic X-rays generated in this process. This is a low probability process and for this reason it requires a large beam currents respect to other IBA, in order to achieve the sufficient statistics both for imaging and analysis through a reasonably fast measurement [Breese et al, 1996].

There are four main physical processes of importance to PIXE: 1) when a charged particle enters the material, it encounters numerous inelastic collisions with the sample atoms; 2) the energy of the ion along its trajectory decreases according to the specific energy loss (stopping power); 3) from some of the numerous ionised atoms along the particle path, characteristic X-rays are emitted with a probability given by the X-ray production cross section; 4) finally, X-rays emerging from the sample are attenuated in the material. Target composition influences particle energy loss, X-rays attenuation and X-rays production probability. So, in a general case as schematically shown in Figure 4, the X-ray yield Y_i for the characteristic X-ray of the i^{th} element in the sample toward the direction of the detector is [Breese et al, 1996]:

$$Y_i = \frac{Q}{e} \beta_i \int_0^d c(x) \sigma_i(E(x)) e^{-\mu x / \cos \theta} dx$$

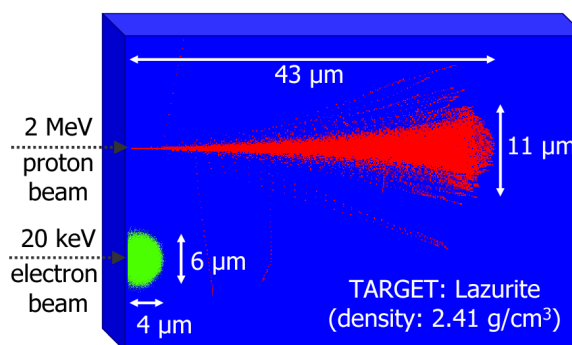


Figure 3. Comparison between 2 MeV protons and 20 keV electrons in lazurite by Monte Carlo simulations (software SRIM and Casino)

where Q is the total beam charge incident on the sample, e is the fundamental charge, $c(x)$ is the concentration profile of the i^{th} element, σ_i is the X-ray production cross section in the i^{th} element, μ is the X-ray attenuation factor and β_i is the transmission coefficient for the i^{th} element, which takes into account the energy lost by the X-rays from the point of incidence to the detector.

The incoming particles lose their energy while passing through the sample according to:

$$E(x) = \int_0^x S(E) dx'$$

where $S(E) = \frac{dE}{dx'}$ is the stopping power. If $c(x)$ is constant, while the X-ray detector has efficiency ε , the relationship between the observed X-rays intensity and the element concentration is given by:

$$I_i = QC_i K_i$$

The calibration parameter K_i is independent of the sample if both geometry of the experiment and the sample matrix composition do not change and is given by:

$$K_i = \varepsilon \int_0^d \sigma_i(E(x)) e^{-\mu x / \cos \theta} dx$$

It is clear from previous equations that for a reliable PIXE analysis several conditions have to be fulfilled. Successful analysis can be performed on well characterized sample (flat surface, known thickness and matrix composition), and fully controlled experimental conditions (in case of thin samples, analysis is much simplified). For quantification procedure, one can either use the fundamental parameter approach by calculating K_i from X-rays production cross sections σ_i , particle stopping power $S(E)$ and X-ray attenuation μ , or compare the unknown sample with standards, thus measuring K_i experimentally, which is most often the case.

Another important aspect is related to the common detector employed for PIXE measurements. A germanium or a Si(Li) detector is generally used to measure the energy of the emitted X-rays. This Ge detector is usually kept separated from the vacuum chamber or from air, if an external beam is used, by a beryllium window which is normally less than 25 μm thick. Since X-rays suffer attenuation also from this Be window they have to pass through to be

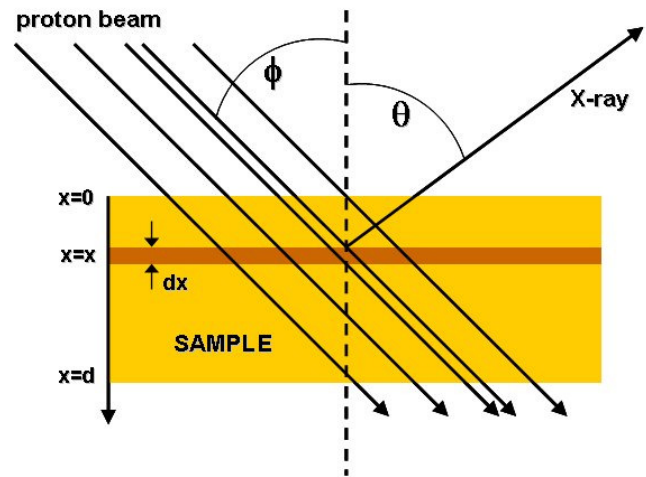


Figure 4. Schematic presentation of the PIXE experiment for a sample of thickness d

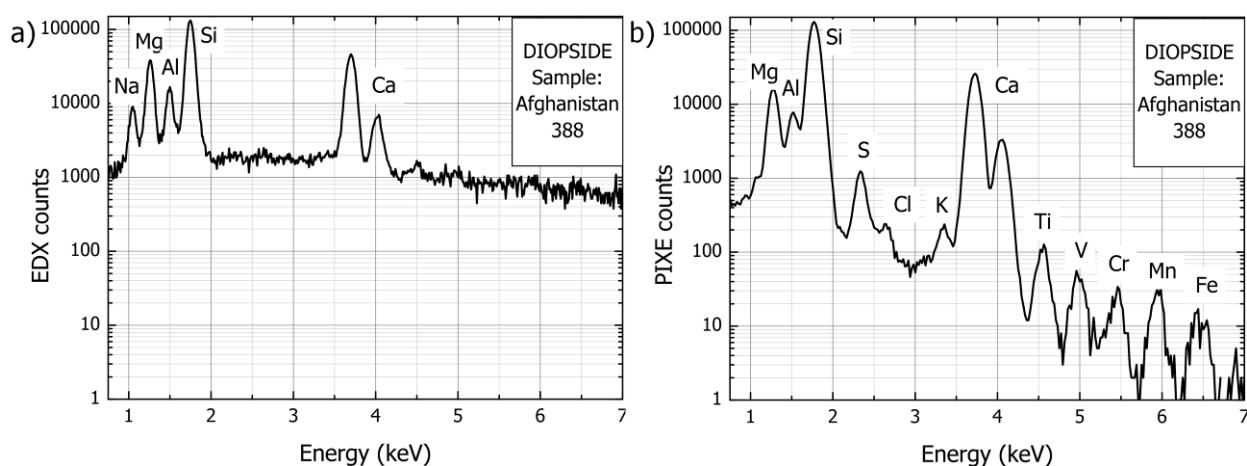


Figure 5. Comparison of X-ray spectra of diopside measured using: a) EDX with 20 keV electrons probe; b) PIXE with 600 keV protons probe

detected, the detection efficiency under 2 keV is poor. This low energy X-rays attenuation and the limited detector resolution (~ 160 eV) restrict the practical use of PIXE to the detection of elements with higher atomic number than fluorine. Moreover Ge detectors have intrinsic low efficiency for energies higher than 35 keV which, in addition to the decrease of the X-rays cross-section production, gives the upper limit of the atomic number which can be detected. It should be noticed that the same kind of detectors are used for EPMA (Electron Probe Micro-Analysis) where X-rays emission is induced by electrons. The dominant source of background is either for PIXE and EPMA coming from brehmsstrahlung, but in the case of a nuclear microprobe it is orders of magnitude less than for electrons as shown in Figure 5. This feature brings for example the EPMA sensitivity of about 100 wppm to the PIXE one at 0.1 wppm for many elements in a low atomic number matrix. The determination of the elemental concentrations from the measured yield is usually carried out with the aid of software packages such as GUPIX [Maxwell et al, 1989; Maxwell et al, 1995].

IL: Ionoluminescence

Ionoluminescence (IL) or Ion Beam Induced Luminescence (IBIL) are the names given to the photon emission in the IR/VIS/UV range from a material excited by an ion beam. This technique is much unusual with respect to PIXE and is involved with the interaction of the incident beam with the excited electrons from the outer-shells of the atoms; for this reason it is the only IBA technique which can give structural information about the probed sample because it is sensitive to local environment of emitting centres and can provide information both on material structure and activator impurity content. It is useful for the identification of chemical phases, as a check for the presence of certain trace elements and for monitoring the build-up of intrinsic and ion induced defects in luminescent materials.

If MeV ion beams are used, IL can hardly provide quantitative data, owing the numerous radiative recombination mechanisms involved in the photon emission process induced by MeV ion bombardment and the degradation with ion dose due to the generation of non radiative recombination centres. However, the coupling of IL with other IBA techniques, like PIXE, PIGE and BS, provides complementary chemical and structural information to complement elemental analyses [Breese et al, 1996]. This synergistic combination has triggered the interest of the IBA community stimulated by the pioneering work of the Lund and Melbourne groups [Yang et al, 1993], which first installed IL set-ups at IBA nuclear microprobe facilities correlating spatial distribution of elements with maps of luminescence centres. In this work the first measurements were performed on zircons ($ZrSiO_4$) and teeth but after that IL was successfully used to characterize a wide variety of advanced materials, minerals, stones and historical/art objects [Vittone et al, 2001; Teo et al, 2003; Calvo del Castillo et al, 2007]. In particular, the increasing interest in the application of IL to archaeometry has to be ascribed to the possibility of carrying out non invasive analysis in air or in controlled atmosphere (usually He), allowing the characterization of delicate or no-vacuum compatible art objects. Moreover, the presence of gas molecules flowing onto the sample surface, in spite of the degradation of the spatial resolution of the beam due to ion scattering in air or He atmosphere, allows a more effective heat dissipation and charge neutralisation, resulting in a reduction of the IL spectral background [Sha et al, 2002]. Besides general peculiarities of IBA techniques, such as the possibility to work in air, the advantages with respect to other luminescence techniques like Photo-Luminescence (PL) or Cathodoluminescence (CL) are: the greater probing depth (up to 0.1 mm), that allows to analyse beyond the surface layers on works of art, and the possibility to perform simultaneous major and trace element analysis by means of PIXE and PIGE.

Usually luminescence, independently from the particles or the radiation used to induce light emission, is divided into two categories: intrinsic and extrinsic luminescence. The former is used to describe the luminescence that results from fundamental properties of the material, such as transitions across the band gap of direct band gap semiconductors or free exciton recombination. The intrinsic luminescence is hardly found in minerals where impurities or defects are instead responsible for light emission. This is called extrinsic luminescence and impurities inducing luminescence are called activators. Of course not all the impurities are able to induce luminescence and rather they can even inhibit light emission (quenchers). These mechanisms are the result of energy transfer between two or more recombination centres in a crystal [Bettiol, 1999].

The intensity of ion beam induced luminescence can be theoretically modelled by the relation [Yang, 1996]:

$$Y_{IL}(c, \lambda) = N_c R(\lambda) F_{esc} \int_0^{\Delta x} F_A(\lambda, x) B_c \left[\left(\frac{dE}{dx} \right)_e + f_n \left(\frac{dE}{dx} \right)_n \right] dx$$

where: N_c is the total number of radiative recombination centres of type c ; $R(\lambda)$ is the signal collection efficiency of the experimental apparatus (light collection system and detector) depending from the wavelength of emitted light; F_{esc} is the ratio of light that emerges from the sample after internal reflections, depending from the refractive index and from the surface quality of the sample; F_A represents the self-absorption term, which is proportional to $\exp(-\alpha x)$, where α is the absorption coefficient of the material (depending from the wavelength) and x is the generation depth; B_c is the radiative recombination efficiency (i.e. the fraction of generated electron/hole pairs that recombine with radiative processes); $(dE/dx)_e$ and $(dE/dx)_n$ are respectively the electronic and nuclear energy loss rates of ions inside the sample. Inside the above described relation there are many experimental parameters which are very difficult to estimate, therefore it is nearly impossible to evaluate theoretically the signal intensity and a quantitative analysis is extremely arduous. Moreover, there are a number of physical and geometrical parameters which affect the detected IL signal. Sample temperature, internal reflection in the sample and beam damage can alter the IL efficiency and spectrum. In particular, with increasing ion fluence, therefore with increasing ion-induced lattice damage, the fraction of electron/hole pairs that recombine with radiative processes decreases, thus quenching the luminescence intensity as described by the following equation [Birks and Black, 1951]:

$$L(F) = \frac{L_0}{1 + k(e^{\sigma F} - 1)}$$

where: L is the luminescence signal [a.u.] after the absorption of a fluence F [ions/cm²]; L_0 is the initial luminescence signal; k is defined as the ratio between non-radiative and radiative recombination centres; σ is the effective ion-damage cross section [cm²].

Electron Probe Analysis

A keV electron beam interacts with matter through a series of phenomena, leading to the emission of backscattered and secondary electrons, of characteristic X-rays and luminescence, just to cite the most common events.

The interactions between electrons and matter can be first grouped into elastic and inelastic scattering events, mainly depending on the amplitude of the deflecting angle. The elastic scattering between electrons and the atoms of the material usually involve "big" deflecting angles and can be modelized with Rutherford's formula:

$$\sigma(> \phi_0) = 1.62 \cdot 10^{-20} \frac{Z^2}{E^2} \cot^2 \frac{\phi_0}{2}$$

where: σ is the cross section [cm^2] expressing the probability of scattering the electron at an angle greater than ϕ_0 ; Z is the atomic number of sample atoms; E is the electron energy [eV]. From this equation we can infer that the inelastic mean free path of electrons increases with increasing electronic energies and decreasing sample atomic number. The electrons that exit from the sample after a series of elastic scatterings are defined as backscattered electrons.

When inelastic scattering processes occur, the electrons lose a part of their energies through a series of phenomena including:

the excitation of valence electrons, that can leave the material to be detected as secondary electrons;

the excitation of core level electrons, leading to the emission of characteristic X-rays (detected in Electron Probe Micro-Analysis technique) or Auger electrons (detected in Auger Electron Spectroscopy);

the emission of continuous Brehmsstrahlung radiation due to the deceleration of electrons in the electrostatic atomic field;

VIS-IR-UV light induced luminescence due to excitation and relaxation processes between extra- or intra-band electronic levels; this phenomenon is known as Cathodoluminescence (CL).

Electron scatterings cause the deviation of electrons from their incidence trajectories and promote their diffusion in the sample; on the other hand the inelastic processes progressively reduce the energies of the electrons, until they are captured by the solid. The shape of the interaction volume for different electron energies and samples has been investigated both experimentally and theoretically, by means of Monte Carlo methods. Generally, it has a characteristic "pear" shape, as shown in Figure 6.

The elastic scattering processes determine the lateral straggling range and therefore the lateral resolution of the technique, while the inelastic scattering processes determine the penetration range and therefore the sampling depth. The

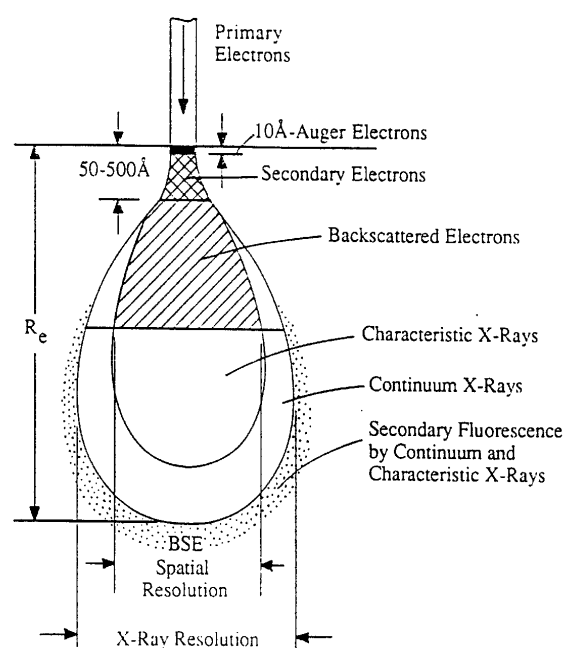


Figure 6. Interaction volume of a keV electron probe beam [Goldstein et al, 1992].

characteristics of generation volume depend from the atomic number of sampled element(s), the electron energy and the incidence angle.

The penetration depth of a keV electron beam can be evaluated neglecting the elastic scattering processes, thus defining the electron range with a relation which is similar to the one used for MeV ions:

$$R_e = \int_0^{E_e} \left(\frac{dE}{dz} \right)^{-1} dE$$

where: R_e is the electronic range; E_e is the electronic energy; (dE/dz) is the inelastic scattering energy loss rate. A more sophisticated formula, in good agreement with experimental data, considers also the effect of elastic processes on the penetration range and it is defined as [Kanaya and Okayama, 1972]:

$$R_{KO} = 0.0276 \frac{A E_e^{1.67}}{Z^{0.889} \rho}$$

where: R_{KO} is the so called "Kanaya Okayama range" [μm]; A is the sample atomic weight [g mol^{-1}]; E_e is the initial energy of electrons [keV]; Z is the sample atomic number; ρ is the sample density [g cm^{-3}].

EPMA: Electron Probe Micro-Analysis

Characteristic X-rays emitted by the sample during an electron bombardment are very useful to qualitatively and quantitatively evaluate its elementary composition. Unluckily the continuous Brehmsstrahlung background is always present and this fact degrades the detection limit for this technique. There are two main techniques to detect X-rays spectra: EDX (Energy Dispersive X-ray Spectrometry) and WDX (Wavelength Dispersive X-ray Spectrometry). The first is more diffused because of its rapidity to obtain a spectrum; in fact few seconds are enough to recognize the main elements inside a sample. Instead WDX has a better spectral resolution (some eV compared to 100÷150 eV of EDX) but requires longer time to obtain a spectrum.

CL: Cathodoluminescence

Cathodoluminescence (CL) is extensively used in various fields, but its widest applications are in geosciences [Marshall, 1988; Pagel et al, 2000; Götze, 2002].

The theory of electron beam induced luminescence is the same as that already described for ion-induced luminescence, since it has been demonstrated that for excitation energies above the band gap energy, the luminescence spectrum is essentially independent of the excitation probe [Klein, 1968]. The main peculiarities of this luminescence technique arise from the energy loss profile of electrons, influencing the penetration depth of the probe, and different damage effects with respect to ions.

RS: Raman Spectroscopy

The physical process behind the Raman spectroscopy is the Raman effect, whose detailed description can be found elsewhere [Long 2002]. Raman spectroscopy probes molecular and crystal lattice vibrations and therefore is sensitive to the composition, bonding, chemical environment, phase, and crystalline structure of the sample material. The sample is illuminated with a monochromatic photon beam (usually a laser), most of which are either absorbed, reflected, or transmitted by the sample. A small fraction, however, interacts with the sample via the oscillating electric field of the incoming photons. The molecules so affected can be considered to reside in 'virtual' excited states, which are highly unstable, decaying instantaneously to the ground state by one of three different processes. Most of the incoming photons that are scattered do so elastically, a phenomenon referred to as Rayleigh scattering, whereby the emission of a photon of the same energy allows the molecule to relax to its ground vibrational state. Rayleigh scattering, therefore, bears no information regarding the vibrational energy levels of the sample. However, for a molecule with certain vibrational frequencies, an even smaller proportion (approximately 1 in 10^6) is scattered inelastically at different energies generating a set of frequency-shifted 'Raman' photons. The energy differences of the Stokes and anti-Stokes Raman photons with respect to the excitation energy relate to either energy lost, or more rarely gained, by a scattered photon as the molecule returns to either a higher or lower vibrational level, respectively. These vibrational energy levels are therefore probed indirectly by Raman spectroscopy, but are the same as those probed directly by IR absorption spectroscopy. Although the vibrational information obtainable by Raman spectroscopy is similar to that obtained by IR spectroscopy, it is not identical, but rather complementary, owing to the different selection rules governing vibrational Raman scattering (mandatory change in polarisation) and IR absorption (mandatory change in dipole moment) [Smith and Clark, 2004].

THE PREVIOUS PROVENANCE STUDIES

Since the 1960's a lot of people have attempted to perform some provenance studies of lapis lazuli for different purposes and with different approaches, obtaining some interesting results. However, at present, a systematic and exhaustive provenance study of the raw material utilized in artworks is still lacking, especially if it is necessary to use non-destructive techniques.

The first thing to notice is the number of sample analysed, always limited if compared to provenance studies of other materials, where hundreds of samples are taken into account [Tykot, 2002]. This is due both to the preciousness and rarity of the material, and also to the localization of the mines, sited in impervious places very difficult to reach because of their altitude, nuclear tests or wars. Another aspect already pointed out by other authors [Ballirano and Maras, 2006; Borelli et al, 1986; Cipriani et al, 1988], is that there is a lack of precise geographical information for many specimens archived in museums or private collections, and this fact makes most of them inadequate to be a reference for a provenance study.

To have more information about these works it is necessary to read all of them (see the bibliography for details), but we can say some words about the main results obtained; the number, the provenance and the kind of samples analysed in each of them are summarized in Table 6, where there is also a distinction if destructive or non-destructive techniques have been used. The first one trying a provenance study of lapis lazuli is Georgina Herrmann [Herrmann, 1968], but in her work she says in few words that using Optical Microscopy (OM), X-Ray Fluorescence (XRF) and Optical Spectroscopy, is not possible to distinguish between Afghan and Siberian Rocks. Few years later, in 1972, Keisch dedicate a short paragraph inside a book [Keisch, 1972] to Isotope Mass Spectrometry, a destructive technique, applied to lapis lazuli and artificial ultramarine pigments. He shows that using an isotope ratio of sulphur (S^{32}/S^{34}) it is possible distinguish the Afghan lapis lazuli both from artificial ultramarine and from Chilean and Siberian provenances. Unfortunately neither Herrmann nor Keisch explain the experimental procedure of their measurements and the details of the results.

Four years later Hogarth and Griffin presented the characterisation of the lazurite of Baffin Island, in Canada, by means of Electron Probe Micro-Analysis (SEM-EPMA) [Hogarth and Griffin, 1976]; they focused only on the main phase of lapis lazuli, the lazurite, and compared it to some samples coming from other quarries and with the results obtained by previous studies on this mineral. They show that the concentrations of the main oxides in lazurite is slightly variable and maybe some variation could be related to the origin of the mineral; unluckily the number of samples of each provenance was too low to find some significant correlations.

Table 6. The provenance studies until now. The numbers represent the samples coming from each provenance; rocks are in bold type, pigments are in italic type, archaeological findings are underlined and the artworks are in normal type. (●) indicates that the exact number is not reported explicitly. The last line represents this work.

Year / Authors	Provenances of rocks and <i>pigments</i>														Rocks	<i>Pigments</i>	Artworks or archaeological samples	Destructive techniques	Non-destructive techniques	
	Afghanistan (Badakhshan)	Tajikistan (Pamir Mts)	Pakistan (Chagai Hills)	Pakistan	Siberia (Lake Baikal)	Russia (Ural Mts)	Myanmar (Mogok region)	Iran	Italy (Latium)	USA	Canada (Baffin Island)	Chile (Coquimbo Region)	Unknown	Synthetic						
1968 Herrmann	●	-	-	-	●	-	-	-	-	-	-	-	-	-	-	●	-	-	●	●
1972 Keisch	3+1	-	-	-	1	-	-	-	-	-	-	4	2	<i>14</i>	10	<i>15</i>	-	-	●	-
1976 Hogarth and Griffin	-	1	-	-	1	-	2	-	2	3	14	1	-	-	24	-	-	●	●	-
1986 Borelli et al	5	-	-	-	8	-	-	-	-	-	-	5	-	-	18	-	-	●	●	●
1988 Cipriani et al	4	-	-	-	8	-	-	-	-	-	-	6	-	-	22	-	-	19	●	●
1990 Delmas and Casanova	2	2	9	-	-	1	-	-	-	-	-	-	-	-	14	-	-	<u>6</u>	●	-
1992 Casanova	7	2	11	-	-	1	-	-	-	-	-	-	-	-	21	-	-	<u>29</u>	●	-
2003 Zöldföldi and Kaszovszky	12	-	-	-	7	4	-	-	-	-	-	4	1	-	28	-	-	-	●	●
2004 Ajò et al	<i>5</i>	-	-	-	<i>1</i>	-	-	<i>1</i>	-	-	-	-	<i>2</i>	<i>18</i>	-	-	<i>27</i>	-	●	-
2006 Zöldföldi et al	20	-	-	-	9	4	-	-	-	-	-	4	9	-	37	9	<u>2</u>	-	●	●
2006 Ballirano and Maras	3	-	5	1	-	-	-	1	-	-	-	1	<i>1</i>	-	10	<i>1</i>	-	-	●	-
2008 Calusi et al	1	-	-	-	-	-	-	-	-	-	-	1	-	-	2	-	-	1	-	●
2009 Bacci et al	1+3	-	-	-	-	-	-	-	-	-	-	1+1	-	-	2	<i>6</i>	-	-	●	-
2009 Smith and Kilnshaw	18+4	4	-	-	4	2	2	-	-	7	2	4+2	3+5	<i>11</i>	46	<i>22</i>	-	-	●	●
2011 Re et al	3	4	-	-	1	-	-	-	-	-	-	4	1	-	13	-	-	4	●	●

Ten years later an Italian group has proposed another scientific approach to the origin of lapis lazuli based on the study the collection of the "Mineralogical Museum" of Firenze [Borelli et al, 1986; Cipriani et al, 1988]. In these two works they used destructive techniques like OM on thin sections, Scanning Electron Microscope with Energy Dispersive X-ray Spectrometry (SEM-EDX) and X-Ray Diffraction (XRD), but they also try to obtain information on some precious artworks in a non-destructive way, putting small objects in the chamber of the diffractometer. The main result of these works is the mineralogical characterization of the samples, that is the recognition of all the different minerals present in a rock and a valuation of how diffuse they are in the sample. This analysis shows for the first time a distinctive marker for the Chilean provenance: the presence of wollastonite as accessory mineral, while both in the Afghan and in the Siberian lapis lazuli it is replaced by diopside. To distinguish the Siberian material from the other provenances, they had to focus on the lazurite only and they found that chlorine is not detectable with SEM-EDX inside Chilean and Afghan lazurite, while it is present at a low but significant concentration in the Siberian one. In these studies they also analysed Italian lazurite, that usually is of very low quality, and they found a high content of potassium compared to other provenances, probably due to the presence of K-feldspar during the formation of the rocks of this provenance.

The next studies on lapis lazuli were devoted to understand the provenance of some cut wastes excavated from Shahr-i-Sokta [Delmas and Casanova, 1990; Casanova, 1992]. They took into account four of the main Asian quarries to find the best resemblance of these stones with their samples. They used Atomic Absorption Spectroscopy (AAS), a destructive physical-chemical technique, and they processed the data using Principal Component Analysis (PCA), a multivariate method to find similarities and differences between the results; with this technique they found that using only six variables (combining the content of Si, Al, Ca, Mg, Ba, Sr) it is possible to distinguish between the four deposits. For the content of barium and strontium, they take inspiration from a previous work [Ivanov et al, 1976] that, analysing the geo-chemistry of the Siberian deposit, suggested these two elements as characteristic of this provenance. The results obtained on the archaeological samples are in agreement with a Pamir Mountains and Chagai Hills provenance, other than Afghanistan, confirming the fact that also other mines could have been exploited during the antiquity.

A similar approach, exploiting PCA to elaborate data, was chosen in other successive works [Zöldföldi and Kasztovszky, 2003; Zöldföldi et al, 2006]; they focused on the use of a neutron reactor to perform Prompt Gamma Activation Analysis (PGAA), a technique that can give information on the chemical composition of the whole sample, but not on the single phases inside it. It must be underlined that this is the first approach that can be totally non-destructive, even though, for these works, some samples have been crushed and powder have been

studied. With this method they obtained a first distinction between provenances showing a graph of sulphur versus chlorine content, even if there is an overlap between some provenances. Apparently this graph can be in contrast with the one presented in a previous work [Borelli et al, 1986], since Zöldföldi and Kasztovszky found a higher content of chlorine in the Chilean samples, while in lapis lazuli from Afghanistan and from Siberia there is more or less the same lower amount of this element. But we have to remember that previous analyses were performed only on one mineral, the lazurite, while the new ones are referred to the whole rock of lapis lazuli and so the results are not directly comparable. Using the PCA they also found some combinations of elements content that permit to divide the results in clusters related to provenances, isolating three main groups: one with the Chilean samples, another one with the samples coming from Afghanistan, and a third one containing samples both from Siberia and Ural Mountains. Unluckily they still do not show the results obtained on archaeological samples and for this reason we can not fully evaluate the validity of this non-destructive approach to analyse objects. In the last paragraph of the second paper, they also suggest the use of Fourier Transform Infrared Spectroscopy (FTIR) to analyse pigments, a method that permits to recognize the natural ultramarine blue from the artificial one.

Actually there are many other works on pigments, also wider and more detailed; some of them also try to find some markers useful for a provenance study, but it is important to note that pigments are less suitable for this purpose, due to the processes involved in their fabrication that could introduce contaminants or remove minerals. Anyway some good results have already been reached, usually combining FTIR with other techniques. Until now the only marker found is an infrared band (at about 2340 cm^{-1}) that seemed to be peculiar of the Afghan provenance [Derrick, 1990; Bacci et al, 2009] or, better, of all the Asian provenances [Ajò et al, 2004]. A recent work [Smith and Klinshaw, 2009] confirms this last hypothesis with a lot of samples coming from different provenances; in the same paper they also try to give a motivation for this band, but on this last question there are different points of view and the debate is still open [Miliani et al, 2008; Bacci et al, 2009; Smith and Klinshaw, 2009].

A very interesting work [Ballirano and Maras, 2006] tries to find the provenance of the pigment employed in the "The Last Judgment", the Michelangelo's fresco. Using various techniques, but all destructive, they find some analogies between the pigment and rocks coming from Asian sources. The result of this work is that the most similar source is the one in Chagai Hills; this fact proves that also in Renaissance the Pakistan deposits could be utilized as source of lapis lazuli to produce ultramarine blue pigments.

Nevertheless lapis lazuli provenance is still an open question and a systematic study on lapis lazuli objects would be helpful in solving such a problem. In particular, because art-works produced using lapis lazuli are valuable, only non-destructive investigations can be carried out

to identify the provenance of the raw materials. On this bases few years ago this work started with the analysis of few samples, two rocks and an art-work, using mainly Ion Beam Analysis (IBA) and in any case non-destructive techniques [Calusi et al, 2008; Colombo et al, 2008]. Despite the low number of samples, the Ionoluminescence (IL) proved to be a very fast way to distinguish between Chilean provenance and others; in fact wollastonite, the typical accessory mineral for the Chilean provenance [Borelli et al, 1986; Cipriani et al, 1988], shows a spectrum very easy to distinguish from the diopside one, the accessory mineral peculiar of the Asian samples.

This work tries to continue on this way, analysing more samples coming from different places, and looking for new markers detectable by means of only non-destructive techniques.

EXPERIMENTAL SETUP

In this chapter we give some details about the instruments and the experimental conditions used for the analyses of this work.

Ion Beam Microprobe facilities

The measurements involving the use of an ion microprobe have been performed at two Italian nuclear laboratories of INFN (the Italian National Institute of Nuclear Physics): the in-vacuum ion-beam facility of the 2.5 MV Van der Graaff accelerator AN2000 at LNL (Legnaro National Laboratories, Padova), and the external beam facility of the 3 MV Tandetron accelerator at the LABEC Laboratory (Firenze). In the following paragraphs the main features of these facilities are briefly summarized.

LNL (Legnaro)

The role of the Legnaro National Laboratories (Padova) is to propose, coordinate and conduct experimental and theoretical research activities in the field of fundamental nuclear physics, as well as in other sectors regarding the study of interactions between matter and radiation or particle beams, such as those generated by the particle accelerators installed at the Laboratories. Nowadays research activities branch into fields that reach even beyond that of fundamental nuclear physics, to embrace issues regarding interdisciplinary applied physics as well. At present, there are four accelerating machines of different potentialities in operation at the Laboratories and one of them is the AN2000 which has been used for the measurements of this work. The AN2000 facility consists in a electrostatic Van de Graaff accelerator; it has a single stage-Belt charging system, and a maximum working voltage of 2.5 MV. Available accelerated ions are single charged ^1H and ^4He . The ion beam is continuous, with a maximum ion energy of 2.5 MeV. The AN2000 accelerator (Figure 7a) is used principally for interdisciplinary studies in materials science, solid state physics, biomedical analysis, radiation and environmental physics and geology. About 20 research groups coming from several national and international universities and research institutions use the LNL facility, for a total effective beam-time of about 2500 hours per year. The accelerator has five beam lines, among which we made use of 0° microprobe line, to perform micro-PIXE experiments [Bollini et al, 1993]. The microprobe line is based on Oxford instrumentation and measurements are taken in vacuum ($\sim 10^{-5}$ mbar). The analysis chamber includes experimental setups for Rutherford and

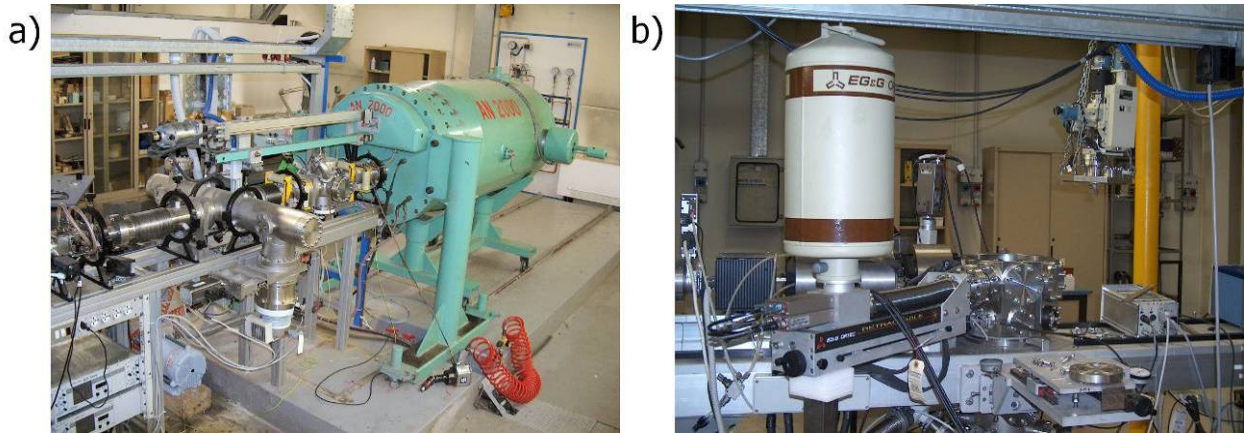


Figure 7. The Legnaro National Laboratories facility: a) AN2000 accelerator ; b) microprobe beamline

Non-Rutherford Backscattering, Ion Channeling, Proton Induced X-ray Emission (PIXE), Elastic Recoil Detection Analysis (ERDA), low energy Nuclear Reaction Analysis (NRA) and Scanning Transmission Microscopy experiments; one optical microscope is available for sample positioning (Figure 8). The ion current is measured either using a faraday cup in front of the beam (or passing through the sample and then collected in the rear) or directly on the sample holder in case of conducting samples. The μ -beam is able to raster scan across the sample surface thanks to the Oxford Microbeam system which is also controlling the acquisition through OM-DAQ software. A remote control allows to move the sample holder along three directions and also to rotate it, so the sample can be easily positioned and orientated with respect to the beam direction. Typical beam spot diameter is around $4\ \mu\text{m}$ and the scanned area ranges from $30\times 30\ \mu\text{m}^2$ to $1200\times 1200\ \mu\text{m}^2$. In Figure 7b there is the terminal part of the microprobe beamline, where it is possible to note the PIXE detector.

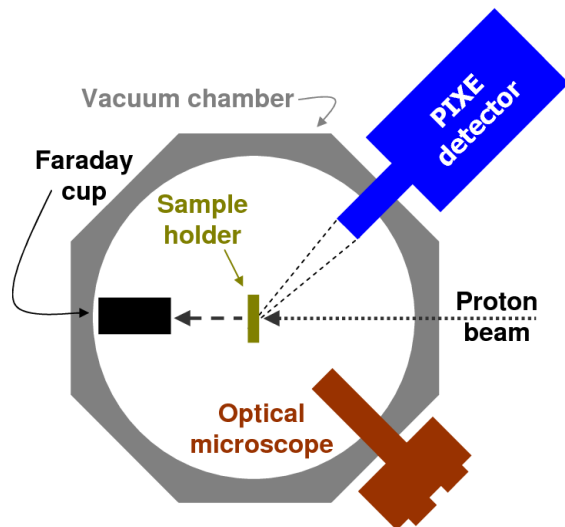


Figure 8. Schematic top view of the AN2000 micro-beam chamber

μ -PIXE set-up at LNL

The PIXE detector used is an iperpure Ge Ortec IGLET-X (crystal area $100\ \text{mm}^2$, crystal thickness $7\ \text{mm}$) with a beryllium window of $12.5\ \mu\text{m}$ and $150\ \text{keV}$ resolution on Mn K_α line. It is positioned at 45° with respect to the beam direction as can be seen in Figure 8 where a schematic view of the microbeam chamber is shown. To simultaneously analyse light and heavy elements with the same detector we used an aluminium funny filter [Gama et al, 2001], that is

a filter with a hole drilled at its centre and placed in front of the detector window. To evaluate the beam dimensions we're used to perform a PIXE map (Cu) of a copper grid (pitch: 60 μm , bar: 15 μm).

The current can be measured in two ways: using a Faraday cup positioned beneath the sample or with a pico-amperometer connected to the sample holder. Since the analyzed samples were not thin enough to allow ions to pass through them, the second method was used, integrating the charge deposited on the sample during the whole run. The first kind of measurement was performed only occasionally, to check the stability of the beam, when the sample was removed and the beam could reach directly the Faraday cup.

Spectra analysis has been carried out through the Gupixwin software (version 2.1.3) and to valuate the H value curve a set of reference mineral standards shown in Table 7. Moreover a different standard of diopside has been analysed to test the validity of the quantitative analyses.

LABEC (Firenze)

LABEC is a laboratory of the INFN established with the main purpose of performing applications of nuclear techniques in the field of cultural heritage. However, applications of nuclear techniques also to other fields are currently being performed: studies on environmental problems (mainly, air quality monitoring), applications to geological studies such as chronological reconstruction of past volcanic eruptions or geochemical modelling of magma evolution, applications to material science in general, and others.

The main equipment of LABEC is a Tandem accelerator, 3 MV terminal voltage (Figure 9a). The accelerator has three independent ion sources, one of which is dedicated to measurements of Accelerator Mass Spectrometry (AMS); the other two sources are instead used to produce all kinds of beams (from protons to heavy ions) mainly for applications of Ion Beam Analysis (IBA), but also for other purposes such as studies of radiation damage to materials exposed to accurately controlled doses (even very weak), tests of radiation detectors responses, etc.

Among the available beam lines, the extracted microbeam line is the one which has been exploited during this work [Giuntini et al, 2007]. The peculiarity of this line, respect to many others micro-beam line in the world, is really the fact that it is an external beam and measurements are performed in air (Figure 9b). This microprobe line is also based on a Oxford

Table 7. Set of mineral standard used for PIXE quantitative analyses of diopside crystals at LNL

Standard	Element	w% in the standard
Haematite	Fe	69.86%
Chromite	Mg	8.20%
	Al	7.30%
	Cr	37.22%
	Fe	13.60%
Apatite	P	18.32%
	Ca	35.63%
Titanium	Ti	99.60%
Diopside	Mg	11.23%
	Si	25.88%
	Ca	18.39%

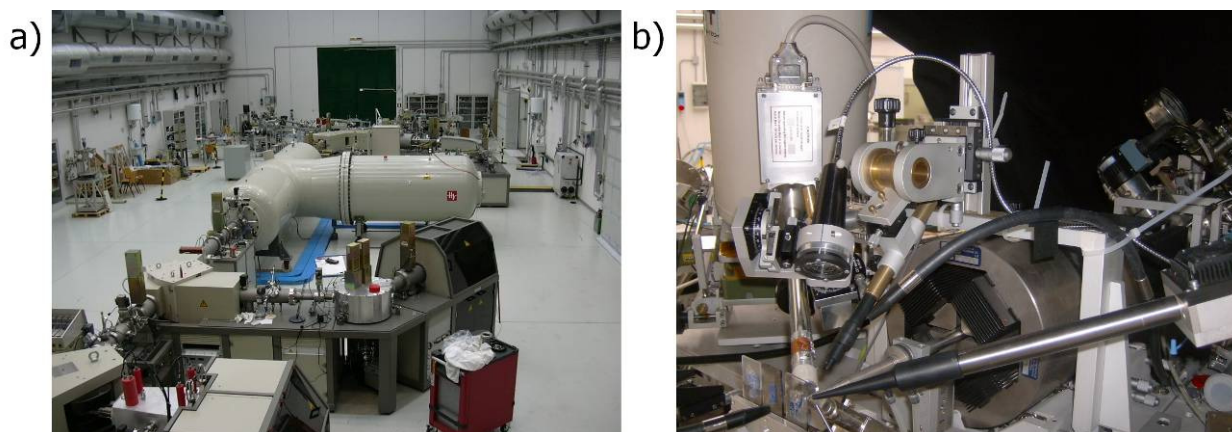


Figure 9. The LABEC facility: a) Tandetron accelerator; b) exit stage of the external microbeam line

Microbeam Ltd. system as well as the data acquisition system OM-DAQ. Typical beam spot diameter in proximity of the exit window is $\sim 10 \mu\text{m}$ and the beam is usually raster scanned along area ranging from $100 \times 100 \mu\text{m}^2$ to $1000 \times 1000 \mu\text{m}^2$. A motorized stage allows a broad range in sample displacement, therefore there are virtually no limits in the analysed object dimensions. The IBA techniques available by now to the external microprobe are PIXE, PIGE, IL, RBS and IBIC (Ion Beam Induced Charge).

μ -PIXE set-ups at LABEC

For PIXE measurements two detectors (Figure 9b) are installed at LABEC which differ in detection efficiency: one suitable for energies below Ca K_{α} lines, which is a SDD Roentec, X Flash detector, Series 1000, with a resolution of 175 eV on Mn K_{α} line (Active area 10 mm^2 , 3.5 mm aperture Zr collimator and effective active area 9.6 mm^2) and a Be window of $8 \mu\text{m}$ and another for high energy X-rays ($Z > \text{Ca}$). This second detector has recently been changed: for the measurements on semi-thin section a HPGe ORTEC IGLET-X-11145-S with a resolution of 130 eV on Mn K_{α} line (Crystal diameter 11 mm, crystal thickness 10 mm) and a Be window of $25.4 \mu\text{m}$ has been used; for the measurements on the objects of the "Collezione Medicea" a SiLi ORTEC SLP-10180-S with a resolution of 157 eV on Mn K_{α} line (Crystal diameter 16 mm, crystal thickness 5.5 mm) and a Be window of $25.4 \mu\text{m}$ has been used. For both the measurements $425 \mu\text{m}$ of mylar and $14 \mu\text{m}$ of aluminium has been used as absorber. More details on LABEC experimental set-up for PIXE can be found in a previous work [Giuntini et al, 2007]. As described for μ -PIXE at LNL, a standard copper grid was used either

Table 8. Set of glass and mono-elemental standard used for PIXE quantitative analyses at LABEC

Standard	Element	w% in the standard
Soda-Lime container	Na	9.45%
	Mg	0.16%
	Al	1.46%
	Si	33.25%
	K	1.67%
	Ca	7.65%
Aluminium (thick)	Al	99%
Titanium (thick)	Ti	99.6%
Copper (thick)	Cu	99.9%
Iron (thick)	Fe	99.5%
Lead (thick)	Pb	99.5%

for the spatial calibration and for the evaluation of the beam spot size. Also in this case spectra analysis has been carried out through the Gupixwin software (version 2.1.3) and to evaluate the H value curve a standard glass with known trace elements quantity and a set of reference mono-elemental standards have been used (see Table 8).

μ -IL set-up at LABEC

The IL apparatus of the external scanning microprobe facility of Firenze is integrated in the PIXE/PIGE/RBS set-up (Figure 9b) and has been developed in the last years mainly for cultural heritage applications. The first version of this system is widely described in [Calusi et al, 2008; Colombo et al, 2008] and consists in a light collector connected to the common end of a Y-shaped optical fibre. One end of the fibre is connected to a spectrometer to quickly obtain a spectrum of an area, while the other end is connected to a photomultiplier tube (PMT), to collect luminescence maps. Besides the panchromatic mode, it is possible to acquire monochromatic maps, thanks to a monochromator system interposed between the fibre and the PMT. To obtain luminescence maps the PMT is connected to a standard amplification electronic chain which delivered TTL signals to the OM-DAQ system.

This system has recently been upgraded, changing the optical fibre, the spectrometer, the monochromator system and the photomultiplier tube; now both systems are available, and can be used depending on which spectral range has to be revealed. The scheme of the new setup is represented in Figure 10 while the main characteristic of the two systems and their

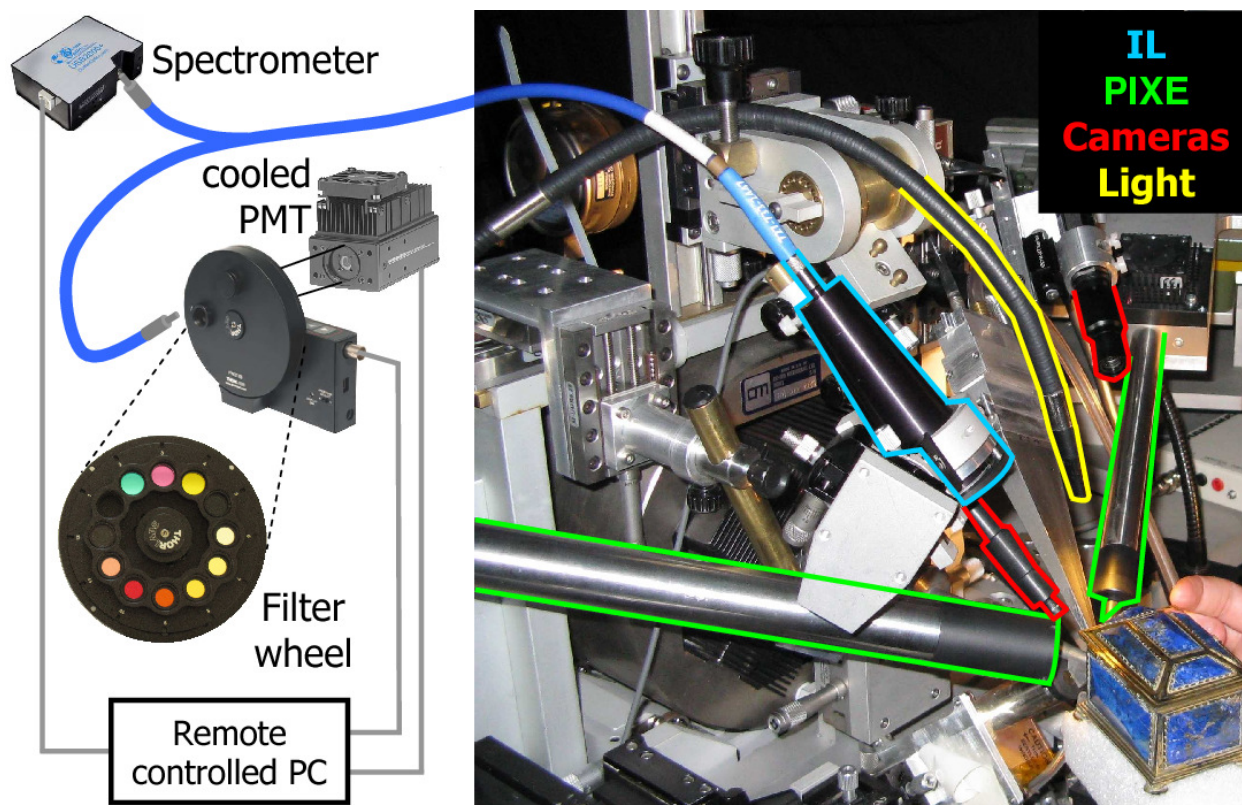


Figure 10. Scheme of the new IL system of the microbeam line at LABEC in Firenze

main differences are reported in Table 9.

In both the systems light was collected through an optical system (1" diameter, 5 cm focal length) based on a Ocean Optics (OO) 84-UV-25 collimating lens, mounted on a manual multistage (xyz, 10 μm resolution; θ and φ, 30" resolution) positioned ~10 cm from the sample and at ~120° with respect to the beam direction. In this configuration the distance from the entrance of the fibre to the collimating lens is ~10 cm and the magnification of the optical system is thus ~1.

The spectrometers were calibrated in wavelengths using an OO HG1 Ar-He lamp while their spectral responsivity was evaluated with an OO LS1-CAL Tungsten Halogen Light Source. The resulting efficiencies of the two systems are shown in Figure 11 and have been used to correct all the spectra collected with each system.

To achieve the optimal performances of the light collection system we periodically aligned the collector moving the manual multistage, to centre the area of maximum collection efficiency in the middle of the scanned area [Calusi et al, 2008]. Moreover, a structure supporting a black cloth was built around and above the beam end-stage to screen the light collection system and the PMT from sunlight during measurements.

For both PIXE and IL measurements the signal was induced by an ion beam extracted in air or in He atmosphere through a silicon nitride window (100 nm thick, 1×1 mm² area) and the beam was raster scanned over the sample located 2.5 mm downstream of the exit window [Giuntini et al, 2007].

Table 9. Characteristics of the two IL setup at the external microbeam line of LABEC in Firenze

IL SYSTEM	[Calusi et al, 2008; Colombo et al, 2008]	upgrade
Optical fiber	OO FIR200VIS	OO QBIF600
diameter	200 μm	600 μm
Spectrometer	OO USB 2000	OO USB 4000
software	OO IBASE32	OO Spectra Suite
pixels number	2048	3648
grating	600 l/mm	600 l/mm
blaze	500 nm	500 nm
bandwidth	200÷900 nm	350÷1000 nm
good response	350÷750 nm	450÷900 nm
PhotoMultiplier Tube	Hamamatsu R376	Hamamatsu H7422
monochromator	linear variable filter VERIL S	Filter wheel ThorLabs FW212A
pre-amplifier	ORTEC 142A	Hamamatsu C9744
amplifier	Bipolar Shaping ORTEC 572	

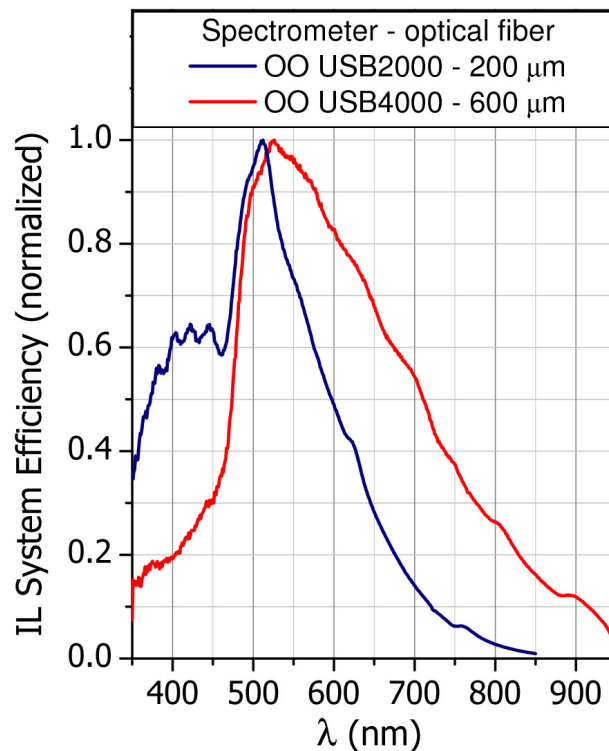


Figure 11. Normalized curves of efficiency of the two IL systems

Defocused-IBIL setup at LABEC

As will be explained in next paragraph, cold-CL gives very quick and useful information to know the distribution of the main phases in a sample, but it requires to put the sample in vacuum. For this reason we thought to design a similar instrument using a defocused ion beam, with the possibility to work in air. This is not just another way to obtain a luminescence map of the sample, but it permits to save a lot of time searching the point of interest on an unknown sample. In fact, due to the non uniformity of lapis lazuli, analysing it by means of a microbeam is very difficult to find a point of interest using only μ -PIXE and μ -IL, since the scanned area is usually quite small and the time required to have a map big enough is high.

To perform these measurements, that require different condition respect to the microbeam, we moved aside the small PIXE detector and put instead of it a CCD colour camera equipped with a zoom lens, at 45° respect to the beam line (see Figure 12). The camera is a Prosilica GC2450C, with a 5 Mpixels detector and an exposure time varying from 25 μ s to 60 s. The objective is a TECHSPEC VZM 1000 Zoom Imaging Lens, with a variable magnification from 2.5 to $10\times$ and a working distance of 35 mm. To avoid to record distorted images, we put the analysed surface of the sample rotated at 45° respect to the beam trajectory and the zoom lens has been aligned to be in front of the object at a distance of 35 mm, to obtain a focused image of the area hit by the beam. With the minimum magnification ($2.5\times$) the recorded area is $3.8\times 3.3\text{ mm}^2$ and, since in this conditions we do not need a micrometric beam, we could afford a thicker (500 nm) and larger ($2\times 2\text{ mm}^2$) silicon nitride window that permits to have a larger beam area. The "microbeam" has been aligned in the middle of the window, then the raster was stopped and the beam has been defocused until it hit all the surface of the window. In this way it was very easy to obtain maps of luminescence of quite large areas in a very short time (from 1 to 20 s with the maximum gain). With the same instrument, changing only the exposure time and the gain, a normal picture in reflection mode of the same area can be collected (after stopping the beam and turning on the light). These pictures are very useful to find exactly the same point on the sample during successive analyses with μ -PIXE and μ -IL.

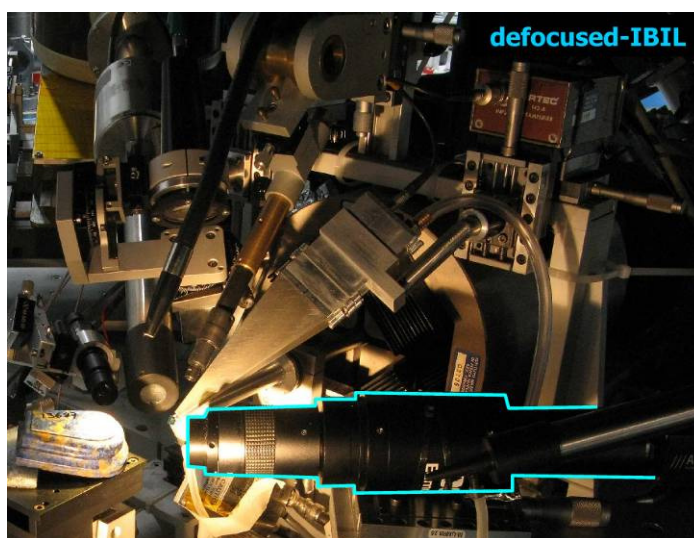


Figure 12. Defocused-IBIL setup at the microbeam line at LABEC in Firenze

Electron probe instruments

All the measurement with electron probes have been performed in the laboratories of the University of Torino. For the compositional analysis we used a SEM-EDX instrument, while for luminescence measurements we used two different instruments: a broad electron beam "cold cathode" apparatus and a SEM-CL system.

cold-CL

A typical cold-CL apparatus consist of an electron source (cold-cathode) and a microscope; the electron beam is not focused like in a SEM, but it is broad and hits the sample obliquely, in correspondence of the optical axe of the microscope. For this reason the analysed area is an ellipse, having an area of about 1 cm².

The cold-CL apparatus used in this work is shown in Figure 13 and it is located at the Petrology and Mineralogy Department of the University of Torino. It is a "CITL Cold Cathode Luminescence 8200 mk3" instrument equipped with a polarized optical microscope Olympus BH2 and a CCD camera Olympus E1 (5 Mpixel). The semi-thin sections were placed in a vacuum chamber with transparent windows and the pressure was maintained at about 0.8 mbar. At this



Figure 13. The cold-cathodoluminescence instrument

stage sample coating was not necessary because the working pressure was high enough to avoid charging effects. During the measurements, the accelerating voltage and current were 15 kV and 500 μ A respectively. Since the electron beam was about 1 cm² broad, the current density was approximately 5 μ A/mm². The penetration depth of the 15 keV electron beam probe is less than 2 μ m and depends on the composition and the density of the mineral. Lapis lazuli showed an intense luminescence in the visible wavelengths so that acquisition time using standard camera conditions ranged from only 1 s to 20 s. The total magnification is 10 \times , due to the microscope objective (4 \times) and a removable lens (2.5 \times). In this conditions the recorded area of each picture is about 1.7 \times 1.3 mm² and thanks to two micro-translators is possible to move the sample on a X-Y plane, taking many picture partially overlapped; putting them together one can obtain a luminescence map of the whole area of interest with a very high resolution.

SEM-EDX

The SEM-EDX measurements for major elements evaluation were carried out using a Leica Stereoscan 420 equipped with an Oxford Pentafet EDX, placed at the I.F.M. Chemistry Department of the University of Torino (Figure 14). It is a standard Scanning Electron Microscope, equipped with both secondary electrons and back-scattered electrons detectors, useful to find the point to analyse. The EDX spectra were automatically corrected and calibrated both in energy and in intensity thanks to measurements performed periodically on cobalt. To obtain the chemical concentration of each phase we also measured a set of reference standards as presented in Table 10. The certified standards were divided in two blocks, one containing minerals and the other oxides; for each element under investigation the standard with the highest content of it was selected. Their EDX spectra were acquired once and then used for the quantification of all the elements, analyzing data by means of INCA Microanalysis Suite software package. The analysis of each crystal have been considered reliable if the sum of the elements was in the range 90÷110%. To compare the data a normalization at 100% have been done and the results presented in this work are always normalized.

For all these measurements the samples have been partially carbon-coated to avoid charging effects; for this reason, except for calcite crystals, we excluded carbon from the quantification, because its quantity is affected by the coating.



Figure 14. The SEM-EDX instrument

Table 10. Set of standard used for SEM-EDX quantitative analyses on various phases. (*) Carbon quantification is always affected by the carbon coating of the samples

Standard	Element	w% in the standard
Calcite	C*	12.02%
Apatite	F	1.91%
	P	18.32%
Jadeite	Na	10.54%
Diopside	Mg	11.23%
Plagioclase	Al	15.10%
	Si	25.34%
Marcasite	S	53.46%
	Fe	46.54%
Tugtupite	Cl	7.58%
Sanidine	K	10.05%
Wollastonite	Ca	34.30%
TiO	Ti	75.40%

Table 11. Set of standard used for SEM-EDX quantitative analyses of diopside crystals

Standard	Element	w% in the standard
Diopside	Mg	11.23%
	Si	25.88%
	Ca	18.39%
Albite	Na	8.60%
	Al	10.34%
Benitoite	Ti	11.58%
Almandine Garnet	Fe	18.09%

The parameters used for all the acquisition were: beam energy of 20 keV, beam current of 200 pA and acquisition time of 120 s. The analysed areas were always very small: using a magnification of 2000 \times , we selected a uniform area with variable dimensions, depending on the size of the crystal; the smallest area have been 3 \times 3 μm^2 , but we've always taken into account the maximum penetration depth and lateral straggling of the beam in the crystal, to be sure not to probe outside or beneath crystals.

For the run of measurements performed on diopside crystals we improve a bit the experimental procedure: to have a more precise quantification, we acquired a spectrum of the standard mineral (Table 11) each time we put a sample in the SEM chamber, without turning off the instrument, so to be sure to have absolutely the same experimental conditions. Moreover, to have more accurate spectra, we doubled the acquisition time, passing to 240 s. We also decided to analyse areas always with the same dimension, to have measurement more comparable; for this reason we used a magnification of 2500 \times , selecting an area of 15 \times 10 μm^2 .

SEM-CL

The instrument used in this work to analyse the cathodoluminescence of single crystals is shown in Figure 15 and it is located at the Petrology and Mineralogy Department of the University of Torino. The SEM apparatus is a "Cambridge Stereoscan S360" equipped with Oxford PentaFET EDX (Si(Li) detector) and a Oxford MONO-CL light collection system that can operate both in monochromatic (MC) or panchromatic (PC) mode (Figure 16). CL is collected with a diamond machined parabolic aluminium mirror which provides a large solid angle of collection and which is retractable for backscattered and secondary electrons imaging as well as EDX. This collector provides a parallel CL beam output incident on a quartz lens at the exit window and is used to improve the light throughput and the wavelength transmission efficiency.



Figure 15. The SEM-CL instrument

CL is collected with a diamond machined parabolic aluminium mirror which provides a large solid angle of collection and which is retractable for backscattered and secondary electrons imaging as well as EDX. This collector provides a parallel CL beam output incident on a quartz lens at the exit window and is used to improve the light throughput and the wavelength transmission efficiency.

A front surface plane mirror allows the CL beam to be directed towards the lens 1, which focuses it on one of the two detection system: the photomultiplier tube (PMT), in order to obtain a panchromatic CL image (PC mode), or the entrance slit of a grating spectrometer, for spectral analysis (MC mode). In both MC and PC modes, the exit light is focused onto a Hamamatsu R376 PMT with fused silica window (wavelength range: 160÷850 nm). In MC mode

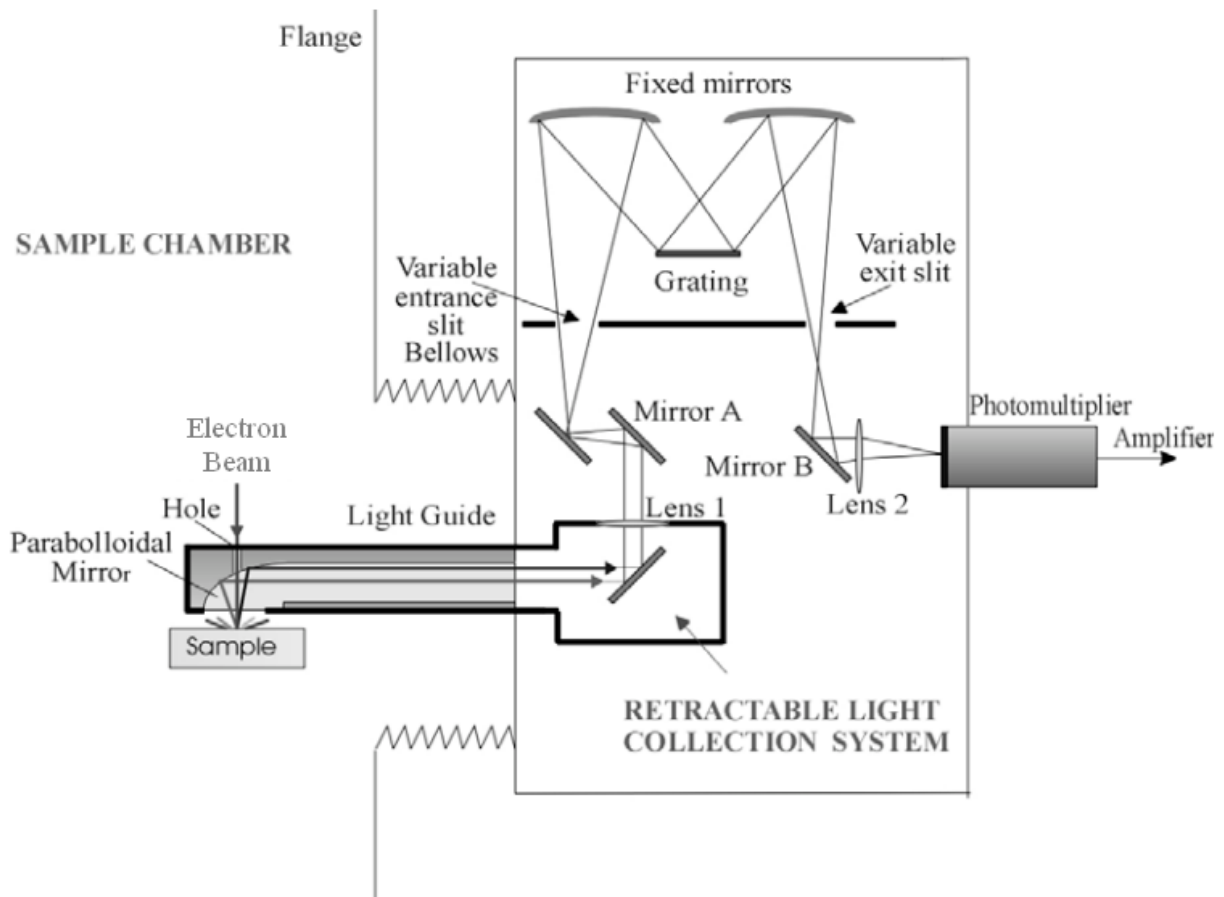
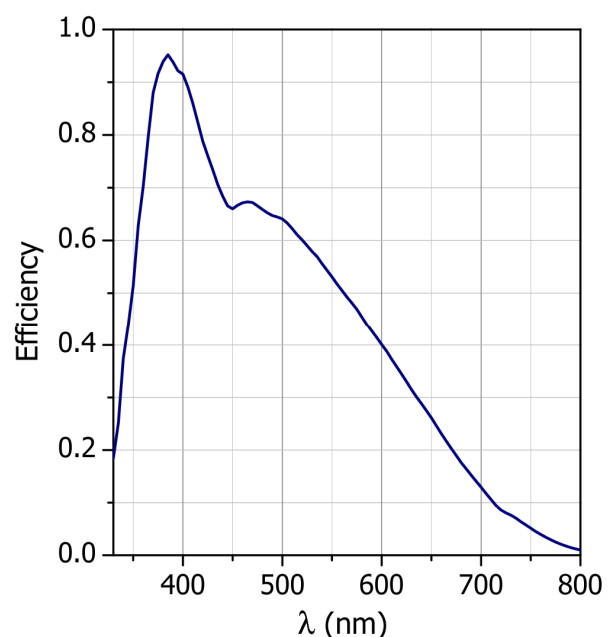


Figure 16. Scheme of the Oxford Instruments monoCL optical collection system in monochromatic mode [Vittone et al, 2001]

the monochromator uses a 1200 lines/mm diffraction gratings, with a spectral range of about 300÷900 nm. Combining the two effects, the instrument has a good response in the range 300÷800 nm and a wavelength resolution of the order of few nanometres, depending on monochromator slits aperture. The acquired spectra have to be corrected for the spectral response of the instrument shown in Figure 17. The range of the calibration where the response is reliable is about 350÷700 nm, even though something can be distinguished up to 800 nm, despite the noise is higher in this region. The spectra presented in this work are already calibrated and are obtained subtracting a constant value to the data, due to the PMT noise, and then dividing by the curve shown in Figure 17.



In order to compare the relevant photons emissions, spectra were collected

Figure 17. Curve of efficiency of the SEM-CL instrument

using the same operating conditions: working distance, magnification (5000 \times , scanning an area of about 20 \times 25 μm^2), probe current (1 nA and 20 nA) and voltage (15 kV). The probe current has two different values because many spectra exhibit a strong dependence on beam current density and therefore such parameter was kept at about 2–40 $\mu\text{A}/\text{mm}^2$, similarly to the value adopted in cold-CL analysis. To measure the real current value a Faraday cup, connected to an external amperometer, was put in the SEM chamber with the sample and the current has been checked before and after the analyses of each sample.

It is worth noticing that besides spectra, both in MC and in PC modes also luminescence maps can be collected, even if CL maps have been acquired mainly in MC mode owing to fluorescence phenomena. During SEM-CL analysis samples were not cooled at liquid nitrogen temperature to simulate measurement conditions on works of art. Also for these measurements, due to the low working pressure, semi-thin sections were carbon coated to avoid surface charging.

Simulations

We used two simulation codes to choose the proper probe energy, one for electrons and one for protons, to be sure to analyse only one crystal and not beneath it. The code for electrons is CASINO (version 2.42) [Drouin et al, 2007] that stands for “monte CARlo SIMulation of electroN trajectory in sOLids”, while for protons we used SRIM (version 2008.04) [Ziegler et al, 2010]. This last one is by now used by the whole IBA community and is essential to understand and predict ions interaction with matter. Its name, SRIM, stands for “the Stopping and Range of Ions in Matter” and it is actually a group of Monte Carlo programs which allow the simulation of a big variety of phenomena related to the interaction of MeV ions with matter: for example TRIM (Transport of Ions in Matter), one of the applications and the most popular, is able among other things to simulate ionisation profiles, ions 2D spatial distribution, damage calculations, ion ranges, surface sputtering, etc. In this work we use it mainly to obtain the dimensions of the probed volume in different minerals, valuating the penetration depth and the lateral straggling of ions of different energies in different mineral phases. In Table 12 the mean values (not the maximum) of both penetration depth and lateral straggling are reported: the

Table 12. The mean penetration depths and lateral straggling of different probes used in this work; the values are obtained by means of CASINO for electrons and SRIM for protons

Technique		CL		SEM-EDX		μ -PIXE			
Probe		15 keV electrons		20 keV electrons		600 keV protons		3 MeV protons	
Mineral	density (g/cm^3)	penetration depth (μm)	lateral straggling (μm)	penetration depth (μm)	lateral straggling (μm)	penetration depth (μm)	lateral straggling (μm)	penetration depth (μm)	lateral straggling (μm)
lazurite	2.41	1.34	0.79	2.24	1.30	6.87	0.40	83.2	3.35
diopside	3.29	0.96	0.56	1.59	0.95	5.18	0.32	60.6	2.54
pyrite	5.02	0.61	0.36	1.00	0.61	3.84	0.31	47.6	2.86

energy values both for electrons and protons are the ones selected for this work. In fact, before to choose the experimental conditions, other parameters to be valuated besides the probed volume are the maximum and minimum energies obtainable with the facility and the intensity of signal coming out from the sample at the selected energy, depending mainly on the cross-section and the geometry. Usually one tries to use the highest energy as possible, where cross sections are higher and consequentially the intensity of the signal. In this work, at the external facility of Firenze, μ -PIXE measurements were carried out on lazurite using a 3 MeV proton beam, that means a maximum penetration depth of about 85 μm . In this way the samples were probed along all their thickness, but the dimensions of analysed lazurite crystals were sufficiently large to avoid the presence of other minerals beneath the investigated ones.

For the characterisation of diopside, since this mineral shows luminescence, we try to find a correlation between luminescence peaks and trace element presence. For a more reliable comparison we choose to probe a volume the closest as possible of that analysed by means of CL (using a 15 keV electron beam), that has a maximum penetration depth of 2 μm and a maximum lateral straggling of about 2.5 μm . For this reason we used the minimum energy as possible, a 600 keV proton beam at the in vacuum facilities of LNL: it has a mean penetration depth of 5 μm and a lateral straggling below 1 μm (Figure 18). Such characteristics represent a good compromise between the reduction of cross section associated with the use of low-energy ions and the proximity to electron probed volume.

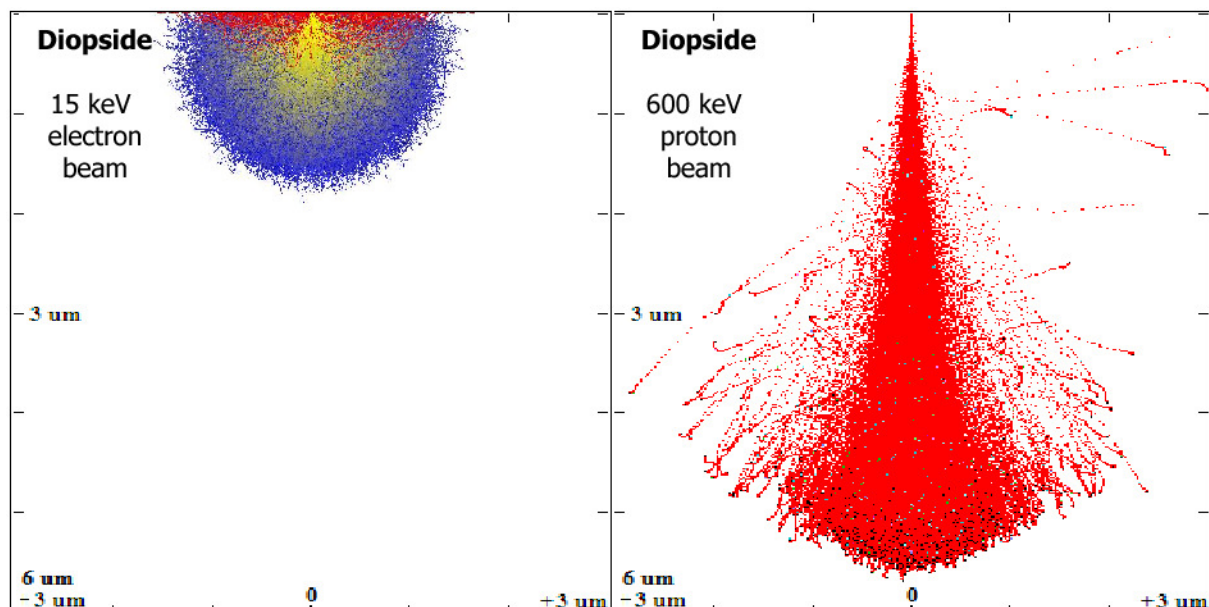


Figure 18. Comparison between 15 keV electrons (on the left) and 600 keV protons (on the right) in diopside by Monte Carlo simulations (software Casino and SRIM)

μ-Raman Spectroscopy

The μ-Raman Spectroscopy instrument used in this work is shown in Figure 19; it is property of the Interdepartmental Centre "G. Scansetti" and it is located at the Petrology and Mineralogy Department of the University of Torino. It is composed by the spectrometer "Jobin Yvon" (Mod. LABRAM HRVIS) and an optical microscope Olympus BX41. The confocal microscope permits transmitted light analyses, with the polarizer and can also acquire images with a colour camera. There are five objectives that permits up to 100× of magnification, with a spot of about 2 μm and the sample holder is motorized to easily find the point of interest.

The spectrometer Horiba Jobin Yvon HR800 has two grating with 1800 and 600 lines/mm and the CCD detector is air-cooled (-70°C). The user can choose between two polarized laser: one HeNe red laser (with a wavelength of 633 nm and a power of 20 mW) and one Nd solid state green laser (with a wavelength of 532 nm and a power of 100 mW). The system is completed by two filters Super Notch Plus for laser lines (633 nm and 532 nm) and by a set of interferential filters. The spectral resolution achievable with the 1800 l/mm grating is 2 cm⁻¹ with the green laser and 1.5 cm⁻¹ with the red laser. On the PC the software Labspec 5 permits to acquire and elaborate spectra.



Figure 19. The μ-Raman Spectroscopy instrument

and the CCD detector is air-cooled (-70°C). The user can choose between two polarized laser: one HeNe red laser (with a wavelength of 633 nm and a power of 20 mW) and one Nd solid state green laser (with a wavelength of 532 nm and a power of 100 mW). The system is completed by two filters Super Notch Plus for laser lines (633 nm and 532 nm) and by a set of interferential filters. The spectral resolution achievable with the 1800 l/mm grating is 2 cm⁻¹ with the green laser and 1.5 cm⁻¹ with the red laser. On the PC the software Labspec 5 permits to acquire and elaborate spectra.

For our measurements we always used the green laser and the 600 l/mm grating; we changed the magnification (20× and 50×), the integration time (from 20 to 30 seconds) and each spectrum is the mean of a number of spectra varying from 1 to 5. To recognise the mineralogical phases we compared the acquired spectra with a reference database (RRUFF, University of Arizona).

RESULTS ON ROCKS

Due to the heterogeneity of lapis lazuli it is very difficult to identify provenance markers analysing elemental composition of the whole rocks or works of art. At the same time it'll require very long time to deeply analyse all the phases inside this stone. For this reason we analysed differences inside single phases instead of the whole stone, mainly focusing on two of the main phases: lazurite, the main phase of lapis lazuli responsible for the blue colour, and diopside, one of the more frequent accessory mineral characteristic of all the Asian samples. Recently we're studying a third phase, the pyrite, but the results are not conclusive yet. This study was performed by means of ion beam techniques (PIXE and IL) but was preceded and completed by means of microanalysis with scanning electron microscopy (SEM-EDX), cathodoluminescence spectra and maps (both cold-CL and SEM-CL) and μ -Raman Spectroscopy measurements. We demonstrated that results obtained by means of PIXE confirm SEM-EDX analyses, providing more information about trace elements; analogously IL spectra are very similar to CL spectra. This is the reason since we decided to use electron probe techniques as a preliminary characterisation and ion probe techniques as a confirmation of the results and to study works of art. Despite the limited number of analyzed samples, results are sufficient to exclude/suggest few features as provenance markers, partly confirming what previously published in literature.

The structure of this chapter is the following: the next paragraph clarifies the procedure adopted for the measurements and presents the preliminary characterization of the samples; in the sequent paragraphs the best results obtained for each phase are collected, mainly focusing on lazurite and diopside; in the last two paragraphs we'll summarize the markers found for each provenance and we'll propose a protocol to distinguish among the four provenances analysed in this work, testing it on a sample of unknown provenance.

Preliminary characterisation

The first step of the characterisation has been the observation of all the samples in reflection mode by means of an optical microscope to have some optical maps to use as a reference during the analyses and as a comparison with other mapping techniques (Figure 20).

After this, even if it was not the aim of this work and the samples were not prepared for this kind of measurements, the semi-thin sections have been observed in transmitted light, to have some basic petrographical information (Figure 21). Because of their thickness, more than

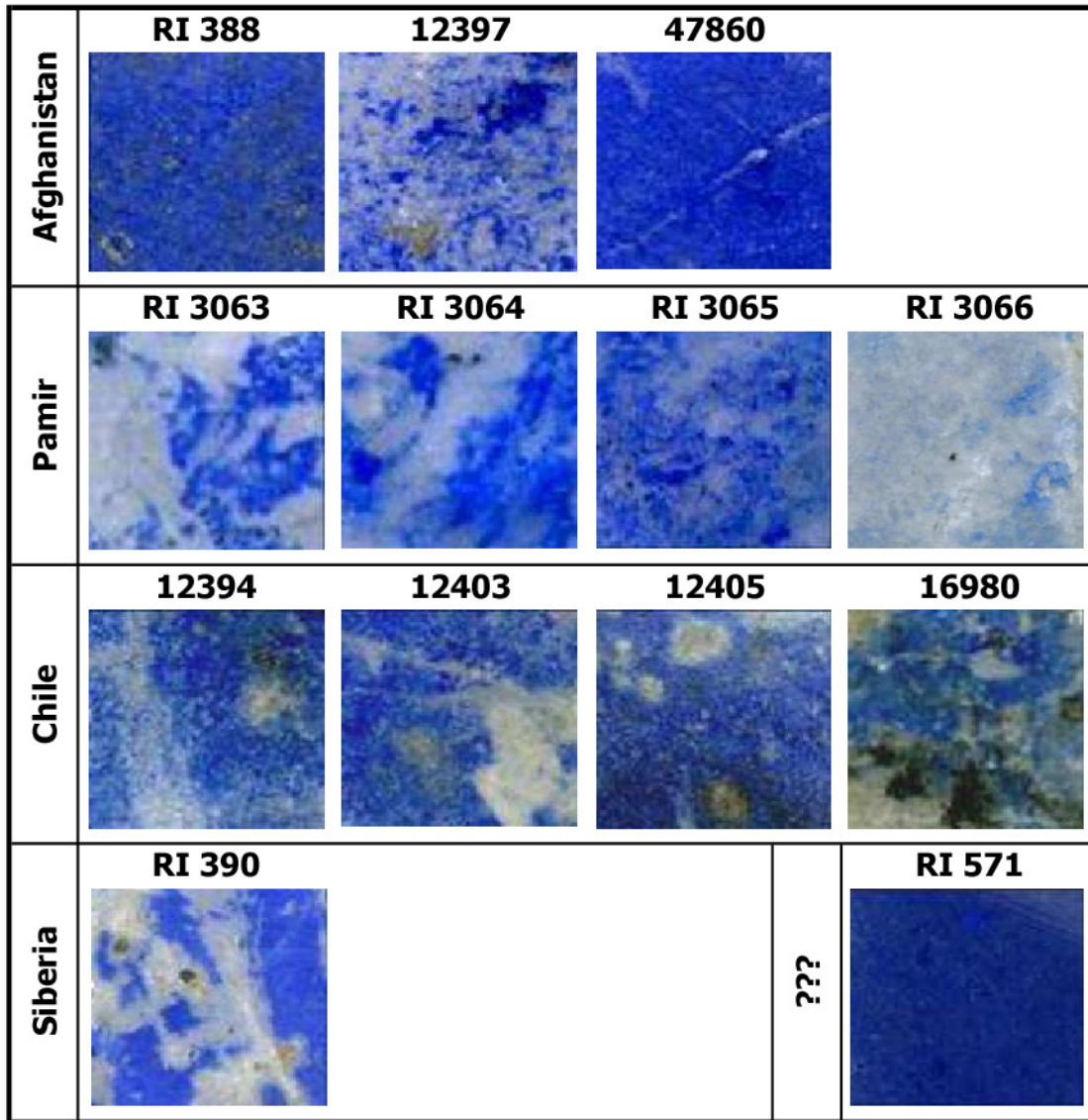


Figure 20. Optical reflection images of the samples: each square is 6 mm wide and is representative of the semi-thin section [Lo Giudice et al, 2009]

double respect to ordinary thin-sections, just one polarizer could be used and not all the samples give us information; in particular the Chilean ones were too thick (about 100 μm) to obtain significant images. From this characterization results that in samples coming from Pamir the distribution of lazurite varies, depending on the sample, from a concentration in nodule of millimetric and sub-millimetric dimensions, to a wide diffusion in all the sample. It is associated to plagioclase and there is also a wide presence of a pyroxene, later recognised as diopside with other techniques. Other crystals that have been detected are: amphibole, calcite, pyrite and white mica. In Afghan samples the same minerals are present, but the texture is different and there is a relevant presence of pyrite crystals uniformly distributed, in some cases reaching dimension of 1 mm. Lazurite crystals, with dimensions of some tenth of microns, create an aggregate very fine, forming large areas of blue mineral, crossed by vein of other minerals or with small inclusions of other minerals diffused in all the sample. The sample coming from

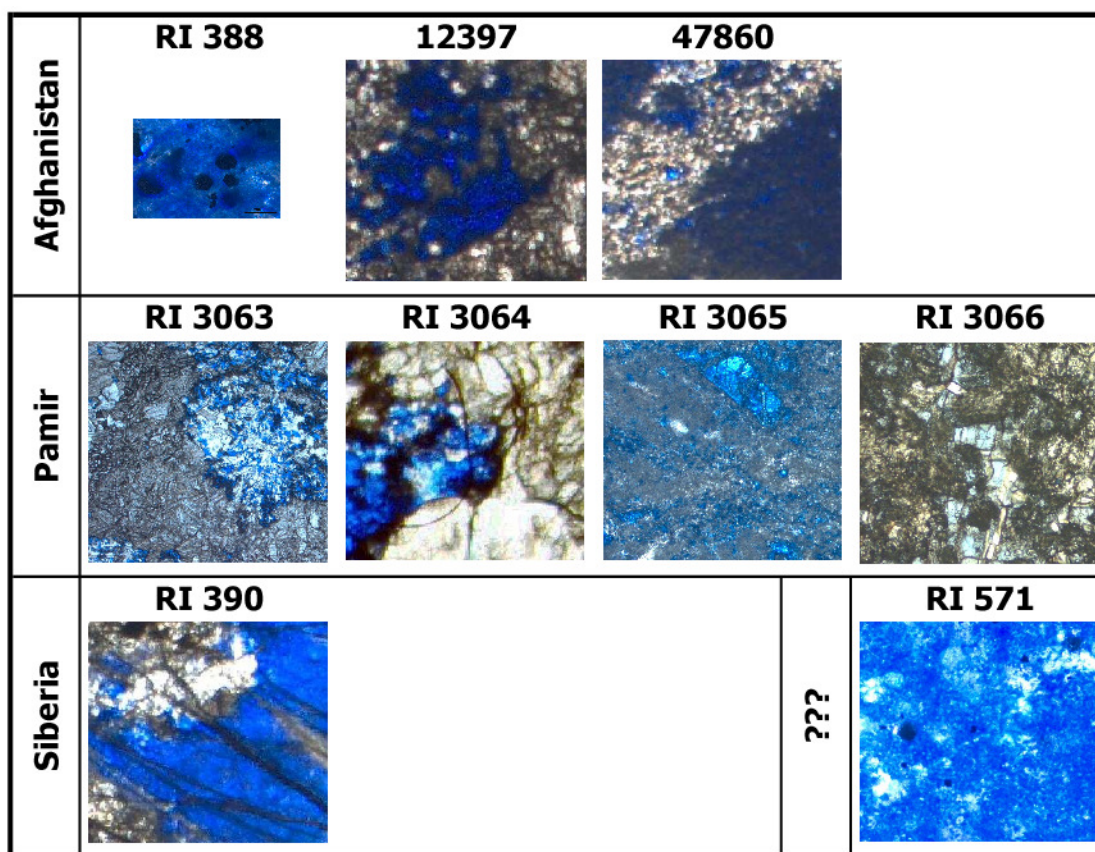


Figure 21. Optical transmission images of the samples: each square is 1.5 mm wide and is representative of the semi-thin section

Siberia has a coarser grain, with big mono-mineral regions of lazurite and diopside, and greater crystals of pyrite respect to samples coming from other provenances. Finally, the sample of unknown provenance is characterised by a very fine grain, with lazurite and pyrite distribution similar to the Afghan one.

The next step for the characterisation have been the cold-CL measurements: images of the whole surface were acquired from all the samples using the experimental conditions already mentioned; only camera integration time was modified during the measurements. To map all the sample, many picture were necessary, since the area of each picture is just $1.3 \times 1.7 \text{ mm}^2$. After the acquisition all the images have been joined to form a complete map of the sample; an example is shown in Figure 22. In Figure 23 a representative collection of the obtained images for each sample is shown. Average luminescence intensity is similar in all samples except for the Siberian sample, which is more than five times less luminescent. From cold-CL images the distribution and intensity of luminescent mineral phases are clear and minerals were later identified mainly by means of EDX analysis. With the exception of the Siberian sample, CL images are dominated by a white-yellow luminescent phase that was identified as wollastonite in Chilean Lapis Lazuli and as diopside in the other samples. Another abundant common mineral phase shows a blue-azure luminescence; it was attributed to K-feldspars and it is the main

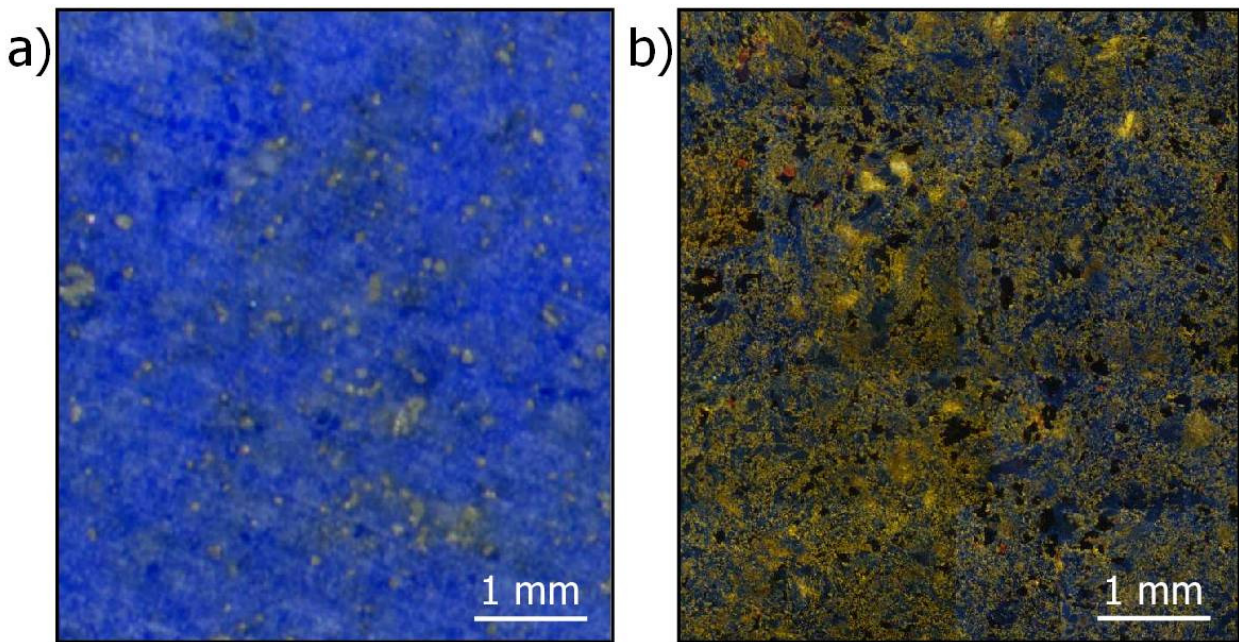


Figure 22. a) Optical image in reflection mode of the central part of the sample Afghanistan RI388; b) cold-CL image of the same area; the CL image is a join of many picture to map all the area of interest.

feature of the Siberian sample. All the K-feldspars observed in lapis lazuli under investigation exhibit a lower luminescence with respect to diopside; this is the reason for the poor luminescence of this sample. Another significant feature is the orange-red colour that was associated to calcite crystals. Lazurite, which is responsible for the blue colour of Lapis Lazuli, shows a very weak luminescence and can be recognized as dark blue; for example in RI3065 the three regularly shaped dark regions are well formed lazurite crystals. The latter phase is dominant in Afghanistan samples. Lastly, pyrite does not exhibit any luminescence and therefore appears as black. Crystal dimensions vary from few microns to hundred of microns but do not seem to be related to different provenances. Apart from wollastonite found only in Chilean samples, all the above-mentioned phases were found in different proportions in all the samples.

After this preliminary mapping we started the analysis on single crystals using a SEM and for this reason it was necessary to carbon-coat the samples to avoid charging effects during the measurements. In this phase we decided to cover only half the sample, leaving uncoated the other half for further analysis that can be influenced by this treatment. Moreover we studied almost the central part of the samples, in correspondence of the hole done for IBA. The crystals to be analysed have been selected among the biggest for each colour on the base of cold-CL maps. We used both SEM-CL, to obtain a luminescence spectrum for each colour in cold-CL maps, and SEM-EDX, to have a quantitative analysis of the main elements in each phase. In order to acquire data with significant statistics, CL and EDX spectra for each luminescent phase were collected in all the samples, for a total of about 450 acquisitions for

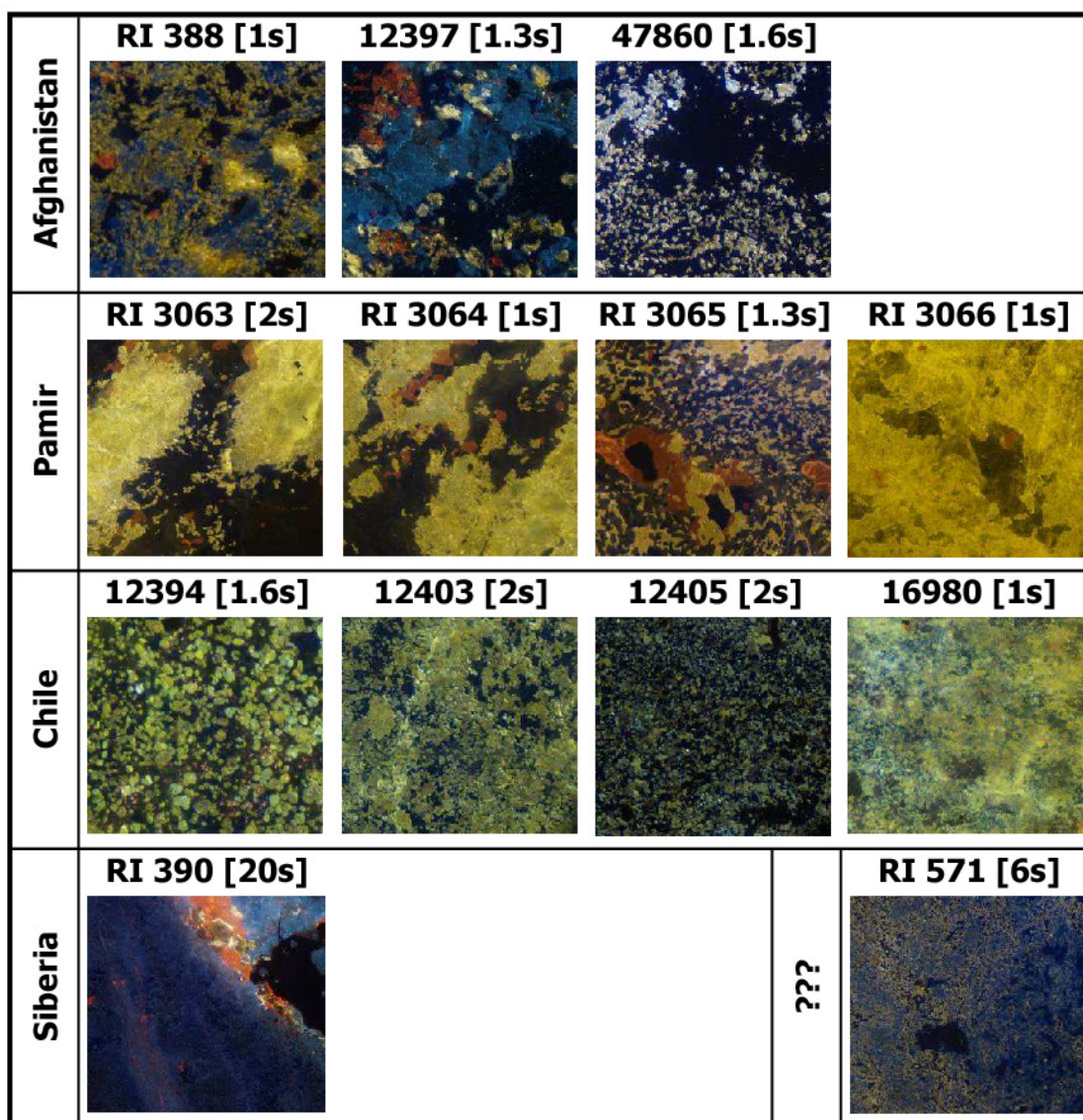


Figure 23. Representative cold-CL images of the samples: each square is 1.3 mm wide; the exposition time is reported in square brackets [Lo Giudice et al, 2009]

each technique. The quantitative analysis allowed to associate a chemical composition to each phase, obtaining in many cases a univocal correspondence between a certain composition and a colour of luminescence. It has often been possible to recognize the phase thanks to the chemical composition, comparing it to the phases already found in lapis lazuli by other authors (Table 2) and acquiring a Raman spectrum of the biggest crystals to confirm the identification of the phase. After this step, for the most important and diffused phases, also the trace elements composition have been investigated, by means of PIXE. In parallel IL measurements have been performed, always confirming the results obtained by means of CL; combining PIXE and IL measurements sometimes it is possible to find a correlation between the presence (or absence) of an element and a certain peak of luminescence, confirming that an element is an activator (or a quencher) for the luminescence.

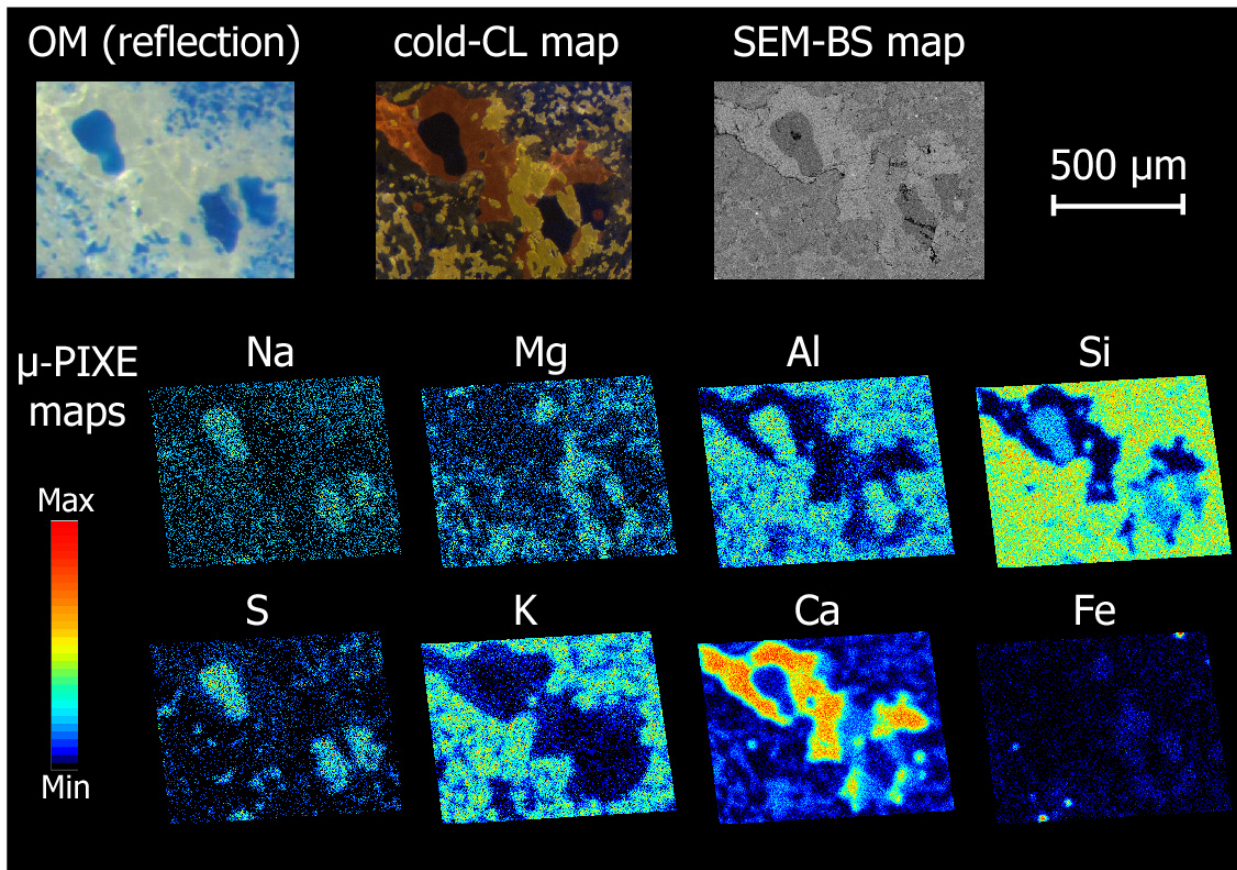


Figure 24. μ -PIXE elemental maps complemented by optical reflection, cold-CL and SEM-BS maps of the same area of sample *Pamir RI3065*. The PIXE measurements were performed at the external microbeam line of LABEC in Firenze. It's easy to recognize the different phases of the lapis lazuli [Re et al, 2011].

To be sure to analyse the same crystal by means of all the techniques, a map was always collected to select the analysing point. For SEM-EDX measurement the point was selected using mainly back-scattered electrons images, while for SEM-CL measurement we used the monochromatic CL maps centred on the wavelength emission of the main mineral (diopside or wollastonite). In Figure 24 a comparison between optical microscopy in reflection mode, BS electron map, cold-CL map and μ -PIXE elemental maps of the same area is shown. The μ -PIXE maps have been obtained at the external microbeam line at LABEC: due to the good spatial resolution, the capability to distinguish and then individually analyse mineral phases in lapis lazuli is evident. The lazurite crystals can be identified thanks to the correlation of both sodium and sulphur distributions. The upper lazurite crystal is embedded in a calcite formation, while one of the lower crystals is surrounded by diopside (characterized by a high magnesium content). All around, many veins of K-feldspars are visible that obviously show a high potassium content while the iron map shows few small pyrite grains.

The last way we developed to rapidly obtain the luminescence map of a sample under IBA investigation is Defocused Ion Beam Induced Luminescence. This technique is suitable for artworks, but we also performed a test on one of the samples already studied with cold-CL. In

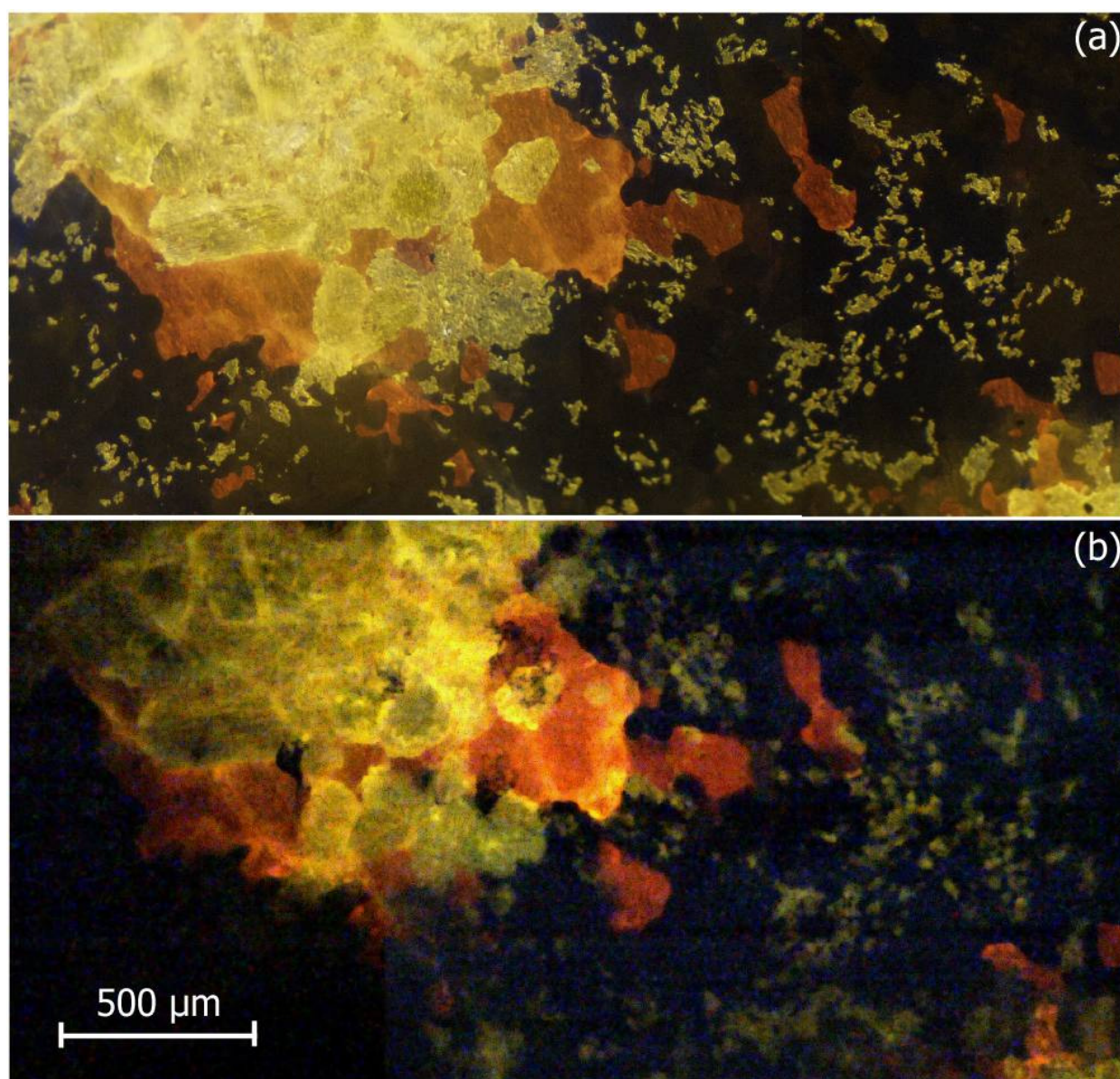


Figure 25. Comparison of the same area of the sample Pamir RI3063 acquired by means of: (a) cold-CL; (b) defocused-IBIL, performed at the external microbeam line of LABEC in Firenze

Figure 25 a comparison between cold-CL map (obtained with 15 keV electrons in vacuum) and defocused-IBIL map (obtained with 3 MeV protons in air) of the same area is shown: the two images present the same colour of luminescence, yellow for diopside, orange for calcite and dark blue for lazurite.

Lazurite

From the examination of cold-CL maps, more than a hundred points of interest in lazurite $((\text{Na,Ca})_8\text{Al}_6\text{Si}_6\text{O}_{24}(\text{SO}_4,\text{S,Cl,OH})_2)$ on all the samples were identified for quantitative SEM-EDX analysis. Some of these points have been analysed also by means of μ -Raman spectroscopy to confirm the identification of this phase comparing them with a reference Raman spectra; all the reference Raman spectra presented in this work have been taken from

the RRUFF database (University of Arizona). In Figure 26 a comparison of lazurite Raman spectra with a reference one is shown; the main peaks are in the same position and have the same relative intensity of the standard; there are some differences only in small peaks, but these can be due both to a signal coming from

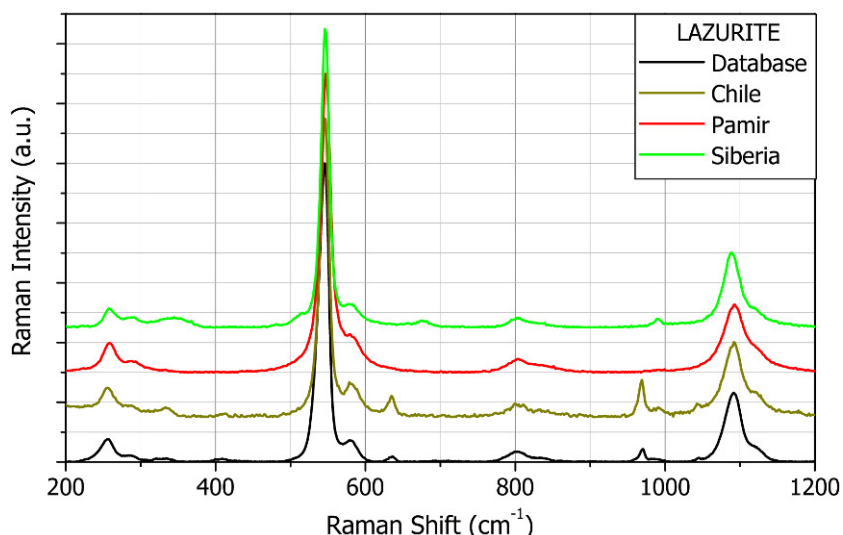


Figure 26. Selection of Raman spectra of lazurite compared to a reference spectrum from the database RRUFF

crystals close to the one under analysis, both to the possibility of different Raman response of different crystals. We have not gone deeper on this aspect (until now) because it was not the main aim of this work.

With SEM-EDX analyses on lazurite only main elements were observed, with a percentage varying slightly inside the same samples and within samples of the same provenance. The presence of Cl^- , OH^- , SO_4^{2-} and S^{2-} ions significantly complicates the calculation of the chemical formula of lazurite, since microprobe analysis does not determine the hydroxyl ion and the sulphate and sulphide ions are measured as total S [Aleksandrov and Senin, 2006]. In Table 13 the mean composition of lazurite is reported. It was compared to other two studies containing many measurements on lazurite from various provenances by means of EDX [Aleksandrov and Senin, 2006; Ballirano and Maras, 2006]: the values are comparable, even if in our samples we detected a lower mean amount of sodium. This fact has often been reported and could be caused by the volatilization of the sodium in the electron beam, even when it is defocused [Deer et al, 2004]. It is worth noting that this was the first run of measurements on these kind of samples and in the future

Table 13. SEM-EDX and μ -PIXE (3 MeV protons at the external microbeam line of LABEC in Firenze) analyses of lazurite crystals; the last two columns are calculated from [Aleksandrov and Senin, 2006; tables from 1 to 4] and [Ballirano and Maras, 2006; table 8]. The mean values are in bold type and the standard deviation are in italic type. All the values are normalized to 100%.

	SEM-EDX (110 points)		μ -PIXE (9 points)		[Aleksandrov and Senin, 2006] (39 samples)		[Ballirano and Maras, 2006] (8 samples)	
Na₂O	10.08	<i>2.63</i>	16.43	<i>3.28</i>	17.44	<i>1.95</i>	18.69	<i>0.66</i>
MgO	0.16	<i>0.77</i>	0.40	<i>0.55</i>	0.14	<i>0.41</i>	0.04	<i>0.04</i>
Al₂O₃	26.00	<i>1.78</i>	28.52	<i>1.07</i>	27.18	<i>1.25</i>	26.96	<i>0.43</i>
SiO₂	34.63	<i>2.12</i>	34.74	<i>3.15</i>	34.00	<i>1.71</i>	34.28	<i>0.41</i>
SO₃	18.55	<i>4.04</i>	12.24	<i>2.48</i>	12.43	<i>2.00</i>	14.11	<i>0.67</i>
Cl	0.80	<i>1.22</i>	0.46	<i>0.21</i>	0.33	<i>0.24</i>	0.62	<i>0.24</i>
K₂O	0.96	<i>1.42</i>	1.17	<i>1.02</i>	0.57	<i>1.06</i>	0.53	<i>0.24</i>
CaO	8.82	<i>3.60</i>	5.84	<i>2.47</i>	7.18	<i>1.76</i>	4.72	<i>0.70</i>
Others	0.01	<i>0.07</i>	0.20	<i>0.61</i>	0.86	<i>1.52</i>	0.06	<i>0.02</i>

we will try to improve the sodium quantification. In Figure 27 the potassium vs sulphur content graph, normalized to the sum of aluminium and silicon contents, is reported in a logarithmic graph; these features represent the more interesting elements in terms of provenance markers. In fact, despite an overlapping of points relevant to Pamir Mountains and Siberia samples, the low concentration of potassium in Chilean stones and

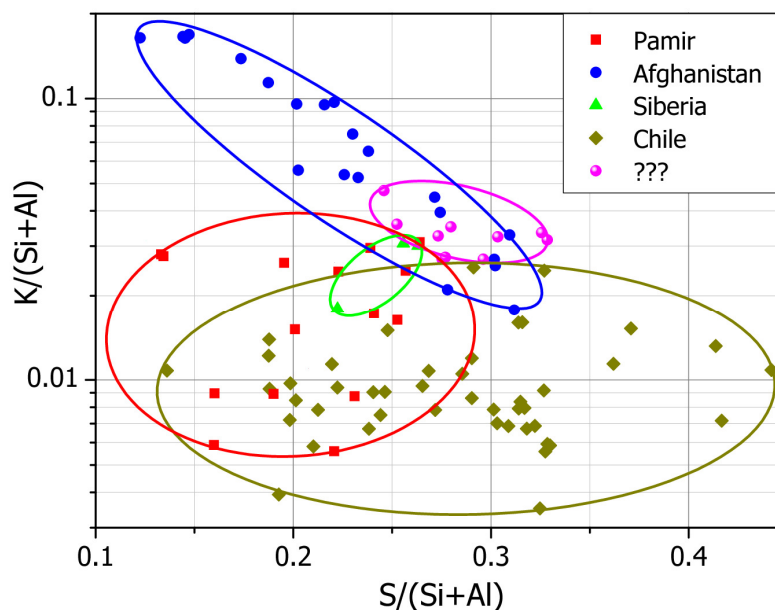


Figure 27. Elemental contents in lazurite from SEM-EDX analysis: potassium vs sulphur, normalized to the sum of aluminium and silicon (all expressed in %w) [Re et al, 2011].

the practically linear correlation in Afghan samples are evident. In particular, it seems that Afghan samples are the only ones characterised by lazurite crystals with both low sulphur and high potassium contents. It is worth noting that 16 point (5 from Chile and 11 from Pamir) present a potassium content below the limit of detection of the instrument and for this reason does not come out in the graph.

About ten points of interest investigated by means of SEM-EDX were also analysed using the μ -PIXE at the external beam facility of LABEC obtaining comparable results. In Table 13 the main elements concentration are reported, while in Figure 28 the results regarding trace elements in lazurite are shown; the coloured column indicates the average elemental content and the dark points represent the individual measurements. At present, significant PIXE information come from barium and strontium contents. In fact all the lapis lazuli samples show a barium contents that is below the instrument sensitivity, with the exception of the Siberian sample, in which the average content is higher than 2%. Also strontium concentration is more than ten times higher in Siberian lapis lazuli (3000 ppm) in comparison with other provenances. Unluckily for the moment we have just one Siberian sample, so we still do not know the variability of barium and strontium in rocks from this provenance, but it is our intention to improve the statistic on other samples with the same origin. In any case these results confirm previous works on Siberian lapis lazuli [Delmas and Casanova, 1990; Ivanov et al, 1976] and can be used to distinguish this provenance from the others. It is important to observe that barium and strontium cannot be incorporated in lazurite but are present in small grains of another phase not yet identified (whose dimensions are below the resolution capabilities of the employed microbeam facilities), as observed by means of a SEM analysis. Similar grains were

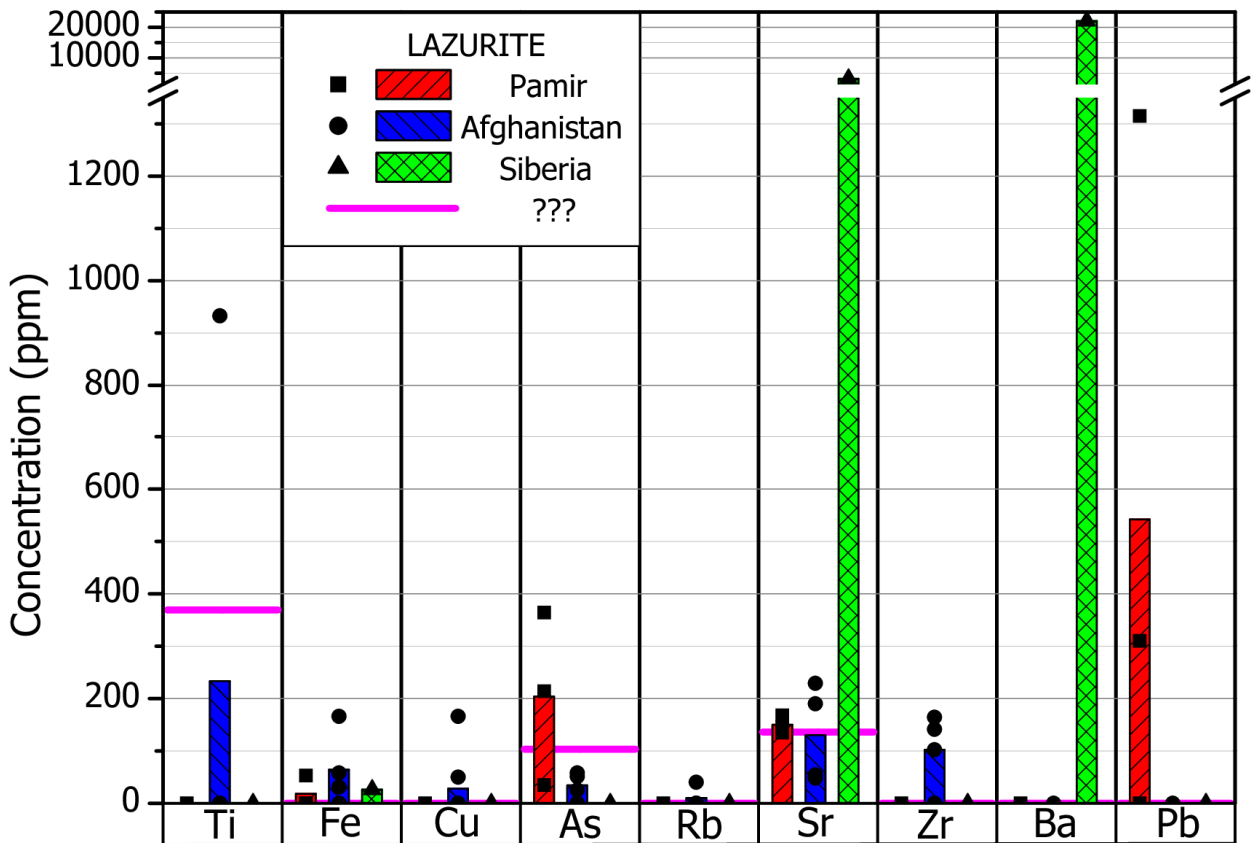


Figure 28. Minor and trace elements in lazurite from μ -PIXE measurements performed at the external microbeam line of LABEC in Firenze. The coloured columns indicates the average elemental content and the dark points represent the individual measurements [Re et al, 2011]

observed also in other lapis lazuli phases. Further results consist in the higher quantity of arsenic in samples from Pamir Mountains, as well as of zirconium in Afghan samples, even if the latter seems to be present in small inclusions of a phase not yet identified. Other elements, detected only in few points are: titanium (in one point in an Afghan sample), iron (in few samples from all provenances), copper (in two points in one sample from Afghanistan), rubidium (only in one point in an Afghan sample), lead (in two points in one sample from Pamir).

In all the samples, lazurite has a very weak luminescence and spectra show the same bands of the main luminescent phases, i.e. wollastonite in Chilean, K-feldspar in Siberian and diopside in the other samples. This can be attributed to the contaminations of these phases inside the lazurite or to luminescence generated by multiple scattering during measurements (i.e. electrons, during SEM-CL analyses, hit strong luminescent phases after backscattering from the detectors that is very close to the surface of the sample). In any case, such luminescence is too weak to be useful for any provenance study.

Diopside

Diopside ($\text{CaMgSi}_2\text{O}_6$) is the second analysed phase; with the exception of Chilean samples, it was found in all lapis lazuli. More than eighty points of interest were selected to be analysed by means of quantitative SEM-EDX and among these a few number have been analysed also by means of μ -Raman

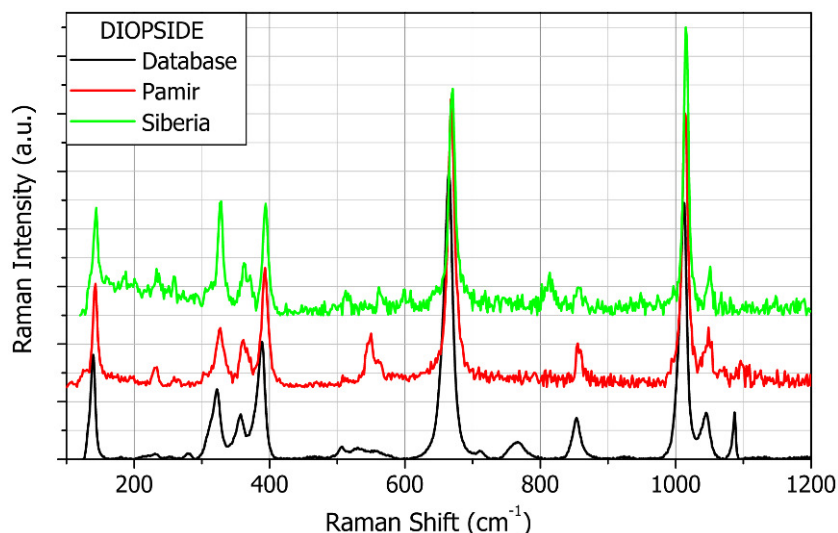


Figure 29. Selection of Raman spectra of diopside compared to a reference spectrum from the database RRUFF

spectroscopy. In Figure 29 a selection of Raman spectra of these points are shown, confirming that the crystals under analysis are diopside. As for the lazurite spectra, the positions and relative intensity of the peaks are the same of the reference spectrum, taken from the RRUFF database. The presence of some minor peaks in the spectra can be due to a crystal near to the one under analysis: for example the peak at 560 cm^{-1} present in the spectrum from Pamir (Figure 29) corresponds to the main peak of the lazurite (Figure 26).

The mean composition of diopside obtained by means of SEM-EDX is reported in Table 14 and is compared to the same two studies already used for comparison of lazurite [Aleksandrov and Senin, 2006; Ballirano and Maras, 2006]. They also contain some measurements on diopside from various provenances by means of EDX and the values are comparable. In Figure 30 the compositional diagram of pyroxenes is shown; the complete

Table 14. SEM-EDX and μ -PIXE (600 keV protons at the in vacuum microbeam line of LNL in Legnaro and 3 MeV protons at the external microbeam line of LABEC in Firenze) analyses of diopside crystals; the last two columns are calculated from [Aleksandrov and Senin, 2006; table 6] and [Ballirano and Maras, 2006; table 9]. The mean values are in bold type and the standard deviation are in italic type. All the values are normalized to 100%.

	SEM-EDX (85 points)	μ -PIXE LNL (19 points)	μ -PIXE LABEC (5 points)	[Aleksandrov and Senin, 2006] (11 samples)	[Ballirano and Maras, 2006] (8 samples)
SiO₂	55.43 <i>1.01</i>	55.96 <i>0.91</i>	53.72 <i>0.67</i>	54.33 <i>0.82</i>	55.35 <i>0.71</i>
TiO₂	0.06 <i>0.24</i>	0.19 <i>0.14</i>	0.09 <i>0.09</i>	0.13 <i>0.24</i>	0.28 <i>0.18</i>
Al₂O₃	2.76 <i>2.07</i>	3.58 <i>1.25</i>	2.85 <i>1.32</i>	2.08 <i>1.48</i>	5.09 <i>1.57</i>
FeO	0.10 <i>0.43</i>	0.20 <i>0.54</i>	0.07 <i>0.07</i>	0.39 <i>0.49</i>	0.04 <i>0.04</i>
MgO	16.84 <i>1.50</i>	14.26 <i>1.12</i>	17.91 <i>1.50</i>	18.09 <i>1.15</i>	15.20 <i>1.34</i>
CaO	23.45 <i>2.01</i>	25.36 <i>1.31</i>	23.92 <i>0.97</i>	24.20 <i>0.81</i>	21.18 <i>1.77</i>
Na₂O	1.26 <i>1.13</i>	-	1.08 <i>1.16</i>	0.74 <i>0.60</i>	2.82 <i>0.88</i>
K₂O	0.03 <i>0.19</i>	0.06 <i>0.06</i>	0.04 <i>0.09</i>	0.00 <i>0.01</i>	0.05 <i>0.02</i>
Others	0.06 <i>0.27</i>	0.40 <i>0.31</i>	0.30 <i>0.33</i>	0.04 <i>0.05</i>	-

overlapping of the composition of the samples from different origin is clear. It can be concluded that the concentration of major elements in diopside cannot be used as a useful criterion for provenance attribution.

μ -PIXE analysis was carried out both at Legnaro laboratory on about twenty points of interest and at the LABEC laboratory on 5 points of interest. There was a very good accordance with SEM-

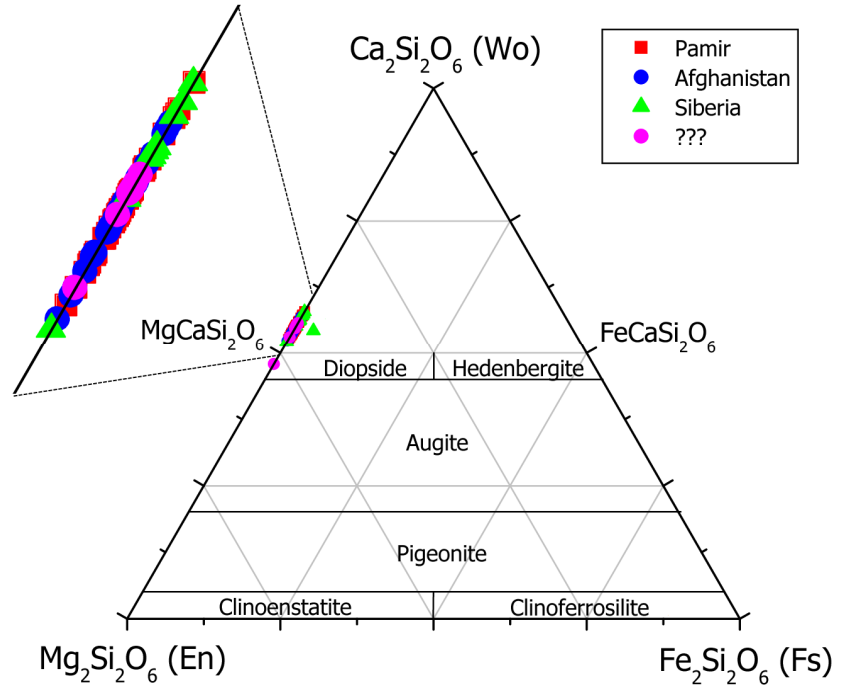


Figure 30. SEM-EDX analyses of major elements contents in diopside displayed in the diagram of piroxenes [Re et al, 2011]

EDX analysis about major elements contents, as shown in Table 14. The only difference is the absence of sodium in the points analysed at the Legnaro laboratory: this is due to the fact that

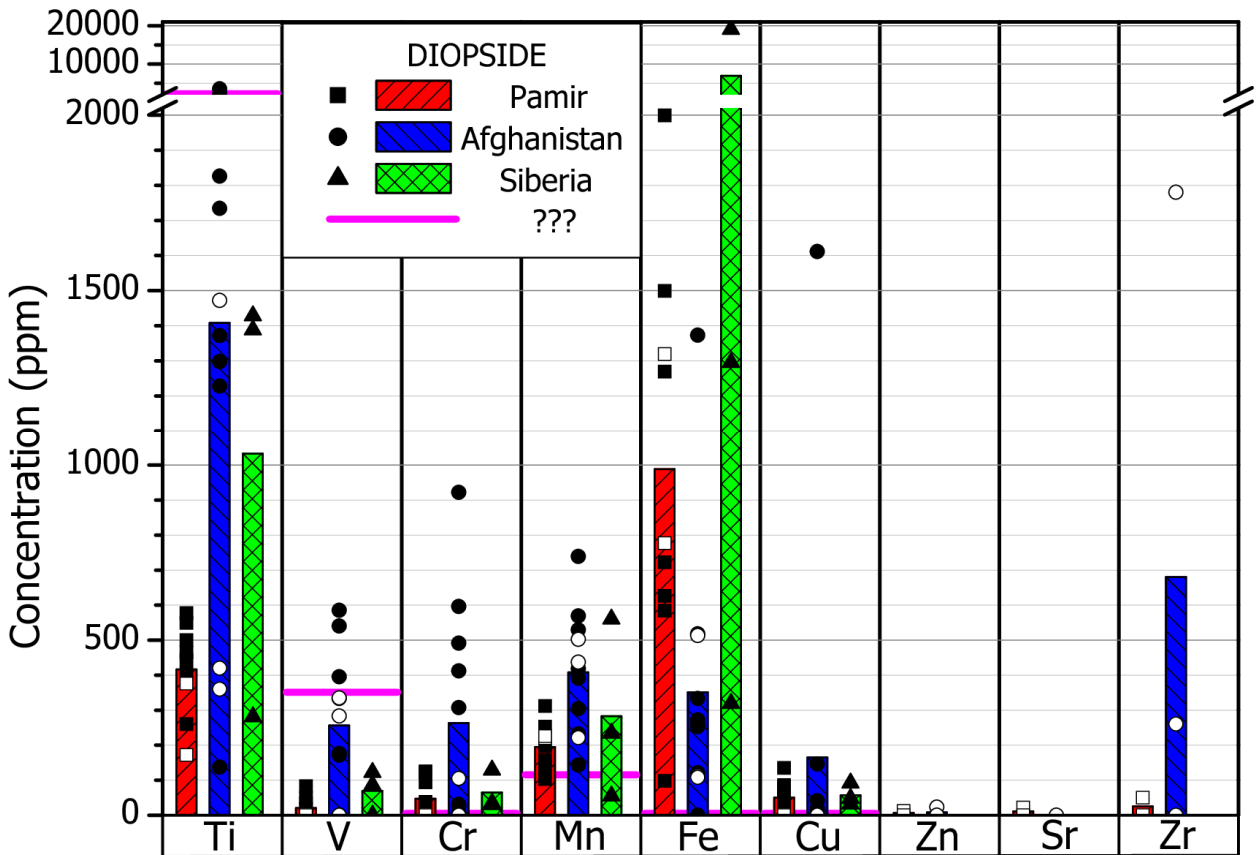


Figure 31. Minor and trace elements in diopside from μ -PIXE measurements performed at the in vacuum microbeam line of LNL in Legnaro with 600 keV protons (in black) and at the external microbeam line of LABEC in Firenze with 3 MeV protons (in white). The coloured columns indicates the average elemental content and the points represent the individual measurements [Re et al, 2011]

using one PIXE detector with an aluminium filter (to be more sensitive to heavier trace elements) we could not detect sodium because its characteristic X-rays are mainly absorbed by the filter and do not reach the detector. Results about trace elements are shown in Figure 31. Identified trace elements are common in all diopside crystals, but they are present at different concentrations, if we compare samples from Pamir Mountains and from Afghanistan. In fact, all the samples coming from Pamir Mountains show concentration in titanium, vanadium and chromium lower than those found in Afghan samples, but on the other hand a higher quantity of iron is observed. Siberian sample does not show any evident difference with respect to the other samples. It is worth stressing that the results have been obtained using two setups with many differences: measurements in vacuum with 600 keV protons at LNL and in air with 3 MeV at LABEC; mineral standard used as references at LNL and mono-elemental standard used at LABEC; one PIXE detector at LNL and two at LABEC. With the detector optimized for heavier elements at LABEC we detected also: zinc (in two points one from Pamir and one from Afghanistan), strontium (in one point from Pamir) and zirconium (in two points from Afghanistan and a very small quantity in one from Pamir).

Almost the same number of points analysed by SEM-EDX (a mean of eight per sample) has also been analysed by means of SEM-CL. The spectra of each sample are quite similar among them, especially for presence or absence of a feature and shape and position of each bands; the only variable inside the sample were the intensity of the bands. A selection of calibrated spectra, one for each provenance, is shown in Figure 32. The position of the bands can be valuated qualitatively, but to compare spectra a fitting procedure is necessary; for this purpose the wavelength (λ) has to be converted in energy (E) with the formula:

$$E(eV) = \frac{1239.8}{\lambda(nm)}.$$

Then a sum of five Gaussian curves has been used to fit each spectrum, as shown in Figure 33 (since this spectrum is expressed in Energy, right and left are inverted respect to the previous one, expressed in wavelength). Two of them just help to fit the extreme parts

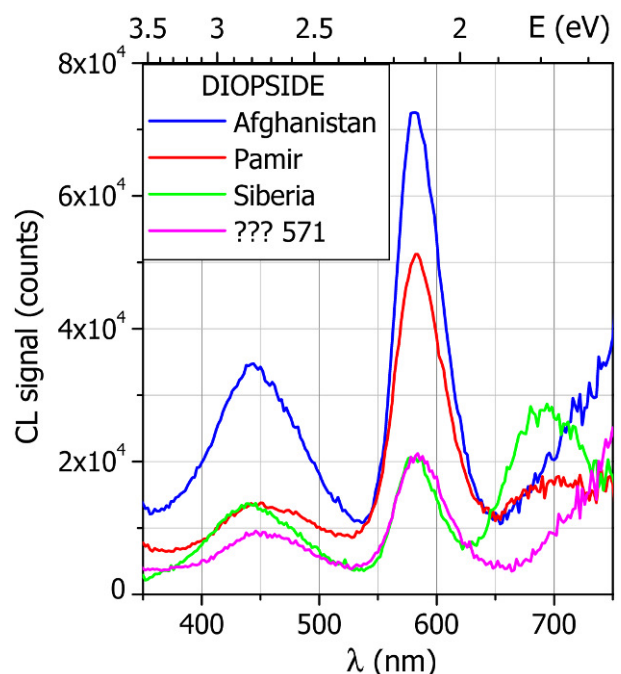


Figure 32. Selection of calibrated CL spectra of diopside in different samples (from *Afghanistan 12397*, *Pamir RI3063*, and *Siberia 390*)

Table 15. Parameters of CL bands in a selection of spectra of diopside; the values reported are mean \pm standard deviation obtained by the fit

Band	Provenance		Energy (eV)	λ (nm)
a	all (9 spectra)	center	2.75 ± 0.04	451 ± 7
		width	0.61 ± 0.07	101 ± 12
b	all (9 spectra)	center	2.12 ± 0.01	585 ± 2
		width	0.17 ± 0.02	47 ± 5
c	Afghanistan (3 spectra)	center	1.69 ± 0.02	733 ± 7
		width	0.17 ± 0.04	72 ± 17
	Pamir (4 spectra)	center	1.79 ± 0.01	693 ± 2
		width	0.21 ± 0.05	82 ± 20
	Siberia (1 spectrum)	center	1.78	696
		width	0.20	78
???	(1 spectrum)	center	1.65	750
		width	0.16	73

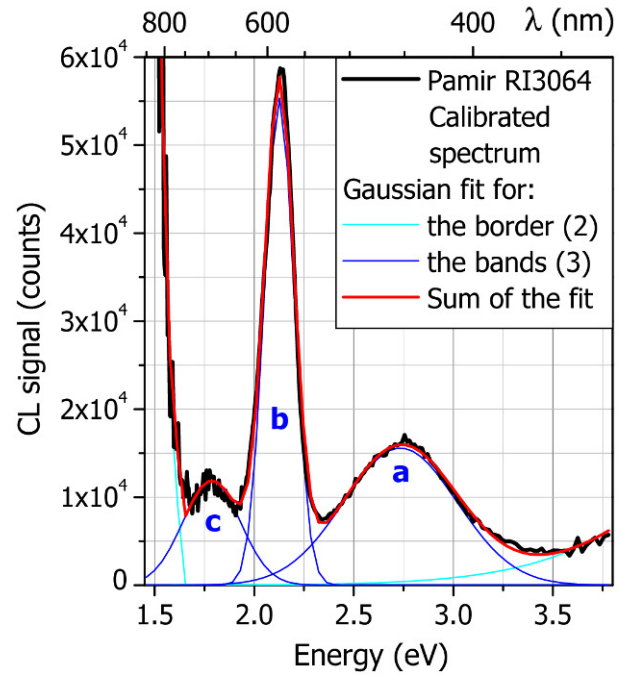


Figure 33. Example of the fit on a calibrated CL spectrum of diopside (Sample *Pamir RI3064*)

of the spectrum, but have no physical meaning; the other three represent the

luminescence bands and their parameters, obtained in Energy, have to be converted in wavelength, for convenience to compare them to other works. The formula used for the fit is:

$$y = \sum_{i=1}^5 \frac{A_i}{w_i \sqrt{\pi/2}} e^{-\frac{2(x-x_i)^2}{w_i^2}}$$

where the parameter x_i is the central position of the band, w_i its width and A_i its area. The values obtained for the main parameters are shown in Table 15 and have been compared to many previous studies of CL on diopside, whose references are collected in other two works [Marshall, 1988; Waychunas, 1988]. All the spectra present a 450 nm band (a), that can be ascribed to the silicate-based network [Abu-Hassan and Townsend, 1988; Moritani et al, 2003; Kitazawa et al, 2004]. Moreover there are an intense band at 585 nm (b) and a weaker band, ranging from 690 nm to 740 nm (c). The band at 585 nm can be ascribed to Mn^{2+} ions in M2 (Ca^{2+}) sites, while the one at 690 nm to Mn^{2+} ions in M1 (Mg^{2+}) sites [Smith, 1949; Walker, 1985]. The infrared part of the spectrum has a less clear origin for the moment: it can be due to Ti^{3+} [Danger et al, 1997; Quaranta et al, 2007] or to Fe-related impurities [Herd et al, 2000]. In our samples coming from Pamir and in the Siberian one the band c is centred at 690 nm, while for the afghan samples it seems to be shifted at higher wavelength; therefore it could represent a good criterion to distinguish among provenances, but it is worth to stress that it is situated in a region of low sensitivity of the instrument used in this work, so further measurements are necessary to confirm this marker.

In order to confirm the possibility to extend the CL results to IL, a number of crystals were selected to be analysed by means of IL. Spectra obtained using CL and IL were compared, exhibiting a good correlation for all the phases analysed (see for example Figure 35 and Figure 36). Moreover we used the new IL apparatus to study the red/IR part the luminescence spectrum of diopside in a sample from Pamir (Figure 34); the band at 690 nm is clearly visible.

At last, no evident correlations between luminescence peaks and trace elements were found. As already mentioned, Ti, Mn and Fe are the main responsible for luminescence in diopside but due to a competition process between activators and quenchers a direct proportionality does not always exist between the intensity of a luminescence peak and element contents.

Other phases

Wollastonite

Wollastonite (CaSiO_3) is one of the strongest luminescent phases and it is common to all Chilean samples. More than forty points of interest were analysed by means of quantitative SEM-EDX and the mean composition is reported in Table 16. CL measurement on wollastonite have been performed in the same condition as on diopside and also a similar fit has been done. The spectra are very similar among them and are characterized by three bands (Table 17 and Figure 35) at about 449 nm, 553 nm and 589 nm. The first band is characteristic of silicate matrix and is common to other phases such as diopside [Long and Agrell, 1965]. The other two closed bands are probably related to $\alpha\text{-CaSiO}_3\text{:Mn}$ and $\beta\text{-CaSiO}_3\text{:Mn}$ polymorphic structures (560 and 620 nm) [Lange and Kressing, 1955; El Marraki et al, 2000]. Such

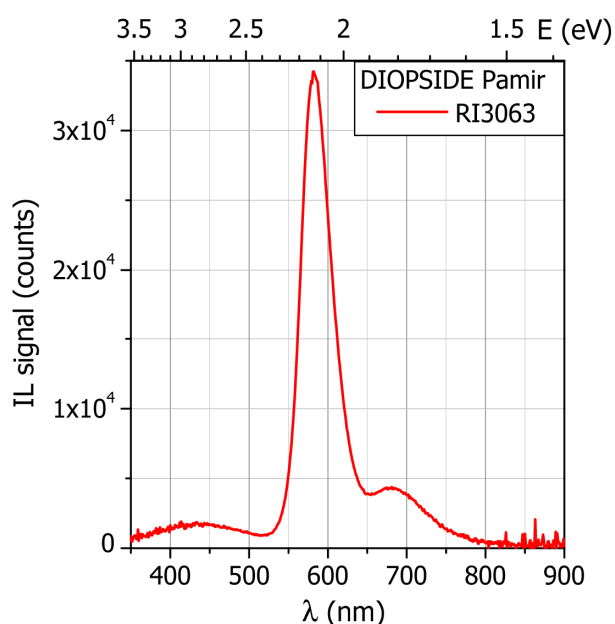


Figure 34. Calibrated IL spectra of diopside (in a sample from Pamir) obtained with the new IL apparatus, more sensitive in the red/IR region

Table 16. SEM-EDX analyses of wollastonite crystals. The mean values are in bold type and the standard deviation are in italic type

	SEM-EDX (41 points)	
SiO₂	40.77	<i>2.91</i>
CaO	58.74	<i>2.80</i>
Cr₂O₃	0.55	<i>0.35</i>

Table 17. Parameters of CL bands in a selection of four spectra of wollastonite; the values reported are mean \pm standard deviation obtained by the fit

Band		Energy (eV)	λ (nm)
a	center	2.76 ± 0.01	449 ± 2
	width	0.42 ± 0.02	69 ± 4
b	center	2.24 ± 0.01	553 ± 1
	width	0.16 ± 0.01	39 ± 2
c	center	2.10 ± 0.01	589 ± 2
	width	0.33 ± 0.01	93 ± 4

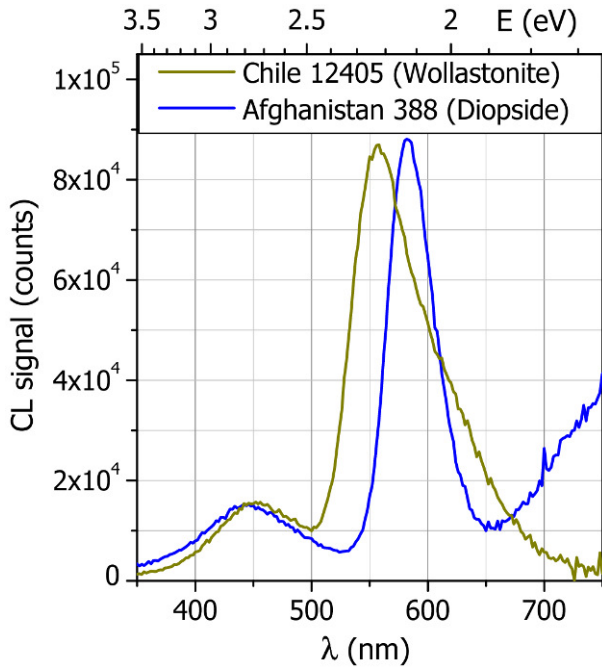


Figure 35. Comparison between calibrated CL spectra of diopside (in a sample from Afghanistan) and wollastonite (in a Chilean sample).

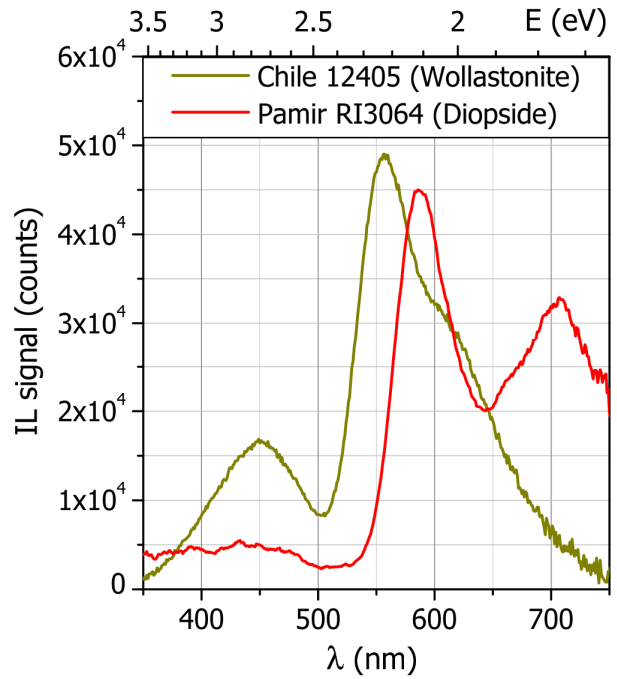


Figure 36. Comparison between calibrated IL spectra of diopside (in a sample from Pamir) and wollastonite (in a Chilean sample).

manganese-related bands were not observed in any other samples and therefore represent a significant fingerprint for Chilean provenance, as already observed in previous works [Calusi et al, 2008; Colombo et al, 2008].

Calcite

Also for this phase (CaCO₃) many points have been selected to be analysed by means both of SEM-EDX and SEM-CL. A Raman spectrum have also been acquired, to check the identification of this phase comparing the spectrum with a reference database (Figure 37).

A quantitative analysis of calcite is very difficult because of the carbon coating of the samples; in Table 18 an evaluation of the quantity of elements inside crystals is proposed, but has to be considered qualitative.

Luminescence spectra

Table 18. SEM-EDX analyses of calcite crystals. The mean values are in bold type and the standard deviation are in italic type

	SEM-EDX (41 points)	
CaO	75.84	<i>12.01</i>
CO₂	23.28	<i>11.97</i>
Others	0.88	<i>1.87</i>

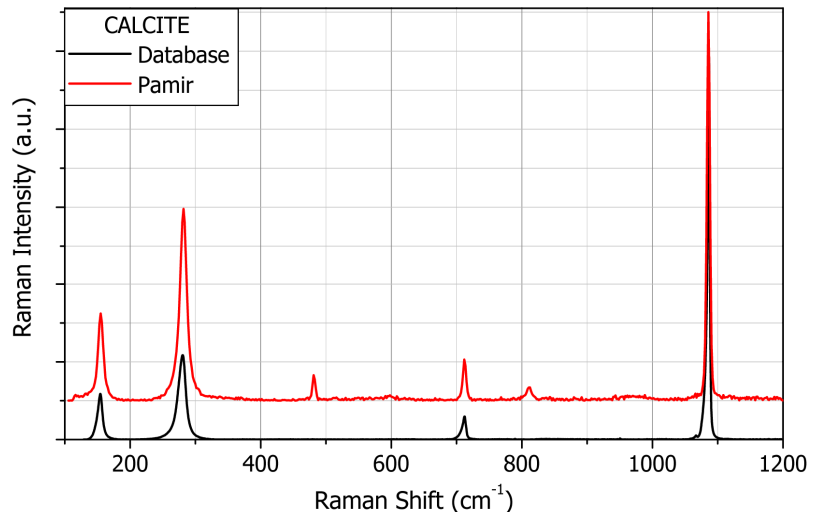


Figure 37. A Raman spectrum of calcite compared to a reference spectrum from the database RRUFF

Table 19. Parameters of CL bands in a selection of five spectra of calcite; the values reported are mean \pm standard deviation obtained by the fit

Band		Energy (eV)	λ (nm)
a	center	3.68 ± 0.28	337 ± 25
	width	1.70 ± 0.22	165 ± 21
b	center	2.01 ± 0.01	617 ± 5
	width	0.21 ± 0.01	66 ± 4
c	center	1.85 ± 0.04	670 ± 14
	width	0.30 ± 0.03	109 ± 10

from calcite exhibit the same features in all the samples: they are characterized by two broad bands at 620 and 670 nm and another one at 340 nm (Table 19 and Figure 38). These bands are due to Mn^{2+} substituting Ca^{2+} and to intrinsic luminescence, respectively [Habermann et al (pages: 331-358) in Pagel et al, 2000].

Phlogopite

At the moment Phlogopite has been identified only in one sample coming from Pamir. Even if in this sample it is very abundant, it is not useful for a provenance discrimination. It shows a brownish luminescence and the results obtained by means of SEM-EDX are shown in Table 20.

K-feldspar

K-feldspar (or Orthoclase, $KAlSi_3O_8$) is

Table 21. SEM-EDX analyses of K-feldspar crystals. The mean values are in bold type and the standard deviation are in italic type

	SEM-EDX (40 points)	
Na₂O	1.02	<i>0.76</i>
Al₂O₃	17.27	<i>1.59</i>
SiO₂	63.97	<i>2.63</i>
K₂O	17.48	<i>4.64</i>
Others	0.25	<i>0.66</i>

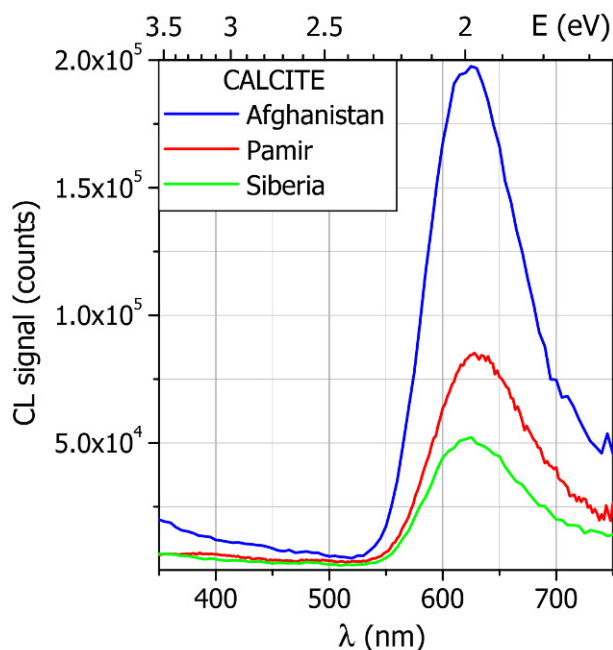


Figure 38. Selection of calibrated CL spectra of calcite in different samples (from *Afghanistan 12397*, *Pamir RI3065*, and *Siberia 390*)

Table 20. SEM-EDX analyses of phlogopite crystals. The mean values are in bold type and the standard deviation are in italic type

	SEM-EDX (10 points)	
F	0.94	<i>0.57</i>
Na₂O	0.06	<i>0.13</i>
MgO	23.30	<i>0.55</i>
Al₂O₃	14.86	<i>0.35</i>
SiO₂	43.65	<i>1.18</i>
K₂O	16.74	<i>0.73</i>
Others	0.45	<i>0.97</i>

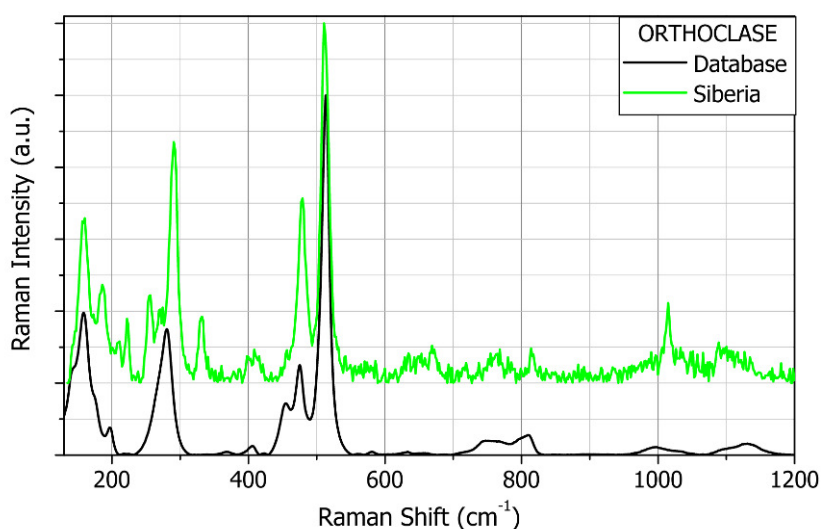


Figure 39. A Raman spectra of K-feldspar compared to a reference spectrum from the database RRUFF

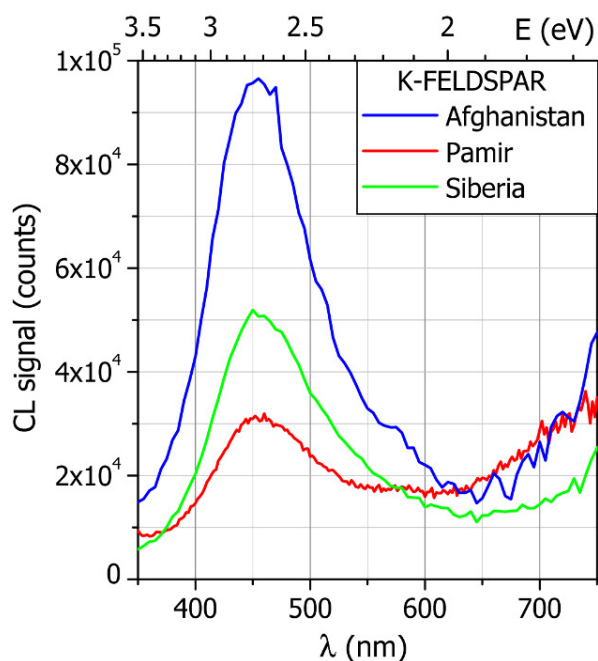


Figure 40. Selection of calibrated CL spectra of K-feldspar in different samples (from Afghanistan 388, Pamir RI3065, and Siberia 390)

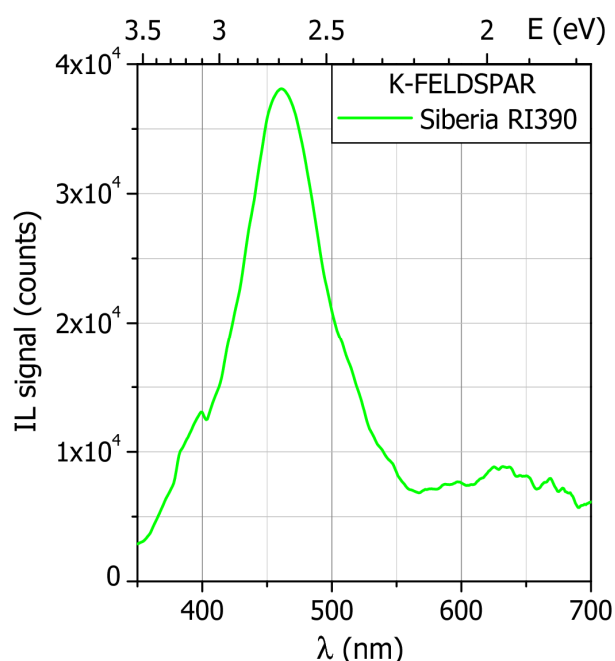


Figure 41. Calibrated IL spectrum of a K-feldspar in the sample Siberia RI390

present in sample from all provenances; a point has been analysed by means of Raman spectroscopy to check the identification of this phase comparing the resulting spectrum with a reference one from a database (Figure 39). Moreover forty crystals have been analysed by means of SEM-EDX and the results are presented in Table 21: besides the potassium, the typical element of this phase, most of the points present also a small amount of sodium.

The luminescence of this phase varies from light-blue to brownish, depending on the intensity of the main band of emission. In fact CL and IL spectra from K-feldspar (Figure 40 and Figure 41) exhibit the same features in all the samples and for this reason they are not useful for a provenance recognition: the main band observed is at 455 nm (Table 22); such emission is very common in this mineral and is due to Al-O-Al defects [Pagel et al, 2000 (pages: 245-270)].

Table 22. Parameters of CL bands in a selection of four spectra of K-feldspar; the values reported are mean \pm standard deviation obtained by the fit

Band		Energy (eV)	λ (nm)
a	center	2.72 ± 0.01	457 ± 2
	width	0.56 ± 0.02	95 ± 3
b	center	2.15 ± 0.03	577 ± 8
	width	0.33 ± 0.03	90 ± 8

Phase of the cancrinite group

The UV detection capabilities of the SEM-CL apparatus allowed the observation of a luminescent phase that was not visible in cold-CL images due to the low camera sensitivity in this wavelength range. SEM-EDX and μ -PIXE measurement of this phase are shown in Table 23: the main elements are clear even if there are some differences, mainly due to the difficulty in the quantification of chlorine, that is very abundant in this phase. Its Raman spectrum is shown in Figure 42 and is compared to four other spectra of phases of the group. The main feature

are the same, so we're confident that this phase belongs to this group, but none of them fit exactly with this phase. Also the composition obtained by means of SEM-EDX and PIXE confirm its compatibility with the cancrinite group, but further analysis are needed to exactly identify it.

A SEM-CL image obtained at 350 nm (10 nm pass band) is shown in Figure 43 in comparison with a cold-CL image of a 200 μm cancrinite crystal. The luminescence spectrum (also shown in Figure 44 and Figure 45) is very interesting and can be attributed to the strong UV emission and to a vibronic structure with ZPL at 2.55 eV. This phase has been abundantly observed only in Pamir samples and therefore it could be used to distinguish this provenance from the others.

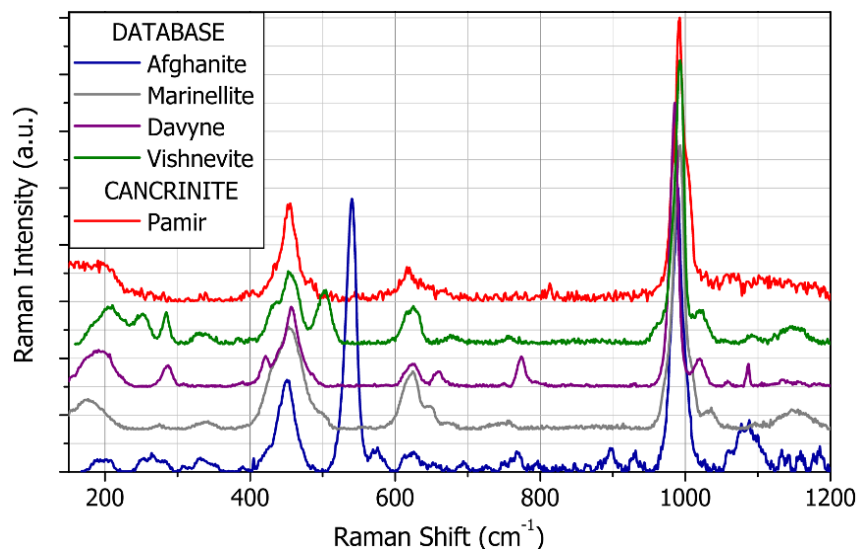


Figure 42. A Raman spectra of the cancrinite phase compared to four reference spectra of the cancrinite group from the database RRUFF

Table 23. SEM-EDX and μ -PIXE (3 MeV protons at the external microbeam line of LABEC in Firenze) analyses of the phase of the Cancrinite group. The mean values are in bold type and the standard deviation are in italic type

	SEM-EDX (2 points)	μ -PIXE (3 points)
Na₂O	9.03 <i>0.01</i>	12.98 <i>0.02</i>
Al₂O₃	23.85 <i>0.07</i>	27.72 <i>0.46</i>
SiO₂	29.91 <i>1.31</i>	30.74 <i>1.21</i>
SO₃	11.80 <i>1.19</i>	10.02 <i>0.42</i>
Cl	11.20 <i>0.86</i>	4.12 <i>0.21</i>
K₂O	3.62 <i>0.63</i>	2.82 <i>0.25</i>
CaO	10.60 <i>0.05</i>	11.59 <i>0.30</i>

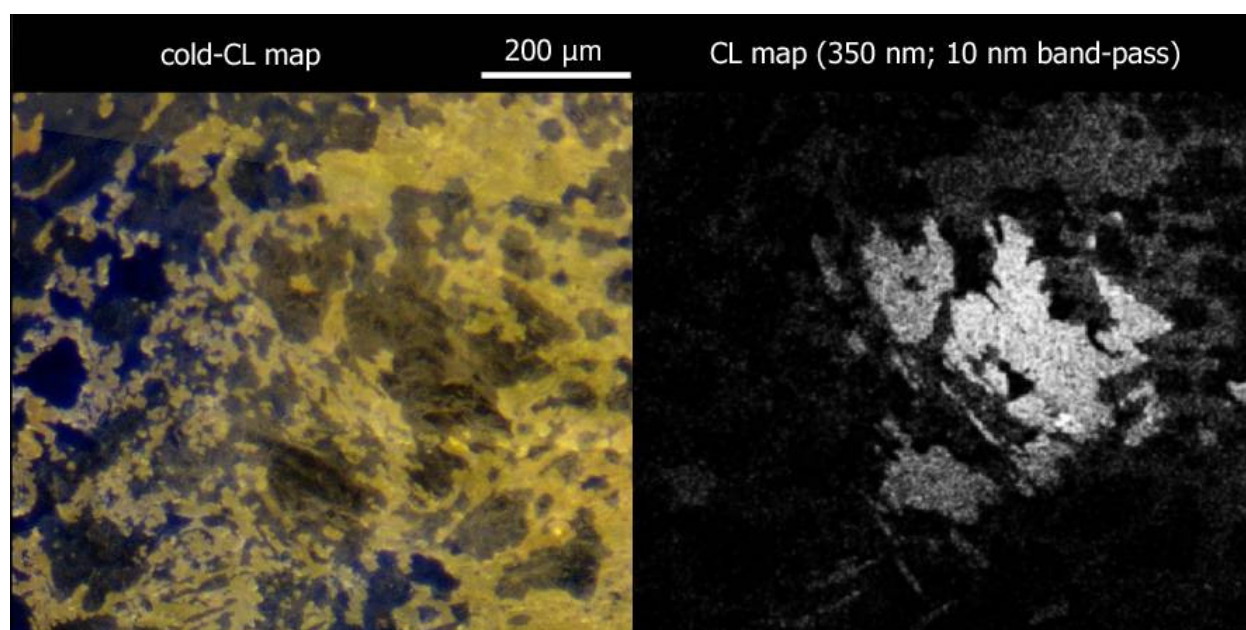


Figure 43. CL images of the sample RI3065 from Pamir: a cold-CL map (on the left) and a CL map (on the right) centred at 350 nm (10 nm band-pass) showing the UV emission of the phase of the Cancrinite group [Lo Giudice et al, 2009]

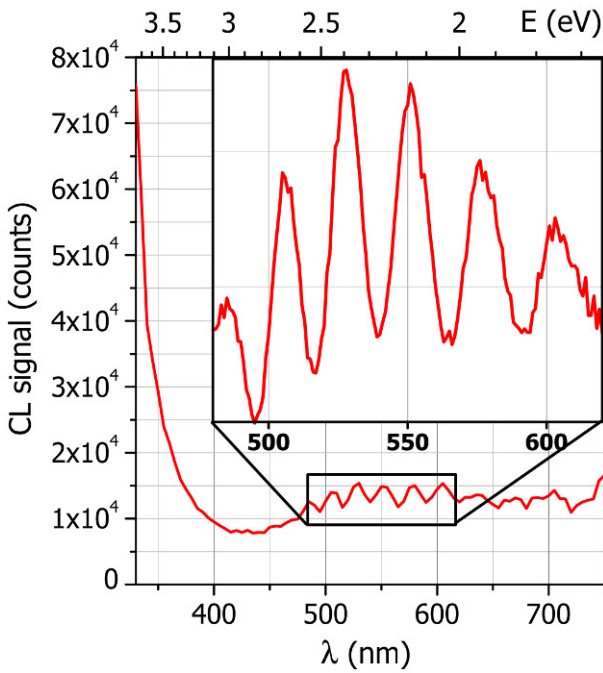


Figure 44. Calibrated CL spectrum of the phase of the Cancrinite group in the sample Pamir RI3065

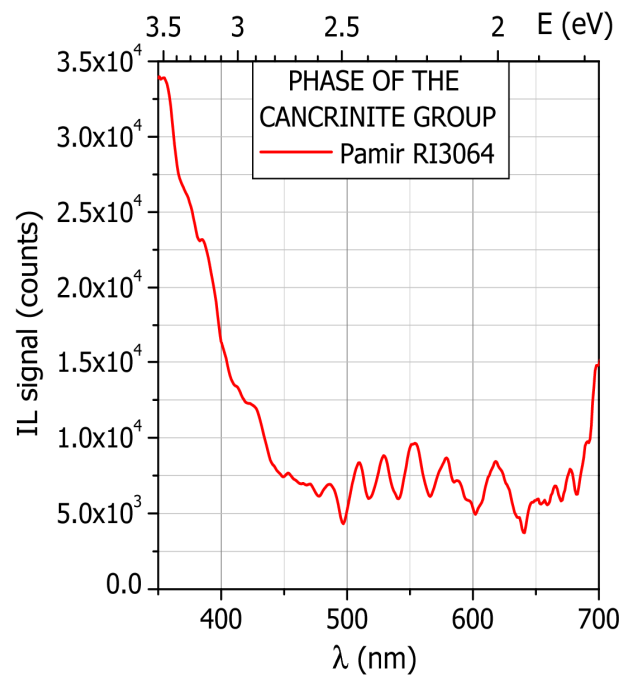


Figure 45. Calibrated IL spectrum of the phase of the Cancrinite group in the sample Pamir RI3064

Phase rich in titanium

Performing μ -PIXE mapping we detected a high quantity of titanium concentrated in some crystals of Afghan samples (see for example Figure 46). SEM-EDX and μ -PIXE analysis of these points are reported in Table 24: the PIXE quantification is quite different from the EDX one, probably because of the probed volumes that maybe give some contribution also from the beneath phase in the PIXE spectra. In any case this

Table 24. SEM-EDX and μ -PIXE (3 MeV protons at the external microbeam line of LABEC in Firenze) analyses of the phase rich in titanium. The mean values are in bold type and the standard deviation are in italic type

	SEM-EDX (6 points)		μ -PIXE (2 points)	
SiO ₂	37.17	<i>2.59</i>	41.64	<i>0.10</i>
TiO ₂	18.51	<i>7.63</i>	5.03	<i>1.07</i>
MgO	18.40	<i>2.42</i>	27.71	<i>0.17</i>
K ₂ O	14.77	<i>1.38</i>	10.09	<i>0.31</i>
Al ₂ O ₃	10.48	<i>0.98</i>	15.01	<i>0.57</i>
Others	0.68	<i>0.41</i>	0.52	<i>0.74</i>

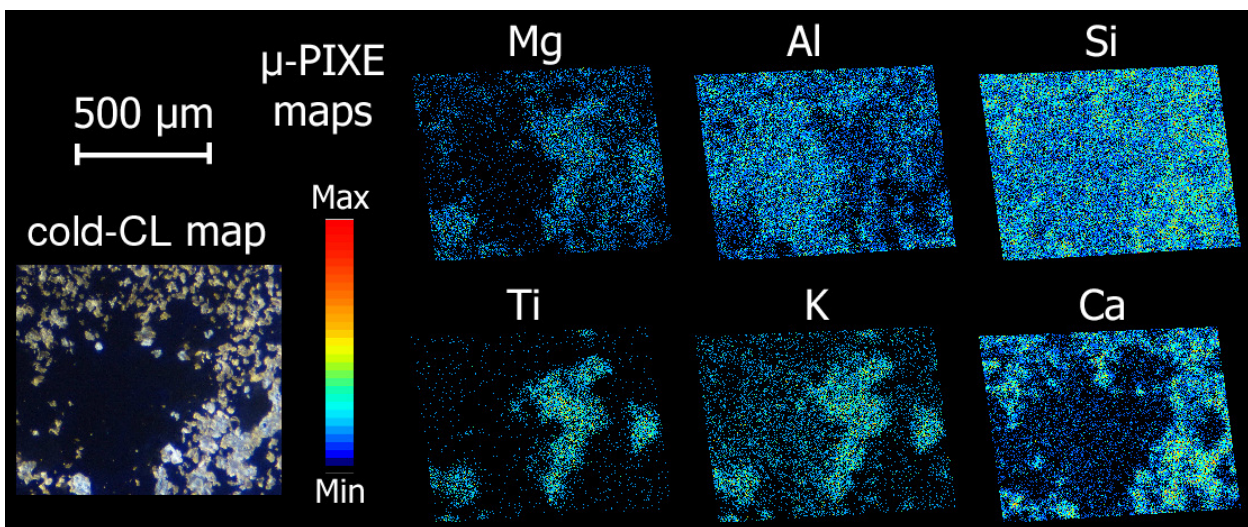


Figure 46. μ -PIXE elemental maps complemented by a cold-CL map of the same area of sample Afghanistan 47860 containing the phase rich in titanium. The PIXE measurements were performed at the external microbeam line of LABEC in Firenze

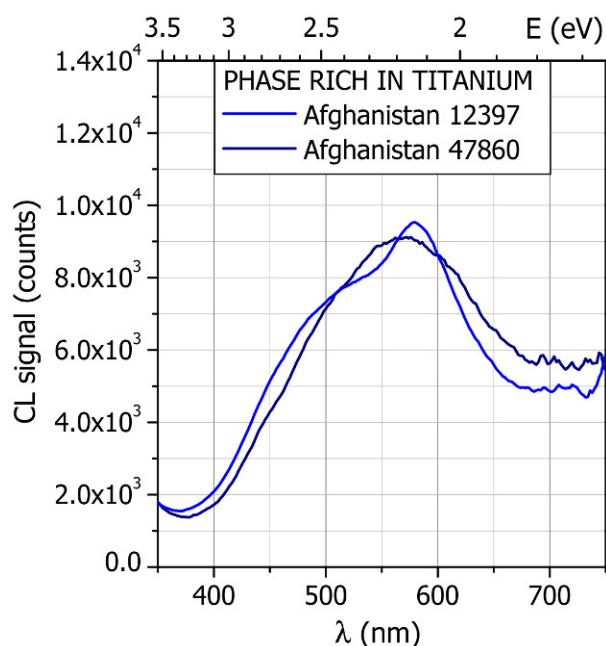


Figure 47. Selection of calibrated CL spectra of the phase rich in Ti in different samples from Afghanistan

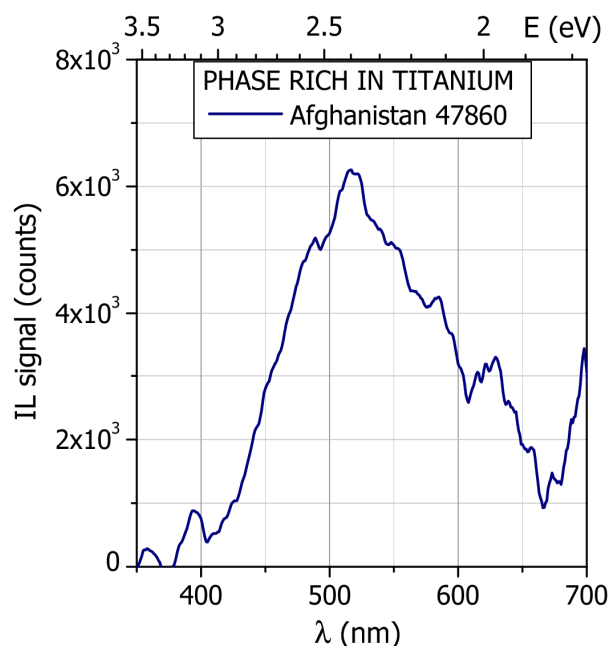


Figure 48. Calibrated IL spectrum of the phase rich in titanium in the sample Afghanistan 47860

high quantity of titanium is peculiar of this phase. Comparing these point of analysis with cold-CL maps, this phase shows a weak brownish luminescence and spectra present a very broad band centred at 540 nm (Figure 47 and Figure 48). Moreover, especially in the CL spectra, there is a contribution of diopside luminescence (band at 585 nm) as shown in Table 25. As for the lazurite, this can be attributed to a contaminations or to luminescence generated by multiple scattering during measurements. In any case, such luminescence is too weak to be rapidly detected for a provenance purpose, while the presence of this phase, that has been detected only in Afghan samples, is quite easy to find by means of μ -PIXE mapping and is a good marker for this provenance.

Table 25. Parameters of CL bands in a selection of five spectra of the phase rich in Ti; the values reported are mean \pm standard deviation obtained by the fit

Band		Energy (eV)	λ (nm)
a	center	2.31 ± 0.02	537 ± 5
	width	0.95 ± 0.11	229 ± 26
b	center	2.12 ± 0.03	585 ± 7
	width	0.19 ± 0.11	54 ± 30

Markers

The markers found in this work are summarized in Table 26, where results from literature are also reported. It is worth observing that in a complex material like lapis lazuli it is unlikely that only a marker or a technique can be sufficient to unequivocally distinguish among different provenances. Moreover some markers are “stronger” because they are a peculiar characteristic of a provenance, while some others can just give an indication if a sample can or cannot come from a certain provenance. The level of confidence of each marker is also indicated in Table 26, but it is worth stressing that all of them has to be verified increasing the statistic on more samples.

Table 26. Markers for provenance recognition of lapis lazuli with non-destructive techniques. The symbols mean:

- (●): probably from this provenance;
- (~): depends on the quantity of the elements or on the intensity of the bands;
- (×): probably not from this provenance;
- (-): nothing can be said.

Provenance	Markers	verified	not verified
Chile	double broad bands of luminescence (560 nm; 620 nm) due to wollastonite [Calusi et al, 2008]	●	×
	large amount of wollastonite instead of diopside [Borelli et al, 1986]	●	×
	lower quantity of K in lazurite	●	~
Afghanistan	higher quantity of Ti or V or Cr in diopside	●	~
	contemporaneous higher quantity of K and lower quantity of S in lazurite	●	~
	presence of Zr in some inclusions	●	-
	presence of a phase rich in Ti	●	-
Pamir	UV luminescence emission due to a cancrinite phase	●	×
	broad bands of luminescence at about 690 nm in diopside	●	~
	higher quantity of As inside lazurite	●	~
Siberia	presence of Ba in some inclusions [Ivanov et al, 1976; Delmas and Casanova, 1990]	●	×
	higher quantity of Sr [Ivanov et al, 1976; Delmas and Casanova, 1990]	●	~

Check on a sample of unknown provenance

The capability to ascribe a lapis lazuli to a quarry using the markers in Table 26 was tested on a the sample *RI 571* of unknown origin. A Chilean origin was excluded due to the absence of wollastonite phase and the correlated double luminescence band at around 600 nm. Moreover a value of $K/(Si+Al)$ concentration ratio ranging from 0.028 to 0.047 was found by means of the major element analysis. These values are higher than the maximum value found for Chilean samples that is $K/(Si+Al)=0.025$ (Figure 27). Taking into account the values of $S/(Si+Al)$ ranging from 0.25 to 0.33, the unknown rock falls in the main sequence of Afghan samples, but very close to Pamir Mountains and Siberian samples. Nevertheless, a Siberian origin was excluded by means of trace elements analysis, since lazurite does not contain barium (Figure 28). Other measured trace elements in lazurite were strontium (240 ppm) and arsenic (160 ppm), at the moment not significant for provenance attribution. The trace elements detected in diopside are compatible with the Afghan provenance, for the high quantity of titanium and vanadium and the absence of iron (Figure 31), while manganese and chromium are not useful for a provenance attribution in this case. Due to the absence of both the UV luminescence characteristic of the cancrinite phase and the 690 nm luminescence in diopside (Figure 32), the Pamir Mountains provenance was excluded. At last, we detected a crystal of the phase rich in titanium by means of SEM-EDX and we therefore conclude that probably the unknown sample comes from Afghanistan, as summarized in Table 27.

Table 27. Test of the markers for provenance recognition of lapis lazuli on the sample RI571. The symbols mean:
 (●): probably from this provenance;
 (≈): depends on the quantity of the elements or on the intensity of the bands;
 (×): probably not from this provenance;
 (-): nothing can be said.

Provenance	Markers	RI571
Chile	luminescence at 560 and 620 nm	×
	presence of wollastonite	×
	lower quantity of K in lazurite	×
Afghanistan	high Ti or V or Cr in diopside	●
	high K and low S in lazurite	≈
	Zr in some inclusions	-
	presence of a phase rich in Ti	●
Pamir	UV luminescence	×
	luminescence at 690 nm in diopside	×
	high As in lazurite	≈
Siberia	Ba in some inclusions	×
	high quantity of Sr	×

RESULTS ON ARTWORKS

In February 2011 a run of measurements have been performed at LABEC laboratory in Firenze, to test if the method developed on rocks works also on artworks. For this reason a special transport of some of the samples of the "Collezione Medicea" has been organized from the museum to the laboratory. This was also the first time we tested some of the new instrumentation on works of art, and in particular the defocused IBIL apparatus.

This run of measurements has to be considered as the first of a series, since has been impossible to check all the markers on all the objects. This is especially due to the fact that to check all the luminescence markers we need two different setup, one optimized for the visible and UV detection and one for the visible and IR range.

Experimental procedure

The first step of the work consists in the selection of the points of analysis: we took many pictures of the samples to easily select areas presenting large crystals (at least with the naked eye) both white and deep blue (Figure 49). We have to pay attention also to the geometry of the objects, because the same point should be analysed both with the defocused IBIL apparatus (with the object at 45° respect to the beam direction) and later with μ -PIXE and μ -IL (with the object orthogonal to the beam direction). With this constraints we acquired maps both in visible light and defocused IBIL of the same areas, selecting the bigger and more homogeneous crystals that for the yellow luminescence or the absence of luminescence could be diopside and lazurite (see Figure 50).

After this first step of mapping with

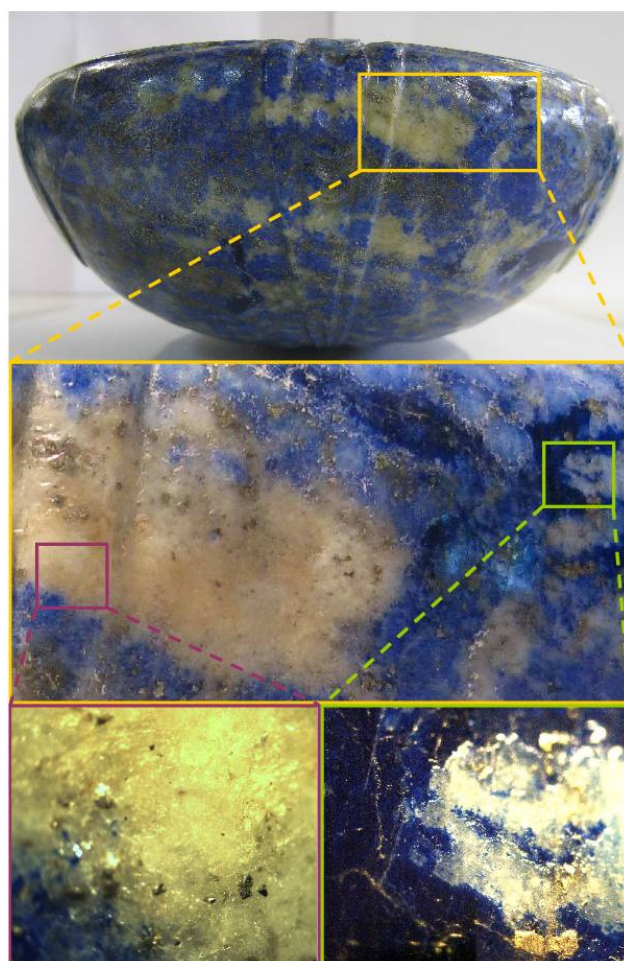


Figure 49. Pictures to select areas of analysis on the oval bowl (13682) from the "Collezione Medicea" of the "Museo di Storia Naturale" in Firenze

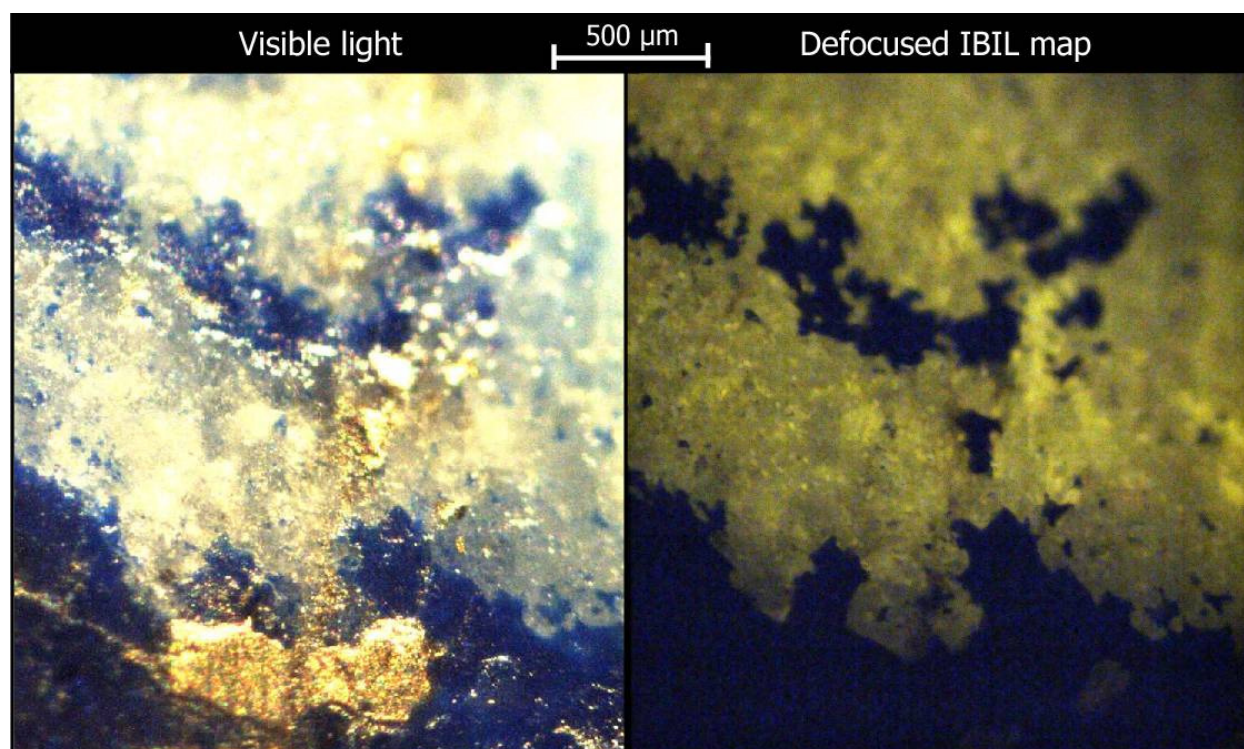


Figure 50. Visible light and defocused IBIL map of the same area of the oval bowl (13682) from the "Collezione Medicea" of the "Museo di Storia Naturale" in Firenze

defocused-IBIL we focused again the beam and started with the contemporaneous μ -PIXE and μ -IL acquisition exactly of the same areas. In this first run we decided to focus our attention mainly on diopside or, better, to the whitish crystals in visible light with a yellow luminescence. This is because the analysis of these crystals allows to easily distinguish among Asian provenances, with the presence of diopside, and Chilean samples, presenting wollastonite. Moreover, analysing the band at $690\div 740$ nm in diopside we can discriminate Afghan and Pamir lapis lazuli. For this reason we used the new apparatus for IL measurements, that is more sensitive in the red/IR region, but not in the UV region. With future measurements, using the other IL apparatus, we'll be able to rapidly detect an UV emission to verify the presence or the absence of the phase of the cancrinite group, typical of the Pamir provenance.

Results

During this run of measurement we could analyse four samples: on the oval bowl we studied one point of lazurite and two of diopside; on the small case and on the saltcellar two points of diopside on each one and on the oval panel one point of diopside. For all these points we acquired both a μ -PIXE and a μ -IL spectra. The results of the μ -PIXE analyses are reported in Table 28 for lazurite and in Table 29 for diopside: the main elements confirm the identification of the phase, while the trace elements can give us some information about provenance.

Oval bowl (13682)

The trace elements found in the lazurite of this sample do not give a clear information about provenance (Table 28 and Figure 51); in fact, the high quantity of arsenic and the absence of barium suggest to exclude the Siberian provenance, but the content of strontium is closer to the level found in the Siberian sample respect to the others. Moving to the two diopside crystals analysed on this object (Table 29 and Figure 52), their trace elements contents are similar: in this case vanadium, chromium and iron do not give information about provenance, while titanium and manganese show the highest detected content until now, that suggest an Afghan provenance for this object. The absence of zirconium inclusions does not give any information about provenance. Looking at the luminescence spectra of diopside (Figure 53), the peak at 690 nm is clearly visible and this could suggest a Pamir Provenance. For this sample we can conclude that a certain attribution is still not possible on the base of the measurements performed until now, but we can exclude a Chilean provenance

Table 28. μ -PIXE analysis of lazurite performed at the external microbeam line of LABEC in Firenze on the objects of the "Collezione Medicea" of the "Museo di Storia Naturale" in Firenze

Lazurite		
Oval bowl (13682)		
Main elements	oxide	%ox error
	Na ₂ O	20.3 1.0
	MgO	- -
	Al ₂ O ₃	25.2 1.3
	SiO ₂	34.1 1.7
	SO ₃	14.0 0.7
	Cl	0.72 0.04
	K ₂ O	0.35 0.03
	CaO	5.2 0.3
others	0.22 0.03	
Traces	element	ppm error
	Fe	330 43
	Zn	70 35
	As	280 84
Sr	1100 220	

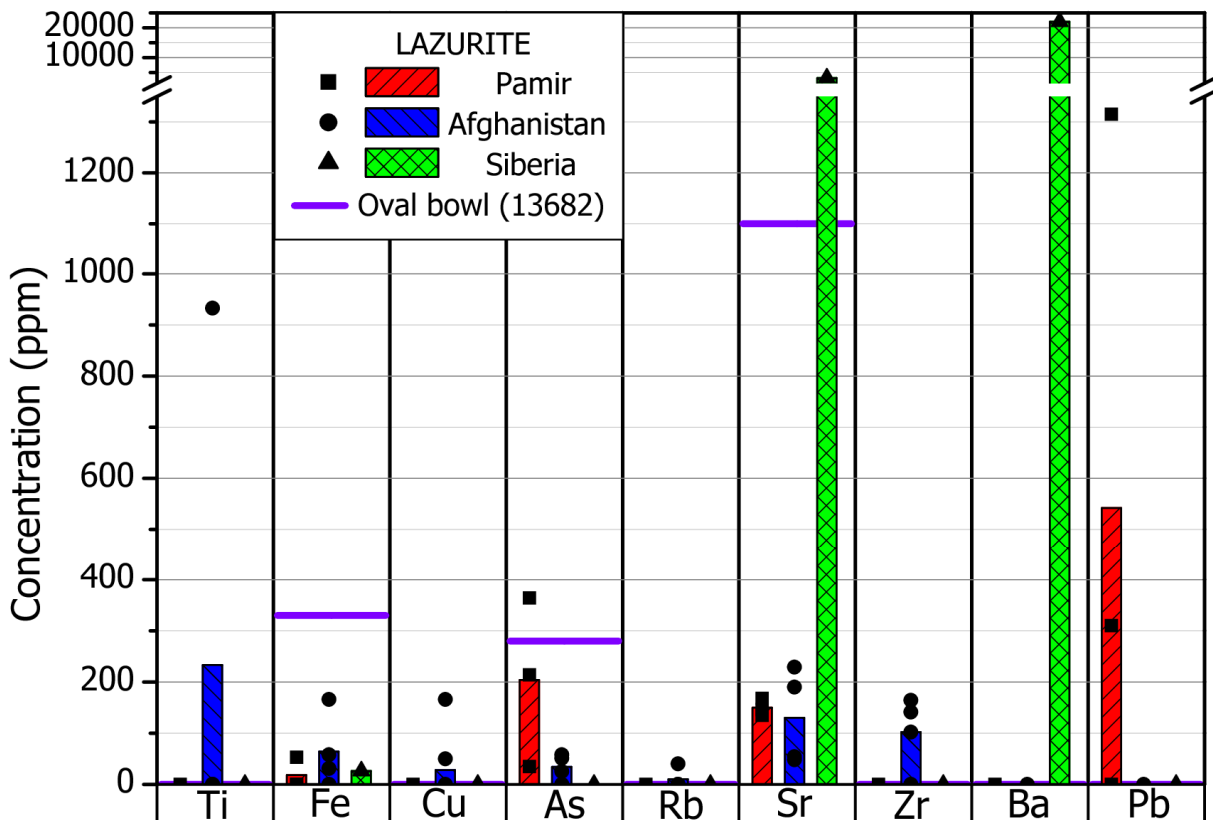
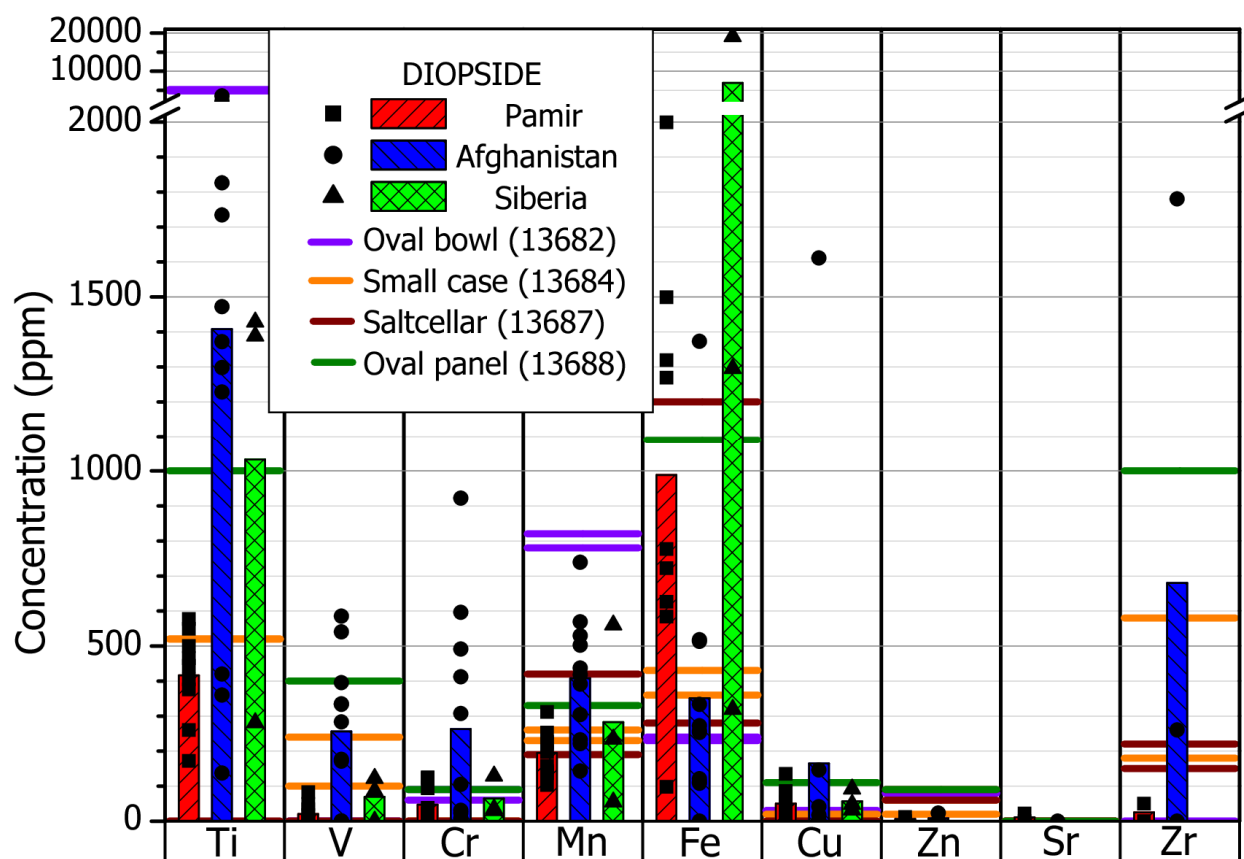


Figure 51. Minor and trace elements in lazurite from μ -PIXE measurements on the oval bowl (13682) performed at the external microbeam line of LABEC in Firenze. The dark points and the coloured columns are previous measurements on rocks of certain provenance and their mean values

Table 29. μ -PIXE analysis of diopside performed at the external microbeam line of LABEC in Firenze on the objects of the "Collezione Medicea" of the "Museo di Storia Naturale" in Firenze

Diopside		Oval bowl (13682)				Small case (13684)				Saltcellar (13687)				Panel (13688)	
Main elements	oxide	%ox	error	%ox	error	%ox	error	%ox	error	%ox	error	%ox	error	%ox	error
	Na ₂ O	3.0	0.2	3.4	0.3	1.9	0.3	1.2	0.1	1.1	0.3	1.4	0.3	1.1	0.2
	MgO	15.8	0.8	9.7	0.5	14.9	0.7	15.2	0.8	13.4	0.7	11.5	0.6	12.4	0.6
	Al ₂ O ₃	5.9	0.3	5.1	0.3	2.4	0.1	1.9	0.1	1.2	0.1	1.9	0.1	3.6	0.2
	SiO ₂	51.3	2.6	55.0	2.7	55.8	2.8	55.7	2.8	55.1	2.8	51.3	2.6	56.7	2.8
	K ₂ O	3.48	0.17	4.45	0.22	-	-	0.05	0.01	0.18	0.01	0.35	0.04	0.58	0.03
	CaO	18.8	0.9	18.7	0.9	24.8	1.2	25.5	1.3	28.5	1.4	31.8	1.6	24.5	1.2
	TiO ₂	0.87	0.04	0.84	0.05	0.09	0.02	0.09	0.02	-	-	-	-	0.17	0.03
	FeO	0.031	0.004	0.031	0.005	0.046	0.003	0.055	0.004	0.036	0.002	0.156	0.008	0.140	0.007
	others	0.84	0.05	2.80	0.15	0.09	0.01	0.37	0.04	0.55	0.04	1.58	0.36	0.74	0.05
Traces	element	ppm	error	ppm	error	ppm	error	ppm	error	ppm	error	ppm	error	ppm	error
	V	-	-	-	-	100	50	240	48	-	-	-	-	400	80
	Cr	90	36	60	36	-	-	-	-	-	-	-	-	90	45
	Mn	820	57	780	94	260	23	230	28	190	19	420	63	330	43
	Fe	240	29	230	35	360	22	430	34	280	14	1200	84	1090	55
	Cu	30	12	30	12	20	10	-	-	-	-	-	-	110	19
	Zn	80	16	80	16	20	8	60	12	60	12	90	27	90	18
	Zr	-	-	-	-	180	54	580	87	150	60	220	110	1000	140
	Rb	230	46	220	44	-	-	-	-	-	-	-	-	-	-
	Pb	290	87	280	84	160	64	380	76	1110	133	3600	360	870	148

because of the presence of diopside and the absence of wollastonite. Further measurement on samples of certain provenance and a deeper study on this object can maybe give a more precise indication about the provenance of the material used for this object.

**Figure 52.** Minor and trace elements in diopside from μ -PIXE measurements on the objects of the "Collezione Medicea" performed at the external microbeam line of LABEC in Firenze. The dark points and the coloured columns are previous measurements on rocks of certain provenance and their mean values

Small case (13684)

For this sample we analysed two points of diopside. The trace element content of iron, manganese, chromium and titanium does not give information about provenance (Table 29 and Figure 52), while the vanadium can suggest an Afghan provenance, even if its quantity is close to that of other provenances. The clear presence of zirconium in both the points it is a good marker for the Afghan provenance. The

luminescence spectra (Figure 53) does not show a strong band at 690 nm and this does not give a clear indication for provenance. Also for this sample a certain provenance can not be given, but we can just exclude the Chilean one.

Saltcellar (13687)

As on the previous sample, we acquired spectra from 2 points of diopside. From the trace element content it is impossible to say something about provenance (Table 29 and Figure 52), also because we did not detect neither titanium, nor vanadium, nor chromium. Also on this sample we detected zirconium indicating an Afghan provenance. From the luminescence spectra of this sample (Figure 53) we can notice a strong band (respect to the other samples) near 700 nm, that can suggest a Pamir Provenance. The conclusion for this sample is the same of the previous ones, excluding Chile as a possible provenance but can not say anything about others.

Oval panel (13688)

On this sample just one point of diopside have been analysed. From the trace elements quantities (Table 29 and Figure 52) we can notice that the amount of vanadium is high as only in Afghan samples has been found; moreover, the presence of zirconium suggests the same conclusion. The luminescence spectrum (Figure 53) is typical of diopside, so we can exclude the Chilean provenance also for this sample, and the band typical of Pamir samples is not present, so we can exclude also this origin. For this sample all the markers that have been analysed until now converge on the Afghan provenance, suggesting a different attribution respect to the

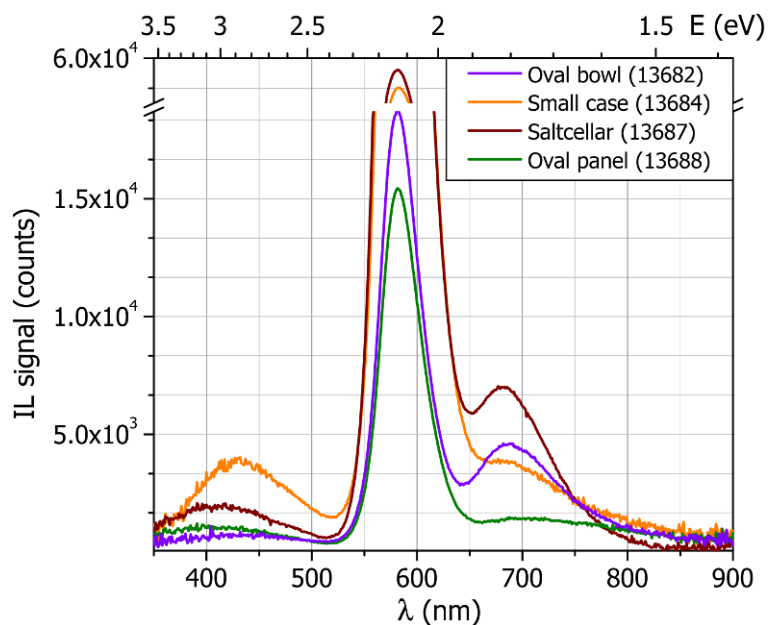


Figure 53. Calibrated IL spectra of diopside in the samples of the "Collezione Medicea" obtained with the new IL apparatus, more sensitive in the red/IR region

previous one that indicates this sample as coming from Siberia. It is worth stressing that only further analysis considering all the markers can give a definitive answer.

Summary

In Table 30 a summary of the markers analysed until now on the objects of the "Collezione Medicea" is reported. As a general consideration we can exclude the Chilean provenance for all the objects. The other markers up to now are not so strong to give a sure identification of the various objects, even if for the "Oval panel" (13688) the Pamir provenance seems to be excluded too. The "Small case" (13684) and the "Saltcellar" (13687) are compatible both with Afghan and Pamir provenance, while the Siberian provenance has not been explored yet. The "Oval bowl" (13682) is compatible both with Afghanistan, Pamir and Siberia provenances, and for this reason also the missing markers has to be analysed to reach a more reliable conclusion. We must note that in the only one Siberian rock sample we analysed in this work there was both high content of barium and strontium, so we actually do not know the variability of these two elements in Siberian samples, and for this reason at the moment we can not suggest or exclude the Siberian provenance for the oval bowl.

Table 30. Test of the markers for provenance recognition of lapis lazuli on the samples of the "Collezione Medicea". The symbols mean:

- (●): probably from this provenance;
- (~): depends on the quantity of the elements or on the intensity of the bands;
- (×): probably not from this provenance;
- (-): nothing can be said.

In gray the markers not yet analysed

Provenance	Markers	Oval bowl (13682)	Small case (13684)	Saltcellar (13687)	Oval panel (13688)
Chile	luminescence at 560 and 620 nm	×	×	×	×
	presence of wollastonite	×	×	×	×
	lower quantity of K in lazurite	-			
Afghanistan	high Ti or V or Cr in diopside	●	~	-	●
	high K and low S in lazurite	-			
	Zr in some inclusions	-	●	●	●
	presence of a phase rich in Ti				
Pamir	UV luminescence				
	luminescence at 690 nm in diopside	●	~	●	×
	high As in lazurite	●			
Siberia	Ba in some inclusions	×			
	high quantity of Sr	●			

CONCLUSION

In this work a systematic study by means of μ -PIXE and μ -IL on lapis lazuli is reported. This is useful to characterize both the elemental composition and the luminescent properties of some of the phases present in this stone. The final aim of the work is to identify useful markers to assign the provenance of raw materials on the basis of four of the main sources used in archaeological finding and works of art.

Despite the limited number of analyzed samples, results are promising and the experimental differences among different samples are significant. All the proposed markers can be identified using external micro ion beam analysis, in particular by means of μ -IL and μ -PIXE. These techniques were applied simultaneously on rocks and objects by means of the external microbeam facility of LABEC in Firenze, where a new defocused-IBIL apparatus has been set-up and tested on artworks, showing its usefulness in the choice of the points to analyse by means of μ -beam techniques.

Spectra obtained by means of CL and IL were compared showing a good correlation so that the possibility of extending the results obtained by means of CL to IL was confirmed. Differences in luminescence spectra arise from the presence of peculiar mineral phases associated with lapis lazuli sources and can be used to distinguish the provenance of the stones.

The elemental analysis of the single phases is also useful to distinguish among provenances: in fact the main elements of lazurite permit in some case to have a clear indication of the provenance of a sample, while in diopside the analysis of only the main elements do not give any information about the origin of a sample. Moreover the analysis of trace elements in the samples by means of μ -PIXE permits to have more markers to distinguish among provenances.

The main distinctive mineral phase in Chilean Lapis Lazuli is wollastonite, which can be distinguished by the intense luminescence at 560 nm and 620 nm. This behaviour was observed in all 4 samples we analysed and confirms what was obtained in previous works [Calusi et al, 2008; Colombo et al, 2008].

Lapis lazuli from Pamir exhibits a luminescence band at 690 nm in the emission spectra of diopside and it is also characterized by a cancrinite phase with a strong UV emission and a vibronic structure with ZPL at 2.55 eV. Moreover a higher quantity of Arsenic in the lazurite from this provenance is a good indication to distinguish it from others.

The samples from Afghanistan show a mean value of some trace elements (titanium, vanadium and chromium) in diopside higher than other provenances and a phase rich in titanium not yet identified has been found only in samples coming from this provenance. Moreover the presence of zirconium in some inclusions seems to be a peculiarity of these samples.

Although differences exist in cold-CL images and relevant CL spectra from Afghanistan and Siberian samples, they are weak because they are based only on different mineral phases ratio. However, Siberian lapis lazuli is characterized by a high content of barium and strontium and therefore the PIXE analysis allows the discrimination of this provenance.

It is worth stressing that all results in this work are related to a limited quantity of samples, and that the reliability of the present conclusion are to be confirmed investigating more samples in future works. However the capability to assign a lapis lazuli sample to a quarry using the identified markers has been tested on a sample of unknown origin and according to our analysis the sample has been attributed to an Afghan origin.

Finally a run of measurements on artworks of the "Collezione Medicea" have been performed: even if this was just the first of a series, it gave encouraging results, showing that this method can be applied to objects. In fact both the trace element content and the luminescence band positions are comparable with the ones already observed on rocks, even if more measurements are needed to reach a conclusive result. In fact the strongest markers we've found until now, that are the presence of a phase peculiar of one provenance, have not been checked systematically on these samples. It is worth noting that some objects present markers characteristic to more than one provenance: this is probably due to the low number of rocks samples we analysed until now, that do not cover all the variability that a marker can have in each provenance. For this reason in the future, with a greater statistic, some of the markers identified until now as peculiar of one provenance could be considered characteristic for more than one provenance or not a marker at all, depending on the variability in each provenance. Another hypothesis, even if this less probable but more fascinating, is that some of the analysed objects come from a provenance not yet analysed presenting the combination of markers we have found. Also in this case only more measurements on samples from different provenances will give a more conclusive answer.

In the last period, to continue this interesting work we already acquired some new samples from Afghanistan, Siberia and Chile, to increase the statistical significance of our results. In parallel we're trying to find samples coming also from other provenances and we're going to continue with measurements on artworks and hopefully also on archaeological samples.

BIBLIOGRAPHY

NOTE: (*) indicates a reference taken from other works and not available to me

- Abu-Hassan L.H., Townsend P.D. (1988) "Luminescence efficiency of silica during ion beam excitation". *Nuclear Instruments and Methods in Physics Research B*, 32: 293-298
- Ajò D., Castellato U., Fiorin E., Vigato P.A. (2004) "Ciro Ferri's frescoes: a study of painting materials and technique by SEM-EDS, X-ray diffraction, micro FT-IR and photoluminescence spectroscopy". *Journal of Cultural Heritage*, 5: 333-348.
- Aleksandrov S.M., Senin V.G. (2006) "Genesis and composition of lazurite in magnesian skarns". *Geochemistry International*, 44(10): 976-988
- Anthony J.W., Bideaux R.A., Bladh K.W., Nichols M.C. (2001) "Handbook of Mineralogy". Mineral Data Publishing (online free pdf files, version 1.2)
- Bacci M., Cucci C., Del Federico E., Ienco A., Jerschow A., Newman J.M., Picollo M. (2009) "An integrated spectroscopic approach for the identification of what distinguishes Afghan lapis lazuli from others". *Vibrational Spectroscopy*, 49(1): 80-83
- Ballirano P., Maras A. (2006) "Mineralogical characterization of the blue pigment of Michelangelo's fresco 'The last judgment'". *American Mineralogist*, 91: 997-1005
- Bauer M. (1904) "Precious stones: a popular account of their characters, occurrence and applications". Charles Griffin & Co, London (*)
- Berthoud T., Cleuziou S., Hurtel L.P., Menu M., Volfovsky C. (1982) "Cuivres et alliages en Iran, Afghanistan, Oman au cours des IV^e et III^e Millénaires". *Paléorient*, 8(2): 39-54 (in French)
- Bettiol A.A. (1999), "Ionoluminescence (IL) with a nuclear microprobe" (PhD thesis). School of physics, University of Melbourne, Australia (*)
- Birks J.B., Black F.A. (1951) "Deterioration of anthracene under α -particle irradiation". *Proceedings of the Physical Society of London A*, 64: 511-512
- Blaise J., Cesbron F. (1966) "Données minéralogiques et pétrographiques sur le gisement de lapis-lazuli de Sar-e-Sang, Hindou-Kouch, Afghanistan". *Bulletin de La Société française de Minéralogie et Crystallographie*, 89: 333-343 (*)
- Bollini D., Cervellera F., Egeni G.P., Mazzoldi P., Moschini G., Rossi P., Budello V. (1993) "The microbeam facility of the AN-2000 accelerator of the Laboratori Nazionali di Legnaro". *Nuclear Instruments and Methods in Physics Research A*, 328: 173-176
- Borelli A., Cipriani C., Innocenti C., Trosti R. (1986) "Caratterizzazione del lapislazuli". *La Gemmologia*, XI: 24-27 (in Italian)
- Bowersox G.W., Chamberlin B.E. (1995) "Gemstones of Afghanistan", Geoscience Press, Tucson, Arizona
- Bradley W.H. (1964), "Lazurite, talc and chlorite in the Green River formation of Wyoming". *The American Mineralogist*, 49: 778-781
- Breese M.B.H., Jamieson D.J., King P.J.C. (1996) "Materials Analysis using a nuclear microprobe". John Wiley & Sons, New York (*)

- Brögger W.C., Bäckström H. (1891) "Die Mineralien der Granatgruppe". *Zeitschrift für Krystallographie und Mineralogie*, 18: 209-276
- Brüggen J. (1921) "Informe jeológico sobre el yacimiento de Lapis LázuLi Flor de Los Andes del señor Santiago M. Merry". Unpublished report, Santiago, Chile, 10 pages (in Spanish)
- Buffon (Georges-Louis Leclerc, Count of Buffon) (1787). "Histoire Naturelle des Minéraux". Imprimerie Royale, Paris: 251-259 (*)
- Bulgarelli G.M., Tosi M. (1977) "La lavorazione ed il commercio delle pietre semipreziose nelle città dell'Iran protostorico (3200-1800 a.C.)". *Geo-Archeologia*, Japadre Editore, L'Aquila, 1-2: 37-50 (in Italian)
- Bussers H. (1984) "Glyptique de Tell ed-Der". Tell ed-Der, L. de Meyer (ed.), Louvain, IV: 63-79 (*)
- Calusi S., Colombo E., Giuntini L., Lo Giudice A., Manfredotti C., Massi M., Pratesi G., Vittone E. (2008) "The ionoluminescence apparatus at the LABEC external microbeam facility". *Nuclear Instruments and Methods in Physics Research B*, 266: 2306-2310
- Calvo del Castillo H., Ruvalcaba J.L., Calderón T. (2007) "Some new trends in the ionoluminescence of minerals". *Analytical and Bioanalytical Chemistry*, 387(3): 869-878
- Canut de Bon C. (1991) "Apreciaciones sobre las reservas de lapislazuli de yacimientos chilenos [Reserve estimates for the Chilean lapis lazuli deposits]". Unpublished report for El Servicio Nacional de Geología y Minería, December 9, 1991 (*)
- Casanova M. (1992) "The Sources of the Lapis Lazuli found in Iran". *South Asian Archaeology, Monographs in World Archaeology*, Prehistory Press, 14: 49-56 (Proceedings of the 10th International Conference of South Asian Archaeologists in Western Europe, Paris - France, 1989)
- Cipriani C., Innocenti C., Trosti-Ferroni R. (1988) "Le collezioni del museo di mineralogia di Firenze: VI) Lapislazuli". *Museologia Scientifica*, V (1-2): 17-30 (in Italian)
- Coenraads R.R., Canut de Bon C. (2000) "Lapis lazuli from the Coquimbo Region, Chile". *Gems & Gemology*, 36(1): 28-41.
- Collon D. (1986) "Western Asiatic Seals in the British Museum: Cylinder Seals III: Isin Larsa to Old Babylonian" (London) (*)
- Colombo E., Calusi S., Cossio R., Giuntini L., Lo Giudice A., Mandò P.A., Manfredotti C., Massi M., Mirto M.A., Vittone E. (2008) "Recent developments of ion beam induced luminescence at the external scanning microbeam facility of the LABEC laboratory in Florence". *Nuclear Instruments and Methods in Physics Research B*, 266: 1527-1532
- Corona Esquivel R., Benavides Muñoz M.E. (2005) "Mineralogía y origen del yacimiento de lapislázuLi Flor de los Andes, Chile". *Boletín de Mineralogía* 16: 57-65 (in Spanish)
- Cuitiño G.L. (1986) "Mineralogía y génesis del yacimiento de lapislázuLi Flor de los Andes, Coquimbo, Norte de Chile". *Revista Geológica de Chile*, 27: 57-67 (in Spanish)
- Da Cunha C. (1989) "Le lapis lazuli: son histoire, ses gisements, ses imitations". Editions du Rocher, Paris, France (in French)
- Danger T., Petermann K., Schwentner N., Sliwinski G., Wong W.C. (1997) "UV-spectroscopy and band structure of Ti:YAlO₃". *Journal of Luminescence*, 72-74: 171-173
- Deer W.A., Howie R.A., Zussman J. (1978) "Rock-forming minerals". Longman

- Deer W.A., Howie R.A., Zussman J. (2004) "Rock-forming minerals". (2nd ed.) Geological society, London
- Delmas A.B., Casanova M. (1990) "The Lapis Lazuli sources in the ancient east". South Asian Archaeology, ed. Maurizio Taddei, Istituto Italiano per il Medio ed Estremo Oriente, Roma, Serie Orientale Roma 66(1): 493-505 (Proceedings of the 9th International Conference of South Asian Archaeologists in Western Europe, Venice - Italy, 1987)
- Derrick M. (1990) "Infrared Spectroscopy in Conservation Science". The Getty Conservation Institute, Los Angeles: 134 (*)
- Dill H.G. (2010) "The "chessboard" classification scheme of mineral deposits: Mineralogy and geology from aluminum to zirconium". Earth-Science Reviews, 100: 1-420
- Dran J.C., Salomon J., Calligaro T., Walter P. (2004) "Ion beam analysis of art works: 14 years of use in the Louvre". Nuclear Instruments and Methods in Physics Research B, 219-220: 7-15
- Drouin D., Réal Couture A., Joly D., Tastet X., Aimez V., Gauvin R. (2007) "CASINO V2.42 - A Fast and Easy-to-use Modeling Tool for Scanning Electron Microscopy and Microanalysis Users". Scanning, 29: 92-101
- El Marraki A., Schvoerer M., Bechtel F. (2000), "Luminescence de cristaux de dévitrification de wollastonite dans des verres non dopés et dopés en Eu, Dy et Tm". Physica status solidi A, 181(2): 491-507 (in French)
- Faryad S.W. (1999) "Metamorphic evolution of the Precambrian South Badakhshan block, based on mineral reactions in metapelites and metabasites associated with whiteschists from Sare Sang (Western Hindu Kush, Afghanistan)". Precambrian Research, 98: 223-241
- Faryad S.W. (2002) "Metamorphic conditions and fluid compositions of scapolite-bearing rocks from the lapis lazuli deposit at Sare Sang, Afghanistan". Journal of Petrology, 43(4): 725-747
- Field F. (1850) "Análisis de lapislazuli de Elqui". Los anales de la Universidad de Chile por 1850 (page 386) (*)
- Gama S., Volfinger M., Ramboz C, Rouer O (2001) "Accuracy of PIXE analyses using a funny filter". Nuclear Instruments and Methods in Physics Research B, 181: 150-156
- Giuntini L., Massi M., Calusi S. (2007) "The external scanning proton microprobe of Firenze: A comprehensive description". Nuclear Instruments and Methods in Physics Research A, 576: 266-273
- Goldstein A.D. (1981) "The Gemstones of Russia, Pamir and Baikal". Jewellery making gems and minerals, 528: 50-51 (*)
- Goldstein J. I., Newbury D. E., Echlin P., Joy D. C. (1992) "Scanning Electron Microscopy and X-Ray Microanalysis: A Text for Biologists, Materials Scientists, and Geologists". Plenum Pub. Corp. (*)
- Götze J. (2002) "Potential of cathodoluminescence (CL) microscopy and spectroscopy for the analysis of minerals and materials". Analytical and Bioanalytical Chemistry, 374: 703-708
- Grew E.S. (1988) "Kornerupine at the Sar-e-Sang, Afghanistan, whiteschist locality: Implications for tourmaline-kornerupine distribution in metamorphic rocks". American Mineralogist, 73: 345-357
- Hassan I., Peterson R.C., Grundy H.D. (1985) "The structure of lazurite, ideally $\text{Na}_6\text{Ca}_2(\text{Al}_6\text{Si}_6\text{O}_{24})\text{S}_2$, a member of the sodalite group". Acta Crystallographica, C41: 827-832
- Herd C.D.K., Peterson R.C., Rossman G.R. (2000) "Violet-colored diopside from Southern Baffin Island, Nunavut, Canada". The Canadian Mineralogist, 38: 1193-1199
- Herrmann G. (1968) "Lapis Lazuli: the early phases of its trade". Iraq, 30(1): 21-57

- Herrmann G., Moorey P.R.S. (1983) "Lapis Lazuli". Reallexikon der Assyriologie und Vorderasiatischen Archäologisch, ed. by W. de Gruyter, Berlin, 6: 489-492
- Hinks P. (1975) "Nineteenth Century Jewellery". Faber and Faber, London (page 56) (*)
- Hogarth D.D. (1970) "Mineral occurrences in the Western Lake Baikal District U.S.S.R.", *The Mineralogical Record*, 1(2): 58-64
- Hogarth D.D., Griffin W.L. (1975) "Further data on Lapis lazuli from Latium, Italy". *Canadian Mineralogist*, 13: 89-90
- Hogarth D.D., Griffin W.L. (1976) "New data on lazurite". *Lithos*, 9: 39-54
- Hogarth D.D., Griffin W.L. (1978) "Lapis lazuli from Baffin Island - a Precambrian meta-evaporite". *Lithos*, 11: 37-60
- Hogarth D.D., Griffin W.L. (1980) "Contact-metamorphic lapis lazuli: the Italian Mountain deposits, Colorado". *Canadian Mineralogist*, 18: 59-70
- Ivanov V.G. (1976) "The geochemistry of formation of the rocks of the lazurite deposits of the southern Baikal Region". *Geokhimiya*, 1: 47-54
- Ivanov V.G., Samoylov V.S., Petrov L.L., Yaroshenko S.K. (1976) "Geochemical features of the genesis of lazurite-bearing metasomatites in the South Baikal Region". *Doklady Earth Science Section*, 227: 200-202
- Jarrige J.F. (1988) "Les cités oubliées de l'Indus: archéologie du Pakistan", *Association Française d'Action Artistique*, Paris (page 28) (*)
- Jensen D.E. (1976) "Lapis lazuli from Edwards, New York". *Rocks and minerals*, 51: 155 (*)
- Kanaya K., Okayama S. (1972) "Penetration and energy-loss theory of electrons in solid targets" *Journal of Physics D: Applied Physics*, 5(1): 43-58
- Keisch B. (1972) "Secrets of the past: Nuclear Energy Application in Art and Archaeology" published by the U.S. Atomic Energy Commission: 96-98
- Kenoyer J.M. (1997) "Trade and technology of the Indus Valley: New Insights from Harappa, Pakistan" *World Archaeology*, 29(2): 262-280
- Kitazawa S.I., Yamamoto S., Asano M., Ishiyama S. (2004) "Radiation-induced luminescence and photoluminescence from sol-gel silica glasses and phosphosilicate glasses by 1 MeV H⁺ irradiations". *Physica B*, 349: 159-165
- Klein C.A. (1968) "Bandgap Dependence and Related Features of Radiation Ionization Energies in Semiconductors". *Journal of Applied Physics*, 39(4): 2029-2038
- Korzinskij D.S. (1947) "Bimetasomatism of phlogopite and lazurite in occurrences of the Archean, Pribaikal". *Akademiya Nauk. SSSR. Trudy Instituta Geologicheskikh Nauk*, 29, Petrograficheskaja Serija 10: 18-25 (*)
- Kostov R. (2004) "Lazurite from central Asia according to the Ethnonym Balkhara". *Bulgarian Geological Society, Annual Scientific Conference "Geology 2004"*
- Kulke H. (1976) "Metamorphism of evaporate carbonate rocks (NW Africa and Afghanistan) and the formation of lapis lazuli". *International Geological Congress, Sydney, Section 3B, Abstract 25* (*)
- Lange H., Kressing G. (1955) "Der Einfluß der Kristallstruktur auf die Lumineszenz des Calciumsilikates (Mn, Pb)". *Zeitschrift für Physik*, 142: 380-386 (*)

- Le Strange G. (1919) [translated by] Hamd-Allah Mustawfi of Qazvin, "The Geographical Part of the Nuzhat al-Qulub": 197 (*)
- Lo Giudice A., Re A., Calusi S., Giuntini L., Massi M., Olivero P., Pratesi G., Albonico M., Conz E. (2009) "Multitechnique characterization of lapis lazuli for provenance study". *Analytical and Bioanalytical Chemistry*, 395(7): 2211-2217
- Long D.A. (2002) "The Raman Effect". Wiley, Chichester (*)
- Long J.V.P., Agrell S. (1965) "The cathodoluminescence of minerals in thin section". *Mineralogical Magazine*, 34: 318-326 (*)
- Majidzadeh Y. (1982) "Lapis lazuli and the Great Khorasan Road". *Paléorient*, 8(1): 59-69
- Marshall D.J. (1988) "Cathodoluminescence of Geological Materials". Unwin Hyman Ltd, Boston, US
- Mathis F., Othmane G., Vrielynck O., Calvo del Castillo H., Chêne G., Dupuis T., Strivay D. (2010) "Combined PIXE/PIGE and IBIL with external beam applied to the analysis of Merovingian glass beads". *Nuclear Instruments and Methods in Physics Research B*, 268: 2078-2082
- Maxwell J.A., Campbell J.L., Teesdale W.J. (1989) "The Guelph PIXE software package". *Nuclear Instruments and Methods in Physics Research B*, 43: 218-230
- Maxwell J.A., Teesdale W.J., Campbell J.L. (1995) "The Guelph PIXE software package II". *Nuclear Instruments and Methods in Physics Research B*, 95: 407-421
- Miliani C., Daveri A., Brunetti B.G., Sgamellotti A. (2008) "CO₂ entrapment in natural ultramarine blue". *Chemical Physics Letters*, 466(4-6): 148-151
- Moorey P.R.S. (1994) "Ancient mesopotamian materials and industries: the archaeological evidence". Clarendon press, Oxford: 85-92
- Morimoto N. (1988) "Nomenclature of Pyroxenes". *Mineralogy and Petrology*, 39: 55-76
- Moritani K., Takagi I., Moriyama H. (2003) "Production behavior of irradiation defects in vitreous silica under ion beam irradiation". *Journal of Nuclear Materials*, 312: 97-102
- Nassau K. (1983) "The physics and chemistry of color: the fifteen causes of color". Wiley & Sons, New York: 149 (*)
- Nibbi A. (1981) "Ancient Egypt and some Eastern Neighbours". Park Ridge, Noyes Publication, chap. 2: 33-55
- Nicholson P.T., Shaw I. (2000) "Ancient Egyptian Materials and Technology". Cambridge University Press: 39-40
- Pagel M., Barbin V., Blanc P., Ohnenstetter D. (2000) "Cathodoluminescence in Geosciences". Springer-Verlag Berlin Heidelberg
- Pauling L. (1930) "The structure of sodalite and helvite". *Zeitschrift für Kristallographie*. 74: 213-225
- Quaranta A., Salomon J., Dran J.C., Tonezzer M., Della Mea G. (2007) "Ion beam induced luminescence analysis of painting pigments". *Nuclear Instruments and Methods in Physics Research B*, 254: 289-294
- Re A., Lo Giudice A., Angelici D., Calusi S., Giuntini L., Massi M., Pratesi G. (2011) "Lapis lazuli provenance study by means of micro-PIXE". *Nuclear Instruments and Methods in Physics Research B*, in press (DOI: 10.1016/j.nimb.2011.02.070)

- Rivano S. (1975) "El lapislazuli de Ovalle (Provincia de Coquimbo, Chile [The lapis lazuli from Ovalle (Coquimbo Province, Chile)]". 6° Congreso Geológico Argentino, 3:165-177 (*)
- Rivano S. and Sepúlveda P. (1991) "Illapel 1:250,000 Geological Map Sheet, Chile". Servicio Nacional de Geología y Minería, Santiago, Chile (*)
- Rogers A.F. (1938) "Lapis lazuli from San Bernardino County, California". *American Mineralogist*, 23(2): 111-115
- Sage B.G. (1777) "Éléments de minéralogie docimastique". Imprimerie Royale, Paris (*)
- Sarianidi V.I. (1971) "The lapis lazuli route in the ancient east". *Archaeology Magazine*, 24(1): 12-15
- Schwarz K.H., Hofmann U. (1970) "Lapislazuli und Ultramarin. II". *Zeitschrift für anorganische und allgemeine Chemie*, 378(2): 152-159 (in German)
- Schreyer W., Abraham K. (1976) "Three stage metamorphic history of white schist from Sare Sang, Afghanistan, as part of a former evaporate deposit". *Contributions to Mineralogy and Petrology*, 59: 111-130 (*)
- Sha Y., Zhang P., Wang G., Zhang X., Wang X. (2002) "Determination of the chemical states of iron in plagioclase by external beam ionoluminescence". *Nuclear Instruments and Methods in Physics Research B*, 189: 408-411
- Silverman D.P. (1978) "50 Wonders of Tutankhamun". An Artabras Book, Crown Publishers, New York (*)
- Smith A.L. (1949) "Some new complex silicate phosphors containing Calcium, Magnesium and Beryllium". *Journal of The Electrochemical Society*, 96(5): 287-296
- Smith G.D., Clark R.J.H. (2004) "Raman microscopy in archaeological science". *Journal of Archaeological Science*, 31(8): 1137-1160
- Smith G.D., Klinshaw R.J. (2009) "The presence of trapped carbon dioxide in lapis lazuli and its potential use in geo-sourcing natural ultramarine pigment". *Journal of Cultural Heritage*, 10: 415-421
- Sofianides A.S., Harlow G.E. (1990) "Gems and Crystals from the American Museum of Natural History". Simon and Schuster, New York (*)
- Strunz H. (1970) "Mineralogische Tabellen". Akademische Verlagsgesellschaft (5th ed.), Leipzig (*)
- Sutherland L. (1991) "Gemstones of the Southern Continents". Reed Books, Sydney, Australia (*)
- Taylor D. (1967) "The Sodalite Group of Minerals". *Contributions to Mineralogy and Petrology* 16: 172-188
- Teo E.J., Bettioli A.A., Udalagama C.N.B., Watt F. (2003) "Ionoluminescence and ion beam induced secondary electron imaging of cubic boron nitride". *Nuclear Instruments and Methods in Physics Research B*, 210: 501-506
- Tikot R.H. (2002) "Chemical Fingerprinting and Source Tracing of Obsidian: The Central Mediterranean Trade in Black Gold". *Accounts of Chemical Research*, 35(8): 618-627
- Tosi M., Piperno M. (1973) "Lithic Technology behind the ancient lapis lazuli trade". *Expedition*, 16(1): 15-23
- Tosi M. (1974) "The Lapis Lazuli trade across the Iranian plateau in the 3rd millennium B.C.". *Gururājamañjarikā, Studi in onore di G. Tucci (extract)*, Istituto Universitario Orientale, Napoli: 3-22

- Tosi M., Vidale M. (1990) "4th Millennium BC Lapis Lazuli Working at Mehrgarh, Pakistan". *Paléorient*, 16(2): 89-99
- Van Peteghem J.K., Burley B.J. (1963) "Studies on solid solution between sodalite, nosean and hauyne". *Canadian Mineralogist*, 7: 808-813 (*)
- Vittone E., Lo Giudice A., Manfredotti C., Egeni G., Rudello V., Rossi P., Gennaro G., Pratesi G., Corazza M. (2001) "Light detection with spectral analysis at the Legnaro nuclear microprobe: applications in material and earth sciences". *Nuclear Instruments and Methods in Physics Research B*, 181: 134-139
- Von Rosen L. (1988) "Lapis lazuli in geological contexts and in ancient written source". *Studies in Mediterranean Archaeology and Literature*, 65; ed. by Paul Aströms förlag, Partille, Sweden
- Von Rosen L. (1990) "Lapis lazuli in archaeological contexts". *Studies in Mediterranean Archaeology and Literature*, 93; ed. by Paul Aströms förlag, Partille, Sweden (*)
- Voskoboinikova, N. (1938) "The mineralogy of the Slyudyanka deposits of lazurite". *Zapiski Vserossiyskogo Mineralogicheskogo Obshchestva*, 67: 601-622 (in Russian) (*)
- Walker G. (1985) "Mineralogical applications of luminescence techniques" (Chemical Bonding and Spectroscopy in Mineral Chemistry, F.J. Berry & D.L. Vaughan, eds.). Chapman & Hall, London, U.K. chap. 4: 103-140
- Warren B.E., Bragg, W.L. (1928) "The structure of diopside $\text{CaMg}(\text{SiO}_3)_2$ ". *Zeitschrift für Kristallographie und Mineralogie*, 69: 168-193 (*)
- Waychunas G.A. (1988) "Luminescence, X-ray emission and new spectroscopies". (Spectroscopic methods in mineralogy and geology). *Reviews in mineralogy*, 18: 639-664
- Webster R. (1975) "Gems, their sources, descriptions and identification". (3rd ed.) Newnes, Butterworths, London: 219-222
- Wood J., Lt. (1841) "A journey to the Source of the River Oxus", ed. John Murray, London, p.265
- Wyart J., Bariand P., Filippi J. (1981) "Lapis lazuli from Sar-i-Sang, Badakhshan, Afghanistan". *Gems and Gemmology*, 17: 184-190
- Yang C. (1996) "Ionoluminescence techniques for geological applications" (PhD thesis). Department of Nuclear Physics, Lund Institute of Technology, Lund, Sweden (*)
- Yang C., Larsson N.P.O., Swietlicki E., Malmqvist K.G., Jamieson D.N., Ryan C.G. (1993) "Imaging with ionoluminescence (IL) in a nuclear microprobe". *Nuclear Instruments and Methods in Physics Research B*, 77: 188-194
- Yurgenson G.A., Sukharev B.P. (1985) "Localization of lapis lazuli bodies of Badakhshan and their mineral zonation". *International geology review*, 27: 230-237.
- Ziegler J.F., Ziegler M.D., Biersack J.P. (2010) "SRIM - The stopping and range of ions in matter (2010)". *Nuclear Instruments and Methods in Physics Research B*, 268(11-12): 1818-1823
- Zöldföldi J., Kasztovszky Zs. (2003) "Provenance study of Lapis lazuli by non-destructive Prompt Gamma Activation Analysis (PGAA)". *BCH Supplément* 51: 677-691 (Proceeding of the 7th International Conference of Association for the Study of Marble and Other Stones in Antiquity, Thassos - Greece, 2003)
- Zöldföldi J., Richter S., Kasztovszky Zs., Mihály J. (2006) "Where does Lapis lazuli come from? Non-destructive provenance analysis by PGAA". 353-360 (Proceeding of the 34th International Symposium on Archaeometry, Zaragoza - Spain, 2004)

WEB BIBLIOGRAPHY

Solid State Physics Group (University of Torino): <http://www.dfs.unito.it/solid>

INFN: www.infn.it

Fondazione per l'arte (Compagnia di San Paolo):
<http://www.compagniadisanpaolo.it/fondazionearte/>

Museo di Storia Naturale (University of Firenze): <http://www.msn.unifi.it/CMpro-v-p-114.html>

LNL: <http://www.lnl.infn.it/index.html>

LABEC: <http://labec.fi.infn.it/>

Interdepartmental Centre "G. Scansetti": <http://www.centroscansetti.unito.it/>

SRIM: <http://www.srim.org/>

CASINO: <http://www.gel.usherbrooke.ca/casino/index.html>

GUPIXwin: <http://pixe.physics.uoguelph.ca/gupix/main/>

RRUFF, University of Arizona (Raman Spectra database): <http://rruff.info/index.php>

Ocean Optics: <http://www.oceanoptics.com>

Oxford Microbeams Ltd.: <http://www.microbeams.co.uk/>

ACKNOWLEDGEMENTS

This work has been carried out and financially supported in the framework of the INFN experiments "FARE" and "DANTE". I gratefully acknowledge the "Compagnia di San Paolo" for the funding of a PhD scholarship on Physics applied to Cultural Heritage that allowed me to carry out this complex as fascinating work.

The first and biggest "thank you" is to my supervisor Alessandro Lo Giudice, to introduce me in the intriguing world of lapis lazuli and to always encourage me, transmitting all his knowledge and passion for research.

I want to thank many other people that worked with me in these three years permitting me to obtain these results. For the "geological part", I warmly thank Giovanni Pratesi, for his precious time and for the availability of the samples: without them this work could not be possible. I also acknowledge Luca Martire for the availability of his cold-CL apparatus, Alessandro Borghi for the precious advices and answers to our "geological" questions, Roberto Cossio for the constant availability of the mineral standards, Margherita Serra for the help with the pyroxenes triangle, Simona Ferrando for the help with the Raman measurements and Angelo Agostino for the availability of the optical microscope.

For the IBA measurements I want to thank all the LABEC people: Silvia Calusi, Nicla Gelli, Lorenzo Giuntini, Novella Grassi, Mirko Massi, Alessandro Migliori, both for the help during the measurements and for the funny atmosphere always present at LABEC. Two special thanks to Silvia, for the commitment during the measurements on artworks and the analysis of the PIXE spectra, and to Novella, for the suggestions about PIXE measurements and Gupix analysis.

For the LNL measurements I want to thank Leonardo La Torre and Luca for the help obtaining the micro-beam and Daniele Ceccato for his precious suggestions and help in the PIXE measurements and analyses at LNL.

A big thanks to all the students that help me with their precious measurements: Maria, Elisa C., Chiara, Debora and Elisa M. (in chronological order); I warmly wish Debora to continue working on this topic with the same enthusiasm she has always shown.

Many thanks to all the people of the group of Solid State Physics for the nice and funny time passed together, the precious advices, the great knowledge that each of you try to pass me and for the cultural growth we've done and we're doing together.

And finally I want to thank all the people that contribute directly and indirectly to this work: sorry not to cite your names explicitly... Among these I want to thank in particular all my friends, old and new, with which I share many important moments of my life...

Un grandissimo grazie a tutta la mia famiglia, specialmente ai miei genitori e a mio fratello, che mi hanno sempre supportato e mi sono sempre stati vicino in tutti questi anni... E infine un grazie infinito a Roby, che ormai conoscerà a memoria questo lavoro a forza di leggerlo: grazie per l'inesauribile impegno che hai dimostrato sopportandomi ed aiutandomi così tanto in questo ultimo periodo, sia per la stesura e la revisione della tesi, che per avermi alleggerito di tutto ciò che ci sta intorno... sei insostituibile...

A ciascuno di voi una sola parola, ma dal più profondo del cuore: **GRAZIE !!!**